# Synthesis and complex self-assembly of AB and ABC amphiphilic block copolymers with a branched hydrophobic poly(2-oxazoline)

**Inauguraldissertation**

Zur Erlangung der Würde

eines Doktors der Philosophie vorgelegt

der Philosophisch-Naturwissenschaftlichen Fakultät

der Universität Basel

von

**Davy Poupin-Daubian**

Basel, 2021



Genehmigt von der Philosophisch-Naturwissenschalftlichen Fakultät

auf Antrag von

Prof. Dr. Wolfgang Meier

(Universität Basel)

Erstbetreuer

Prof. Dr. Cornelia Palivan

(Universität Basel)

Zweitbetreuerin

Prof. Dr. Nico Bruns

(Universität Strathclyde)

externer Experte

Basel, den 17.11.2020

Prof. Dr. Martin Spiess

(Dekan)

# Synthesis and complex self-assembly of AB and ABC amphiphilic block copolymers with a branched hydrophobic poly(2-oxazoline)

**Davy Poupin-Daubian**

University of Basel

Department of Chemistry

Davy Poupin-Daubian: *Synthesis and complex self-assembly of AB and ABC amphiphilic block copolymers with a branched hydrophobic poly(2-oxazoline)*,
Basel, Autumn 2020

Dedicated to ma Maman, my Cerf-Volants und meine Julia

Without their precious love and support,
none of this would have been possible.

Klar Zum Entern, Sine Metu and Tiger4ever

## Abstract

Amphiphilic block copolymers (ABPs) have been the focus of numerous studies thanks to their ability to self-assemble into materials with diverse applications, including drug delivery and nanocatalytic reactors. In order to increase the number of ABPs available and broaden the range of self-assembled structures and increase their morphological complexity, this work describes the synthesis of new families of linear AB and ABC amphiphilic block copolymers with a branched hydrophobic poly(2-oxazoline).

First, we synthetized poly(ethylene oxide)-*block*-poly(2-(3-ethylheptyl)-2-oxazoline) (PEO-*b*-PEHOx), a new biocompatible amphiphilic AB diblock copolymer obtained in one step via microwave-assisted polymerization of EHOx using a new nosylated PEO macroinitiator. Kinetics of the polymerization in different solvents was crucial to optimize the synthesis and revealed a controlled, yet fast polymerization of the AB copolymer. Differential scanning calorimetry (DSC) proved that PEO-*b*-PEHOx shows glass transition temperatures below room temperature, making it suitable for a wide range of self-assembly method, especially in mild and solvent-free conditions. Self-assembly of PEO-*b*-PEHOx was then performed using film rehydration and solvent switch. In both cases, we were able to show the formation of various complex structures (multi-compartment micelles (MCMs), pseudo-vesicles and yolk/shell nanoparticles) by dynamic and static light scattering (DLS/SLS), transmission electron microscopy (TEM) and cryogenic transmission electron microscopy (Cryo-TEM). Our results show that PEO-*b*-PEHOx is a potent new AB copolymer due to its unique self-assembly behaviour.

In the second part of this thesis, building upon the synthesis of PEO-*b*-PEHOx, we leveraged the living nature of the polymerization of oxazolines. Via sequential microwave-assisted polymerization, we synthetized in one-pot poly(ethylene oxide)-*block*-poly(2-(3-ethylheptyl)-2-oxazoline)-*block*-poly(2-ethyl-2-oxazoline) (PEO-*b*-PEHOx-*b*-PEtOz), a new biocompatible amphiphilic ABC triblock copolymer. Depending on the hydrophilic weight fraction of the copolymers, nanoscopic micelles, worms and polymersomes were formed as well as multicompartment vesicles (MCV). The self-assemblies were thoroughly analysed regarding their size and shape using dynamic and static light scattering, TEM and Cryo-TEM. By varying the ratio of PEO to PEtOz, we were able to drive the asymmetry of the polymersome membranes and proved it by two independent methods, bicinchoninic acid (BCA) assay and 2D-$^{1}$H-NOESY NMR, which confirmed the presence of a longer PEO block (45 units) and the absence of a shorter PEtOz (less than 32 units) on the outer surface of the polymersomes. Thus, from this new family of ABC triblock copolymers, asymmetric polymersomes with a thin membrane (6-10 nm) can be obtained, justifying a potential future use in biomedical applications with the directed insertion of transmembrane proteins.

# Acknowledgments

**PhD Defence Committee:**

First and foremost, I thank the committee members Prof. Wolfgang Meier, Prof. Cornelia Palivan and Prof. Nico Bruns for evaluating my thesis. I sincerely thank Prof. Wolfgang Meier and Prof. Cornelia Palivan for supervising my work and for providing a great working environment. For examples, by giving me responsibilities over synthesis laboratories and various instruments, by giving me the freedom to bring my own scientific ideas to the table, by letting me take a major part in writing manuscript, to name a few…I learned a tremendous amount of personal and professional skills for my future. I can't thank you enough for having given me the opportunity to come for a PhD in your group. Merci beaucoup!

I thank Prof. Nico Bruns very much for being my co-referee. I deeply appreciated discussing with him at the Macromolecular colloquium Freiburg 2020.

I thank the BioEM Lab, Dr. Mohamed Chami and Carola Alampi for the Cryogenic transmission microscopy measurements and useful discussions.

**Tiger PhD Odyssey Gratitude Project:**

Early-on for scientific reports in our weekly group meetings, I began to use the title "Without those amazing people I wouldn't be here today, Merci!" on my Acknowledgements slide. I thought and still think that sentence very sincerely. I would like to express my thanks in my own crazy Tiger way from the bottom of my heart. All those people made my PhD an incredible adventures filled with countless lessons and unforgettable memories.

One of the habit/skillset/mindset/whatever I developed the most throughout my PhD is "Gratitude". I have always been very grateful for all the awesome people I met throughout my life but I failed to express it by fear of judgments, paralyzing doubts they wouldn't like it etc…Thanks to my inspiring muse of a soulmate, Julia, I overcame this barrier and began to write little notes, emails, craft cards etc…whenever my crazy Tiger mind wanted to do so…gifting them to the people that had a positive and meaningful impact on me no matter how small. Because I realized that people generally receive any positive comments, thanks or compliments (very) well. And no matter how they receive it in the end, it can never do harm and it brings me a great deal of happiness to prepare and send all those little gifts and

messages. This is why, I won't just write some lines of acknowledgements in a thesis that may never reach the people I truly want to thank them for their contribution to my PhD Odyssey.

In my upcoming "PhD Tiger Odyssey Gratitude Project" I will reach out personally to all those people to thank them, tell them how amazing they are in my eyes and wish them all the best:

| | | |
|---|---|---|
| Dr. Evgeniia Konishcheva | Dr. Gesine Gunkel-Grabole | Claire Meyer |
| Dr. Samuel Lörcher | Dr. Serena Rigo | Dr. Saziye Avsar |
| Dr. Pascal Richard | Dr. Andreas Belluati | Dimitri Hürlimann |
| Maya Greuter | Dr. Sagana Thamboo | Dr. Myrto Kyropoulou |
| Gabriele Persy | Riccardo Wehr | Dr. Roland Goers |
| Sven Kasper | Dr. Csaba Fodor | Dr. Adi Dinu |
| Dr. Cora-Ann Schönenberger | Christoph John | Alessandro Angelini |
| Dr. Jens Gaitzsch | Luisa Zartner | Maryame Bina |
| Shabnam Tarvirdipour | Xinan Huang | Stefano Di Leone |
| Paul Gneupel | Alexandra Fillion | Dr. Sonja Kübelbeck |
| Dr. Grit Baier | Dr. Oliver Spangenberg | Ludovic Amruthalingam |
| Carl Emerson | Carola Alampi | Pierre Thesmar |
| Ronan Rocaboy | Alain Baiyoumy | Alexis Vrignaud |
| Marina Charrieras | Family Pestke | Horst Beran |

**Ma Maman, my Cerf-Volants und meine Julia: my happiness pillars**

Ma Maman chérie d'amour, sans toi, sans ton soutien sans failles tant financier qu'affectif, je ne serai pas là où je suis aujourd'hui, tu m'as permis de tellement m'épanouir! Merci de t'être rapprochée de moi avec Belfort et ces vacances d'été en Bretagne! Je t'aime très fort! <3

My Cerf-Volants, Antoine « Le Viking » Clémot, Marine « Némésis/Hamtaro » Bain, Alexia « L'iguane » Leyret and Bastien « Breton Pur Beurre » Jégo, my dear best friends, despite the distance, be it crazy Skypes, WhatsApp discussions or awesome WEs together…it always had a wonderful positive impact on my well-being. Thank you so much! Love you guys! <3

Meine Julia, dieses PhD Abenteuer hätte ich nie ohne dich beginnen oder schaffen können. Meine Seeleverwandte, Ensemble für ein Ewigkeit oder zwei, ich liebe dich so beaucoup! <3

## Contents

# List of figures

# List of tables

## List of main abbreviations used

**ABPs:** Amphiphilic Block Copolymers

**AB polymer:** amphiphilic linear AB diblock copolymer

**ABC polymers:** amphiphilic linear ABC triblock copolymers

**BCA:** Bicinchoninic acid

**CROP:** Cationic Ring Opening Polymerization

**Cryo-TEM**: Cryogenic Transmission Electron Microscopy

**DLS**: Dynamic Light Scattering

**DSC**: Differiential Scanning Calorimetry

$Đ_M$: Dispersity (polymers)

**EtOH**: Ethanol

***f***: hydrophilic weight fraction

**FR:** Film Rehydration

**GPC:** Gel Permeation Chromatography

**MCM:** Multicompartment Micelles

**MCV:** Multicompartment Vesicles

$M_n$: Number average molar mass

**MWCO**: Molecular Weight Cut-Off

**NOESY**: Nuclear Overhauser Effect SpectroscopY

**NMR**: Nuclear Magnetic Resonance

**PEO-Nos:** Nosylated Poly (ethylene oxide)

**PEO-*b*-PEHOx:** Poly(ethylene oxide)-*block*-poly(2-(3-ethylheptyl)-2-oxazoline)

**PEHOx-*b*-PEtOz:** Poly(2-(3-ethylheptyl)-2-oxazoline)-*block*-poly(2-ethyl-2-oxazoline)

**PEO-*b*-PEHOx-*b*-PEtOz:** Poly(ethylene oxide)-*block*-poly(2-(3-ethylheptyl)-2-oxazoline)-*block*-poly(2-ethyl-2-oxazoline)

$R_g$: Radius of gyration

**$R_h$:** Hydrodynamic radius

**SLS**: Static Light Scattering

**SS:** Solvent Switch

**TEM**: Transmission Electron Microscopy

**THF:** Tetrahydrofuran

# 1. Introduction

*In this chapter, the reader will be introduced to amphiphilic block copolymers (ABPs), from their synthesis to their unique ability to self-assemble in aqueous solutions, notably nanoscopic polymersomes. This introduction will start with an overview of the possible strategies to synthetize ABPs efficiently with a focus on linear ABC triblock copolymers. It will follow up with the principles of the self-assembly in solution of linear AB diblock and ABC triblock copolymers. The important criteria underlying the self-assembly of ABPs and which tools are available to characterize the resulting self-assemblies are showed. As a conclusion, the motivation behind this present work will be presented.*

Inspired by nature, ABPs have been developed to self-assemble in aqueous solutions into different structures relevant for biomedical applications like drug delivery, catalytic nanocompartments or cell mimics.[3-9] Their self-assembly is driven by the hydrophobic interactions between the spatially separated hydrophilic and hydrophobic blocks. Thanks to the vast variety of monomers available and development of polymerization techniques, an ever-increasing range of different block copolymers are produced, including complex architectures like graft, star, dendritic and cyclic.[10]

This Chapter contains parts adapted from the ref[1] and ref[2]:

(1) Evgeniia Konishcheva, **Davy Daubian**, Jens Gaitzsch and Wolfgang Meier. "Synthesis of Linear ABC Triblock Copolymers and Their Self-assembly in Solution". *Helv. Chim. Acta.* (2018), 101, e1700287.
(2) Evgeniia V. Konishcheva, **Davy Daubian,** Serena Rigo and Wolfgang P. Meier. "Probing membrane asymmetry of ABC polymersomes". *Chem. Commun*. (2019), 55, 1148.

The simplest type of ABPs are linear and their self-assembly lead already to a wide range of morphologies. Linear AB diblock copolymers (From now on referred to as “AB polymers”), where A is an hydrophilic block and B an hydrophobic block, can self-assemble into micelles, cylindrical micelles (worms), polymersomes and hollow tubes.[11-17] Linear ABC triblock copolymers polymers (From now on referred to as “ABC polymers”) can reach a higher level of complexity and flexibility in the design of self-assembled structures compared to traditional AB polymers.[18-19] ABC polymers can form morphologies not accessible with AB polymers, such as raspberry shapes, waffle-like self-assemblies, half-moon structures, cloud-like aggregates or 3D networks.[20-22]

Poly(ethylene oxide)-*block*-poly(propylene oxide)-*block*-poly(ethylene oxide) (PEO-*b*-PPO-*b*-PEO), better known as poloxameres or pluronics, the first reported ABPs, have been extensively studied and used as micelles in pharmaceutical formulations.[23-26] By varying the block composition of the ABPs, it is possible to functionalize the resulting self-assemblies: biocompatibility, biodegradability, stimuli-responsiveness, etc… Choosing the individual segments of the ABPs not only dictate its properties or the available morphologies by self-assembly but also how difficult is its synthesis.

There are various ways to obtain linear ABPs. In the next section, the challenges of the synthesis of ABC polymers and the available tools to overcome them will be presented. The same principles can be applied to AB polymers. Their synthesis is easier with one less step needed.

## 1.1 Synthesis of ABC triblock copolymers

The synthesis of an ABC polymer is never straightforward: the choice of the correct solvent is crucial, the high purity of the monomer is mandatory, and often the change of polymerization technique or an end-group modification is required for the synthesis of the next block. These challenges require a deliberate design of the polymerization route to synthesize a narrowly dispersed polymer with the desired block sequence.

We will now give an overview over different synthetic strategies to obtain linear ABC architectures relevant for self-assembly studies. Table 1 summarizes examples of ABC polymers with subscripts indicating the length of the corresponding block, its average molecular weight $M_n$, its dispersity $Đ_M$, and the polymerization technique used. They all show a monomodal and narrow molecular weight distribution, confirming the controlled character of the polymerization performed.

**Table 1.** Examples of ABC triblock copolymers and their characterization a) $M_n$ calculated form $^1$H NMR. b) $Đ_M$ obtained from GPC. c) $M_n$ obtained from GPC, calculated against PS standards

| Example Triblock | $M_n$ [g.mol$^{-1}$] | $Đ_M$ [b] | Synthetic route | Ref |
|---|---|---|---|---|
| PDMAEMA$_8$-*b*-PLMA$_{39}$-*b*-POEGMA$_8$ | 15600[a] | 1.19 | Sequential RAFT | [27] |
| PEO$_{120}$-*b*-PHEMA$_{11}$-*b*-PtBA$_{46}$ | 17600[a] | 1.30 | Sequential ATRP | [28] |
| PS$_{51}$-*b*-PB$_{28}$-*b*-PtBMA$_{21}$ | 104000[a] | 1.07 | Sequential AP | [29] |
| PEO$_{42}$-*b*-PAGE$_{15}$-*b*-PtBGE$_{12}$ | 3400[a] | 1.07 | Sequential AROP | [30] |
| PODFOx$_{20}$-*b*-PEPOx$_{20}$-*b*-PEtOx$_{40}$ | 7990[c] | 1.12 | Sequential CROP | [31] |
| PE$_{20}$-*b*-PEO$_{20}$-*b*-PCL$_{10}$ | 2540[a] | 1.23 | ROP | [32] |
| PEO$_{44}$-*b*-PEtOx$_{263}$-*b*-PCL$_{175}$ | 46600[a] | 1.31 | CROP + ROP | [33] |
| PEO$_{45}$-*b*-PCL$_{103}$-*b*-PMOXA$_4$ | 14000[a] | 1.14 | ROP + CROP | [34] |
| PEO$_{45}$-*b*-PDMS$_{40}$-*b*-PMOXA$_{67}$ | 13070[a] | N/A | AROP + CROP | [35] |
| PEEP$_{135}$-*b*-PCL$_{50}$-*b*-PDMAEMA$_{118}$ | 44900[a] | 1.31 | AROP + ROP + ATRP | [36] |
| PEO$_{45}$-*b*-PMCL$_{47}$-*b*-PDMAEMA$_{31}$ | 12890[a] | 1.25 | ROP + ATRP | [37] |
| PEO$_{30}$-*b*-PS$_{90}$-*b*-PCL$_{62}$ | 19600[a] | 1.09 | ATRP + ROP + Click | [38] |

There are two main approaches when choosing the best technique to achieve the desired ABC polymer. In the sequential approach, the same polymerization technique is used to polymerize the monomers one after the other. Once a monomer is fully consumed, the polymerization continues with the next one and an appropriate initiator in the suitable conditions. The second approach combines different polymerization techniques, which means that intermediate products need to be purified and sometimes end-groups are modified to serve as a precursor for the next step.

We will now go through the sequential approach presenting various polymerization techniques with examples and then cover the second approach with different polymerization techniques.

### 1.1.1 Sequential polymerization

**Sequential RAFT** - Reversible addition-fragmentation chain transfer (RAFT)[39] polymerization has been widely used for the synthesis of triblock copolymers with various architectures.[40,41] This polymerization is advantageous due to a large number of available vinylic monomers like (meth)acrylates, (meth)acrylamides, acrylonitrile, styrene, butadiene, vinyl acetate and N-vinylpyrrolidone. Moreover, RAFT is very versatile as it can be performed in many solvents, including water, and its conditions are compatible with many functional groups. Nevertheless, the synthesis of a suitable initiator can be challenging, and this radical polymerization is controlled but not completely living due to the probability of chain recombination followed by a decrease in active chain ends. This means that the intermediate polymers need to be purified after each step, which then require a reinitiation to synthetize the next block. By using sequential RAFT, Skandalis and Pispas et al.[27] synthetized a series of poly[2-(dimethylamino)ethyl methacrylate]-*block*-poly(lauryl methacrylate)-*block*-poly(oligo

ethylene glycol)methacrylate (PDMAEMA-*b*-PLMA-*b*-POEGMA) polymers (Figure 1). In the first step, they polymerized DMAEMA in 1,4-dioxane using azobisisobutyronitrile (AIBN) as initiator and 4-cyano-4-[(dodecylsulfanylthiocarbonyl) sulfanyl]pentanoic acid as chain transfer agent (CTA). The resulting PDMAEMA homopolymer was then used as the macro-CTA for the addition of LMA under the same conditions. This yielded the AB polymer which served as the macro-CTA for polymerization of OEGMA under similar conditions. Methyl iodide was then used for quaternization of the PDMAEMA block to transform the ABC polymer into an amphiphilic ABC electrolyte.

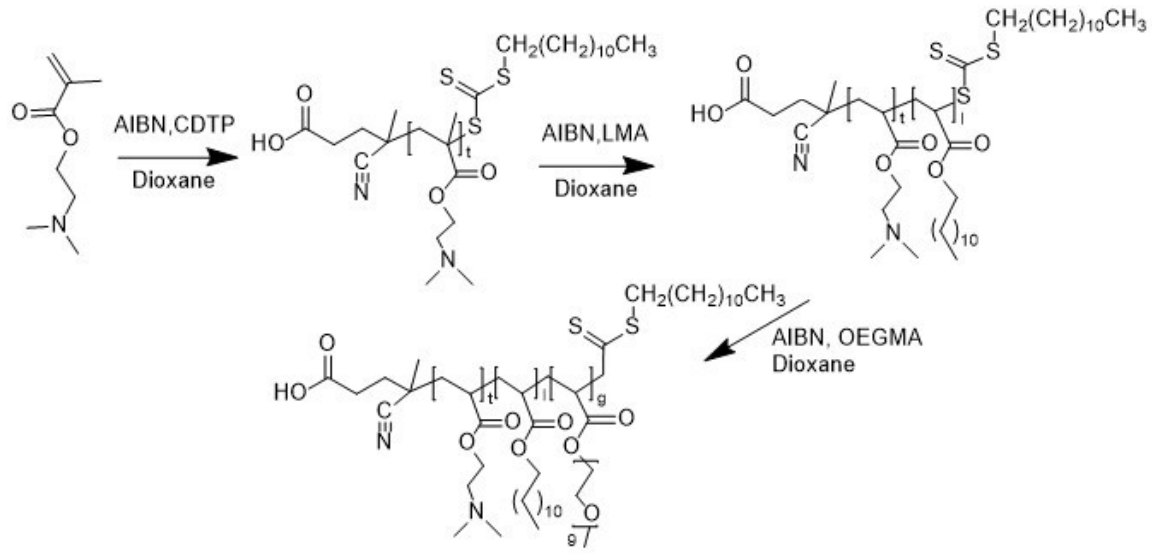


**Figure 1.** Schematic representation of the synthesis of PDMAEMA-*b*-PLMA-*b*-POEGMA by sequential RAFT.POEGMA).[27]

**Sequential ATRP** – Atom transfer radical polymerization (ATRP)[42] is, like RAFT, a controlled radical polymerization and gives access to a wide selection of vinylic monomers. A range of styrenes, (meth)acrylates, (meth)acrylamides and acrylonitrile can be polymerized, and ATRP can be conducted in many solvents including water.[43] However, this polymerization requires a metal catalyst, the most versatile and successful one is Cu(I).[44] But its toxicity might limit potential biomedical applications of polymers synthetized via ATRP, although solutions for

this problem have been presented.[45] Being a living polymerisation, sequential ATRP was used to synthesize ABC polymers. For example, Jin et al[28] synthetized poly(ethylene oxide)-*block*-poly(2-hydroxyethyl methacrylate)-*block*-poly(*tert*-butyl acrylate) (PEO-*b*-PHEMA-*b*-P*t*BA) through a two-step ATRP of HEMA and *t*BA by using PEO-Br as a macroinitiator (Figure 2). The first step involving HEMA was done in methanol with CuBr/bipyridin as a catalyst. The last step with *t*BA was performed in dimethylformamide (DMF) to cope with the solubility of the copolymers, again in the presence of CuBr as catalyst but now ligated with pentamethyldiethylenetriamine (PMDETA). Azide groups were then introduced to the PHEMA blocks by reaction of OH side groups with 2-bromoisobutyryl bromide followed by sodium azide. Click reaction between the azido-modifed PHEMA blocks and dialkynetrithiocarbonate yielded reactive micelles with cross-linked cores and P*t*BA/PEO corona.

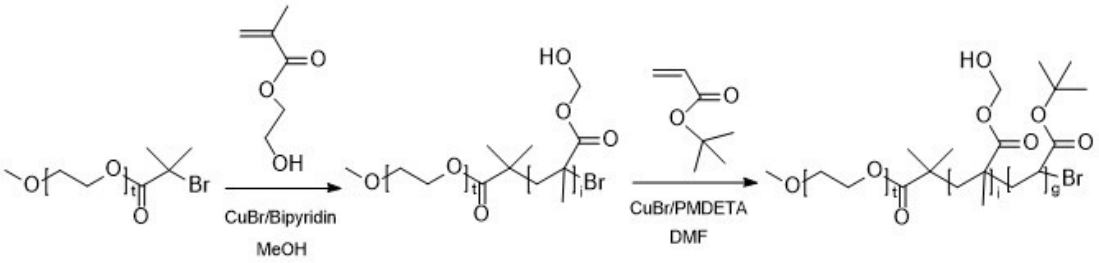


**Figure 2.** Schematic representation of the synthesis of PEO-*b*-PHEMA-*b*-PtBA.[28]

**Sequential AP** – Anionic polymerization (AP)[46] is another important living polymerization for polymers obtained from vinyl monomers. This technique is less versatile than RAFT and ATRP and requires monomers with substituents that stabilize the negative charge through charge delocalization, such as styrene, dienes, vinyl pyridine and vinyl epoxide. Müller and co-workers[29] used sequential AP to synthetize a series of polystyrene-*block*-polybutadiene-*block*-poly(*tert*-butyl methacrylate) (PS-*b*-PB-*b*-P*t*BMA) triblock copolymers (Figure 3). Sec-butyl lithium (sec-BuLi) and styrene were first mixed in THF. Once the polymerization of styrene was complete, 1,3-butadiene was added. The resulting PS-*b*-PB diblock copolymer was mixed

with 1,1-diphenyl-ethylene (DPE) to produce the precursor for *t*BMA polymerization. Degassed methanol was then added to terminate the polymerization of *t*BMA. The bulk morphologies of those ABC polymers were then thoroughly studied to map their bulk phase behaviour.

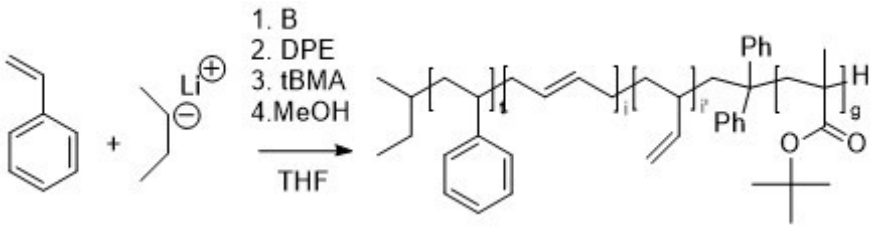


**Figure 3.** Schematic representation of the synthesis of PS-*b*-PB-*b*-PtBMA via sequential AP.[29]

**Sequential AROP** – Anionic ring-opening polymerization (AROP)[47,48] is an important polymerization technique for producing polyesters, polycarbonates, polyamides, polyurethanes and polyphosphates in a living fashion. Compared to RAFT and ATRP, AROP is very sensitive to impurities and cannot be performed in protic solvents. Amongst others, Barthel et al.[30] synthetized poly(ethylene oxide)-*block*-poly(allyl glycidyl ether)-*block*-poly(*tert*-butyl glycidyl ether) (PEO-*b*-PAGE-*b*-P*t*BGE) using sequential AROP (Figure 4). A PEO macroinitiator with terminal OH group was activated using sodium hydride, and the sequential polymerization of AGE and *t*BGE yielded ABC polymer. The middle block, PAGE, was then additionally modified by post-polymerization addition of 2,3,4,6-tetra-O-acetyl-1-thio-β-D-galactopyranose via thiol-ene chemistry, resulting in PEO-*b*-$PAGE_{Gal}$-*b*-P*t*BGE. This step was done to further modify the weight fraction of the hydrophobic parts (PAGE, P*t*BGE) and obtain new micellar morphologies.

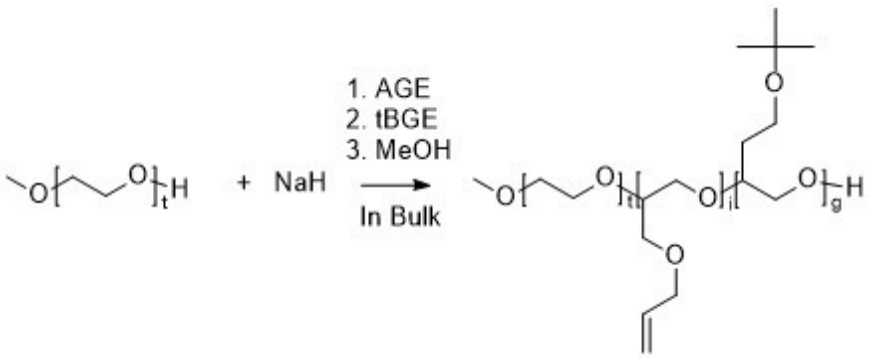


**Figure 4.** Schematic representation of the synthesis of PEO-*b*-PAGE-*b*-PtBGE via sequential AROP.[30]

**Sequential CROP** – Cationic ring-opening polymerization (CROP)[47] enables to polymerize different monomers including cyclic amines and cyclic ethers. It is notably used to produce polyoxazolines.[49] Like AROP, CROP is very sensitive to impurities and limited to specific solvents like acetonitrile, chlorobenzene and nitromethane. Through the sequential addition method, Hoogenboom et al.[50] prepared a library of 30 triblock copolymers from 2-methyl-, 2-ethyl-, 2-nonyl-, and 2-phenyl-2-oxazoline. Following this development, Kempe et al.[31] designed new amphiphilic triblock copoly(2-oxazoline)s containing a fluorinated segment. Starting with methyl tosylate as an initiator, 2-(2,6-diflurophenyl)-2-oxazoline (ODFOx), 2-(1-ethylheptyl)-2-oxazoline (EPOx) and 2-ethyl-2-oxazoline (EtOz) were added sequentially to obtain a series of triblock copolymers PODFOx-*b*-PEPOx-*b*-PEtOz through microwave polymerization performed in nitromethane (Figure 5). This ABC triblock copolymer self-assembled in water into vesicular and aggregated cylindrical micellar structures.[51]

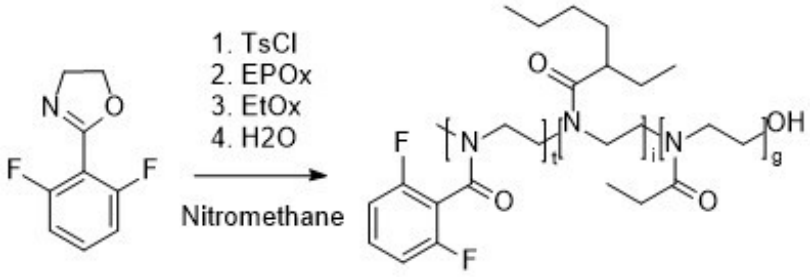


**Figure 5.** Schematic representation of the synthesis of PODFOx-*b*-PEPOx-*b*-PEtOx via sequential CROP.[31]

All of these examples show that sequential polymerization is a powerful tool to obtain ABC polymers. The Luxenhofer group even managed to push the limits of living nucleophilic ROP of N-substituted glycine N-carboxyanhydrides (NCAs) towards polypeptoids by performing 10 chain extensions.[52] However, side reactions like chain termination and chain transfer may hinder the controlled synthesis of well-defined and longer triblock copolymers via this method. Using commercially available macroinitiators reduces this problem as less chain extensions need to be performed.

### 1.1.2 Using macroinitiators or click reactions

**Commercially available macroinitiators.** Synthesizing ABC polymers can become synthetically less demanding if a commercially available starting block (like poly(ethylene oxide), polystyrene or polyethylene) can be used as a macroinitiator. For example, PEO is a frequent choice because of its advantageous properties (hydrophilic, non-inflammatory, biocompatible) and broad commercial availability.[53] Sun et al. used a PEO macroinitiator for a ROP of NCAs towards polypeptides, namely PEO-*b*-$P_L$Lys-*b*-$P_L$Glu ($P_L$Lys = poly(L)lysine, $P_L$Glu = poly(L)glutamic acid).[54] Both, the lysine and glutamic acid units were protected during the polymerization. The final ABC polymer self-assembled in acidic water (pH 2.2, 0.5 M NaCl) into vesicles with a symmetric (ABC-CBA) membrane due to strong interactions of the helical protonated $P_L$Glu chains.[54]

Wang et al.[32] synthetized a series of polyethylene-*block*-poly(ethylene oxide)-*block*-polycaprolactone (PE-*b*-PEO-*b*-PCL) polymers. Using commercially available AB (PE-*b*-PEO) diblock copolymer as a macroinitiator, the synthesis of the ABC polymer required only ROP of ε-caprolactone (ε-CL) catalysed by stannous(II) octoate ($Sn(Oct)_2$) in DMF. This $Sn(Oct)_2$-catalyzed ROP of ε-CL is called coordination-insertion ROP and is the main technique used to

obtain polycaprolactone. However, in most cases, a tailor-made macroinitiator is required for the corresponding polymerisation of the desired monomer, especially if different polymerization techniques are used.

**Clicks reactions to combine AB and C.** ABC polymers can also be engineered via covalent binding of AB diblock copolymer and C homopolymer. Such approach requires pre/post polymerization modification reactions to obtain the corresponding building blocks with required functional end-groups. For example, He et al.[38] used a combination of ATRP, coordination-insertion ROP and click chemistry to obtain poly(ethylene oxide)-*block*-polystyrene-*block*-polycaprolactone (PEO-*b*-PS-*b*-PCL). The diblock precursor PEO-*b*-PS containing terminal Br group was prepared via ATRP of styrene on a PEO macroinitiator, which was obtained by esterification of PEO by 2-bromo-2-methylpropionyl bromide. The terminal bromine group on PEO-*b*-PS was then transformed in an azide group by nucleophilic substitution with sodium azide. The third block, propargyl-terminated PCL, was prepared via ROP of ε-caprolactone initiated by propargyl alcohol in the presence of $Sn(Oct)_2$. The final ABC polymer, PEO-*b*-PS-*b*-PCL, was then synthetized by the copper catalysed azide alkyne click (CuAAC) reaction of those two precursors in the presence of a CuBr/PMDETA catalytic system in DMF (Figure 6).

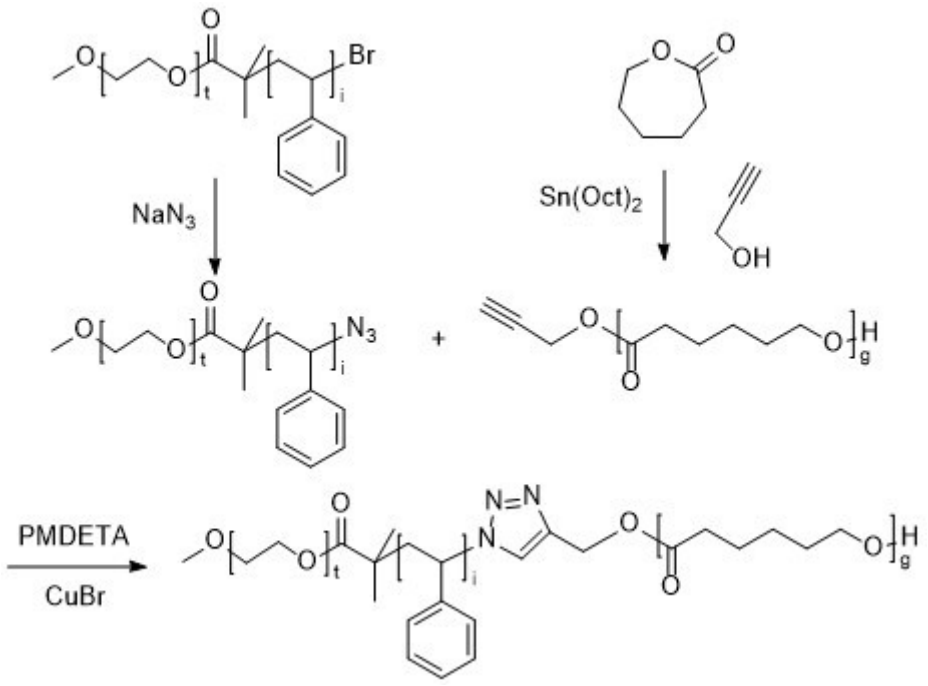


**Figure 6.** Schematic representation of the synthesis of PEO-*b*-PS-*b*-PCL.[38]

### 1.1.3 Combination of different polymerization techniques

This synthetic path involves several different polymerization techniques to obtain the desired ABC polymer. For example, Petrova et al.[33] endcapped α-methoxy-ω-hydroxy-poly(ethylene oxide) with p-toluenesulfonyl chloride (TsCl) to use it as a macroinitiator for the CROP of 2-ethyl-2-oxazoline (EtOz) in acetonitrile. The latter step was terminated by a KOH/methanolic solution to introduce hydroxyl units as chain ends. The resulting AB diblock copolymer was then used as a macroinitiator for the ROP of ε-CL yielding PEO-*b*-PEtOz-*b*-PCL. In this case, a carefully chosen termination step introduced the terminal functionality on the AB polymer needed for the next polymerization step. However, when the AB polymer is not readily functional, it needs to be modified to enable the polymerization of the C block. One example where this strategy was applied, is the synthesis of poly(ethylene oxide)-*block*-poly(dimethylsiloxane)-*block*-poly(2-methyloxazoline) (PEO-*b*-PDMS-*b*-PMOXA).[35,55] In the first step, PEO-*b*-PDMS is synthetized via AROP using PEO as a macroinitiator. In order to

polymerize 2-methyl-2-oxazoline (MOXA) via CROP on this resulting AB polymer, PEO-*b*-PDMS was ω-functionalized with trifluoromethanesulfonic anhydride (triflate). The resulting PEO-*b*-PDMS-*b*-PMOXA self-assembled into polymersomes with asymmetric membrane that induced a directed insertion of transmembrane proteins. A similar principle was also used for the synthesis of poly(ethylene oxide)-*block*-polycaprolactone-*block*-(poly-2-methyl-2-oxazoline) (PEO-*b*-PCL-*b*-PMOXA).[56,34] PEO-*b*-PCL was synthesized via $Sn(Oct)_2$-catalyzed ROP of ε-CL using PEO as a macroinitiator. In a similar fashion as for PEO-*b*-PDMS, to polymerize MOXA via microwave-assisted CROP on this resulting AB polymer, PEO-*b*-PCL was ω-functionalized with TsCl (Figure 7). The obtained PEO-*b*-PCL-*b*-PMOXA self-assembled into different microscale structures, notably polymersomes with asymmetric membrane.

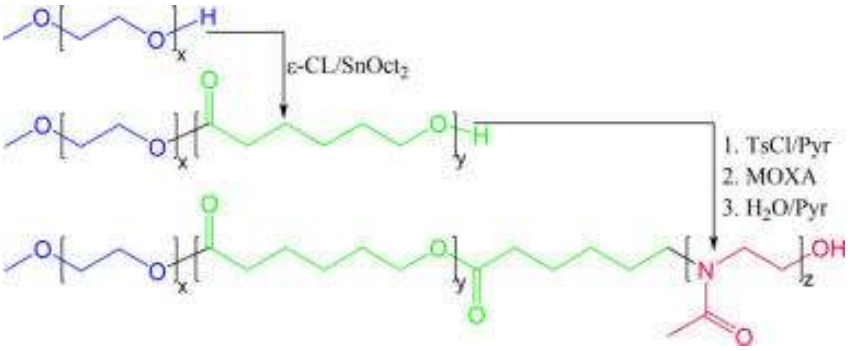


**Figure 7.** Schematic representation of the synthesis of PEO-*b*-PCL-*b*-PMOXA.[34]

Using several polymerization techniques grants access to a wider pool of monomers and functionalities. This increased versatility is very helpful in engineering ABC polymers. For example, Bian et al.[36] synthetized poly(ethylethylene phosphate)-*block*-polycaprolactone-*block*-poly[2-(dimethylamino)ethyl methacrylate] (PEEP-*b*-PCL-*b*-PDMAEMA) via a combination of coordination-insertion ROP and ATRP. In a similar way, Matter et al.[37] synthetized poly(ethylene glycol)-*block*-poly(γ-methyl-ε-caprolactone)-*block*-poly[2-(dimethylamino)ethyl methacrylate] (PEO-*b*-PMCL-*b*-PDMAEMA) via a combination of coordination-insertion ROP and ATRP yielding ABC polymers.

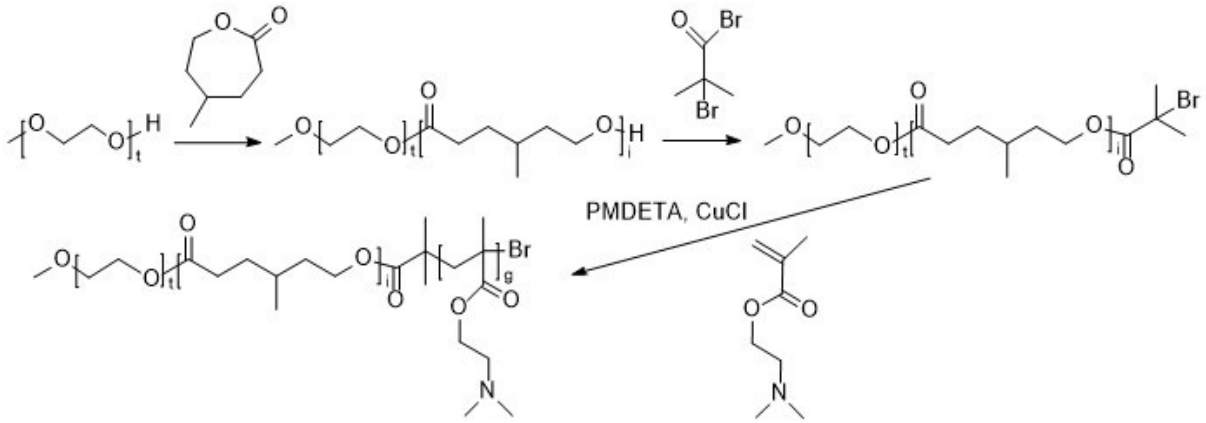


**Figure 8.** Schematic representation of the synthesis of PEO-*b*-PMCL-*b*-PDMAEMA.[37]

In conclusion, to engineer AB or ABC polymers, there is a wide range of polymerization techniques available. Each system requires its own specific combination of reaction conditions. The large effort in synthesis pays off in their intriguing self-assembly behaviour, which we will discuss next.

## 1.2 Self-assembly of linear ABPs

Due to the versatile design of linear ABPs allowing for fine tuning of the morphology and properties of their self-assemblies, structures assembled from ABPs open new opportunities in many fields like biomedical applications. In the next section, the principal methods to characterize self-assemblies and the principles behind their self-assembly is reviewed.

### 1.2.1 Characterisation methods of self-assembled structures

The morphology and size of nanoscopic (< 1 µm) self-assemblies can be characterized by various scattering methods. Dynamic light scattering (DLS) can be conducted to assess hydrodynamic radius ($R_h$) and size distribution while static light scattering (SLS) provide weight-average molecular weight ($M_w$) and radius of gyration ($R_g$). By combining DLS and SLS, it is possible to determine the structure of the self-assemblies.[57-58] Small angle X-ray/neutron scattering (SANS/SAXS) can also be used to study the morphology of the self-assemblies.[59] Transmission electron microscopy (TEM) and Cryogenic-TEM (Cryo-TEM) are also powerful techniques to observe these structures with fine details thanks to its high resolution (1 nm) and determine their morphology. In particular, Cryo-TEM by freezing the self-assemblies allows their visualisation in their native environment without any staining and thus provides additional information like membrane thickness.[60-61]

Compared to nanoscopic structures, microscopic structures (> 1 µm) due to their larger size can also be characterized by optical microscopy. Light/fluorescence/confocal scanning microscopy can be used to visualize those structures. When matching the size of cells, microscopic structures can be analysed by flow cytometry which determine the size, granularity and fluorescent properties.[62] Both micro- and nanoscopic structures can be characterized by fluorescence correlation spectroscopy (FCS). By labelling the self-assemblies

with a fluorescent dye, FCS can be used to provide data on lateral diffusion coefficients and molecular organisation in membranes.[61,63]

### 1.2.2 Self-assembly techniques in solution

There are many different procedures available to obtain self-assembled structures from block copolymers. But they are not all equal. By using various self-assembly methods with different approach, it can potentially lead to different self-assembled structures using the same block copolymer. Direct dissolution is used when the block copolymer is water-soluble. By adding the block copolymer at a concentration above its CMC, it induces its self-assembly into micelles.[64] When the block copolymer is not water-soluble, solvent switch or film rehydration can be used. In the solvent switch method, the block copolymer is first dissolved in an organic solvent miscible with water, like THF. Water is then added dropwise to the aqueous solution. The organic solvent is then removed by dialysis against water. One disadvantage of this method is that traces of organic solvent may linger in the system and be incompatible with biomedical applications.[65] This can be avoided by using the film rehydration method in which the block copolymer is first dissolved in a suitable volatile organic solvent which is then evaporated under reduced pressure to create a thin polymeric film. This film is then rehydrated with an aqueous buffer and generate self-assemblies after an appropriate period of stirring.[34, 66-67]

### 1.2.3 Self-assembly of linear AB and ABC copolymers

ABC polymers offer unique opportunities for the development of sophisticated structures which cannot be accessed with conventional AB polymers. With respect to the solvent in which self-assembly is performed, ABC polymers can contain one soluble block (terminal A/C or middle B) and two soluble blocks (adjacent blocks A/C and B, or terminal blocks A and C).

In this section, we focus on self-assembly of ABC polymers with two soluble A and C blocks compared to the self-assembly of AB polymers.

ABC polymers with A and C soluble blocks are advantageous for the production of self-assembly structures with domains in their corona, commonly referred to as "patchy" structures. Triblock copolymers of this type can self-assemble into structures with mixed, patchy, and Janus corona[68-77] with diverse potential applications ranging from materials science to biomedicine.[78-79] There are already a number of polymers available, but we will focus on systematically investigated PEO-*b*-PCL-*b*-PMOXA polymers, where PEO and PMOXA are water-soluble, and PCL is a semicrystalline hydrophobic block.[20, 34] Their aqueous self-assembly was investigated depending on PCL and PMOXA block lengths (PEO length was constant) and the method of preparation.

Similar to AB polymers, self-assembly of such ABC polymers was investigated depending on the hydrophilic weight fraction *f*:

$$f = \frac{M_{hydrophilic}}{M_{hydrophilic} + M_{hydrophobi}} = \frac{M_A + M_C}{M_A + M_C + M_B} \qquad (1)$$

In the case of AB polymers with fixed A block length, *f* can be varied through the change in the length of the B block, and a typical self-assembly trend is polymersomes – elongated micelles (worms) – micelles with increasing *f*. Such a tendency was directly reported for PEO-*b*-PMCL,[80] PEO-*b*-PB,[12-13], PEO-*b*-PDEAMA[81], PMOXA-*b*-PDMS,[67] PEO-*b*-PS,[82] PG-*b*-PBO[66] and PAA-*b*-PSS (PAA = poly(acrylic acid)).[14] In the case of ABC polymers with fixed A block length *f* can be varied through the change in B or C block length, and the accessible structures are much more diverse compared to the ones formed by AB polymers. For PEO-*b*-PCL-*b*-PMOXA, the morphology changes in the row irregularly shaped particles (Figure 9.C) – polymersomes

(Figure 9.D) – spherical particles (Figure 9.B) with an increase in *f*, when *f* is varied through the length of B (PCL) (Figure 9.A, red and blue dashed lines). When *f* is varied through the length of the C (PMOXA) block for polymers with B around 60 to 130 units, the morphology of the assemblies changes in the row spherical particles (Figure 9.B) – polymersomes (Figure 9.D) – cloud-like aggregates (Figure 9.E) with an increase in *f*. The number of the self-assembled structures formed by ABC polymers can be increased even further by using different preparation methods.

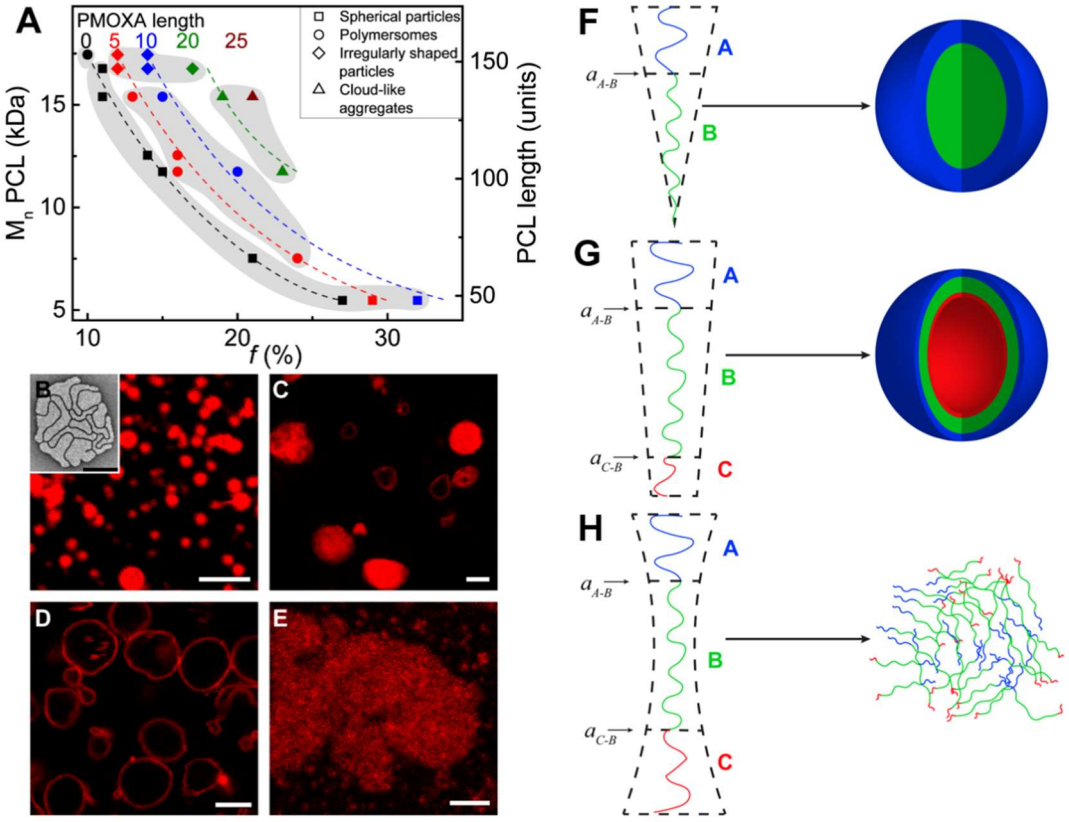


**Figure 9**. (A) Morphology diagram showing structures formed by PEO-*b*-PCL and PEO-*b*-PCL-*b*-PMOXA in aqueous solution as a function of the molecular composition. Points of each color correspond to polymers with a certain PMOXA length. Points of each shape correspond to a certain morphology: spherical particles (squares), polymersomes (circles), irregularly shaped particles (diamonds), cloud-like aggregates (triangles). The gray areas point out regions of the same morphology. Representative LSM images of (B) spherical particles, (C) irregularly shaped particles, (D) polymersomes, (E) cloud-like aggregates. Structures were stained with Bodipy 630/650. Scale bars are 5 µm. B inset is a representative TEM image of negatively stained spherical particles; scale bar is 200 nm. Illustration of

the packing geometry of polymers with fixed A and B (~60 – 130 units) but different C block lengths: (F) AB, (G) ABC with short C block, and (H) ABC with long C block. Adapted from ref.[20]

Formation of the observed self-assembled structures can be explained using the packing geometry model (Figure 9.F-H). In the case of AB polymers, packing geometry is defined by packing parameter *p*:[83]

$$p = \frac{v_B}{a_{A-B} \cdot l_B} \qquad (2)$$

where $a_{A-B}$ is the optimal area of the hydrophilic block A at the interface A–B, $v_B$ and $l_B$ are the volume and critical length of the hydrophobic block B, respectively. AB polymers self-assemble into spherical particles, and therefore their packing geometry corresponds to a cone (Figure 9.F). Adding the C block presumably introduces the area $a_{C-B}$ at the C–B interface (Figure 9.G), because PEO and PMOXA polymers are immiscible in aqueous solution.[84-85] In the discussed case, the A block is longer than the C block, which results in a packing geometry of ABC molecules corresponding to a cylinder slightly truncated at the C side. The resulting polymersomes now consist of an inner surface formed by a shorter C block, and an outer surface formed by a longer A block. Further increase in C block length results in stronger repulsive forces within the hydrophilic corona which compete with attractive hydrophobic forces between B chains. In this case, the packing geometry of ABC molecules approaches the double cone shape resulting in cloud-like aggregates (Figure 9.H).

### 1.2.4 Asymmetric polymersomes from ABC polymers

The most common application of ABC polymers with A and C soluble blocks is probably the formation of polymersomes with an asymmetric membrane. In principle, there are three possibilities of polymersome membrane composition: A block outside, C block outside or A

and C blocks form a patchy or mixed membrane. Typically, a longer block is located on the outer surface of polymersomes due to a larger radius of the outer curvature compared to the inner curvature. Polymersomes with asymmetric membrane have been reported for PEO-*b*-PDMS-*b*-PMOXA,[55, 86] PAA-*b*-PS-*b*-PVP,[87] PEO-*b*-PCL-*b*-PAA,[88] glycosylated PEO-*b*-PB,[89] PEO-*b*-PCL-*b*-PDEAEMA,[90] PMPC-*b*-PDPA-*b*-PDMEAEMA,[91] PEO-*b*-PMA-*b*-PAA (PMA = poly(methyl acrylate)),[92] and PEO-*b*-PCL-*b*-PMOXA.[34] In the case of charged blocks, such as PAA, PDMAEMA, and PVP, asymmetry was proven by measuring ζ-potential of the structures in solution at different pH, because (de)protonation influenced the surface charge.[87-88, 92] However, this method does not exclude the possibility of the presence of the second hydrophilic block on the outer polymersome surface and cannot be applied when both blocks are neutral. Asymmetry of polymersomes formed by glycosylated PEO-*b*-PB was proven by interaction of gold nanoparticles with glucose detected by Raman spectroscopy. The absence of PEO on the outside was suggested by the absence of interactions between the PEO block and the glycosylated PB block revealed by 2D-$^{1}$H-NOESY NMR. For PEO-*b*-PDMS-*b*-PMOXA with a fluorescently labelled PMOXA block (longer than PEO), its presence outside was shown by quenching the fluorescence of the attached dye by an externally added quencher. To determine asymmetry of PEO-*b*-PCL-*b*-PMOXA polymersomes, two independent approaches were used. In the first approach, ABC polymersomes contained terminal functional groups either on A or C side which could couple with a reactive fluorescent dye. The reaction between the A block and a dye occurred, indicating the presence of the A block outside. The absence of the reaction between C blocks and a dye suggested the absence of C chain ends on the outside. Bicinhoninic acid assay (BCA)[93] could selectively react with PMOXA, which was additional prove of the asymmetry. Another strategy to create polymersomes with an asymmetric membrane was shown by Schrage et al.[94] The authors used two diblock

copolymers, PB-*b*-PCsMA (PCsMA = poly(cesium methacrylate)) and PS-*b*-P4VP (P4VP = poly(1-methyl-4-vinylpyridinium iodide)), which self-assembled in THF due to electrostatic interactions between the PCsMA and P4VP blocks. In this case the corona blocks, i.e. PS and PB, presumably segregated on different sides of the polymersome membrane due to their strong incompatibility and different space requirements.

ABC polymersomes with an asymmetric membrane allow for more flexibility in the design of sophisticated systems compared to conventional symmetric membranes. Depending on the nature of A and C blocks, the inner and outer surfaces can possess different chemical and physical properties for selective catalysis, responsiveness to certain stimuli, immobilization of specific molecules, etc. For example, an ABC membrane can induce the directed insertion of transmembrane proteins as it was shown for the insertion of histidine-tagged Aquaporin 0 into polymersomes made from PEO-*b*-PDMS-*b*-PMOXA.[55] The formation of an ABC membrane (i.e., PEO outside) induced an insertion with 72 % of His-tags on the outside. A CBA membrane on the other hand (i.e., PMOXA outside), induced the reversed orientation with 19 % of His-tags outside. No preferred orientation (47 % of the His-tags outside) was recorded for polymersomes made from the symmetric PMOXA-*b*-PDMS-*b*-PMOXA block copolymer. In addition to preferential orientation, polymersomes from ABC polymers enhance the delivery of some drugs.[90, 95-96]

## 1.3 Motivation

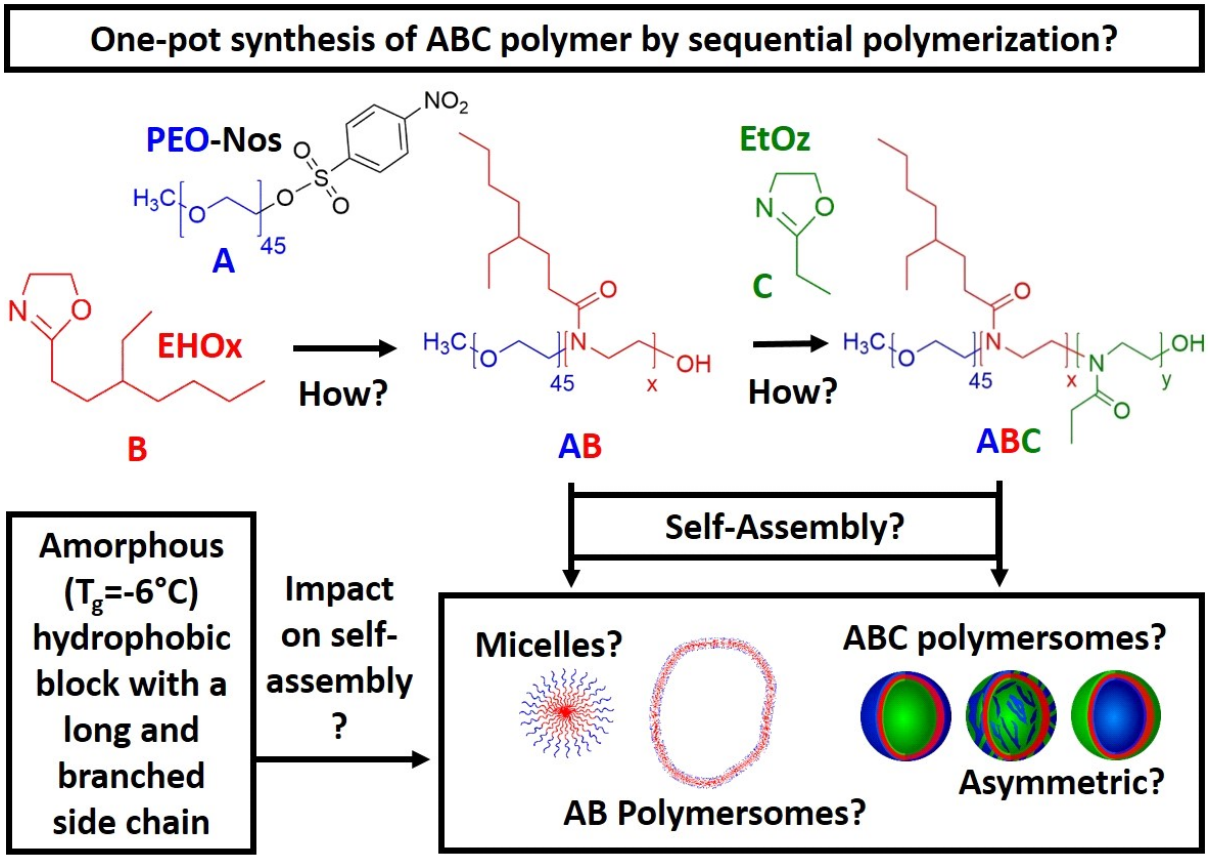


**Figure 10.** Graphical abstract of the aim of this thesis.

*This PhD work revolves around designing a novel biocompatible amphiphilic ABC triblock copolymer with a facile synthesis using a poly(2-oxazoline) with a long and branched side chain as a hydrophobic block. By comprehensively studying its self-assembly, the aim is to create a reproducible platform of diverse self-assemblies with a focus on asymmetric polymersomes for the directed-insertion of transmembrane proteins as a future application.*

**How does a B hydrophobic block with a long and branched side chain impact the self-assembly of an AB polymer? Is there any novel interactions during its self-assembly?**

Despite AB polymers being the focus of numerous studies, there are only few works investigating AB polymers including a B hydrophobic block with a long and branched side

chain. This could generate additional hydrophobic-hydrophobic interactions during the self-assembly and lead to more complex morphologies. An AB polymer was designed accordingly to be used as a model for this study. We used a novel hydrophobic poly(2-oxazoline) with a side chain of nine carbon atoms including an ethyl branching, namely poly(2-(3-ethylheptyl)-2-oxazoline (PEHOx). With a $T_g$ of -6°C, PEHOx is thus perfectly suitable as a hydrophobic block in an ABP. Its polymerization on a PEO macroinitiator was optimized to create a library of PEO-*b*-PEHOx with an extensive spectrum of different *f.* This allowed us to carry out a complete study of its self-assembly comparing two different techniques: film rehydration and solvent switch (**Chapter 2**).

**Can we create an ABC polymer by a controlled one-pot synthesis which self-assemble successfully and accurately into asymmetric polymersomes?**

One of the core characteristic of biological membranes is its asymmetry which is essential for the orientation of inserted membrane proteins like proton pumps which are vectorial molecules. To mimic this feature, a direct strategy is to obtain asymmetric polymersomes by self-assembly of ABC polymers with A and C chemically distinct hydrophilic blocks of different lengths. Due to the complexity of the synthesis of such ABC polymers, only a few studies have been reported. To bridge that gap, we proposed a one-pot synthesis of an ABC polymer. Building upon our previous work on PEO-*b*-PEHOx, using microwave-assisted sequential polymerization, we created a comprehensive library of PEO-*b*-PEHOx-*b*-PEtOz with different PEHOx and PEtOz block lengths. Their self-assembly was studied in depth, notably the formed polymersomes. Using two independent methods, the surface composition of the polymersomes from the self-assembled ABC polymers was thoroughly characterized to determine if they are asymmetric. **(Chapter 3)**.

## 2. Efficient Synthesis and Complex Self-Assembly of the Amphiphilic PEO-*b*-PEHOx polymers into Multicompartment Micelles, Pseudo-Vesicles and Yolk/Shell Nanoparticles

Within this chapter, the synthesis and self-assembly of the AB polymers PEO-*b*-PEHOx is presented. First, by studying the kinetics of the polymerization of EHOx on a PEO macroinitiator under different conditions, the synthesis of PEO-*b*-PEHOx was optimised and a library of PEO-*b*-PEHOx was obtained with different block length of PEHOx. An in-depth study of their self-assembly by two methods was conducted. It lead to the discovery of various complex structures which showed the unique self-assembly behaviour of PEO-*b*-PEHOx and the potential of hydrophobic blocks with a long and branched side chain.

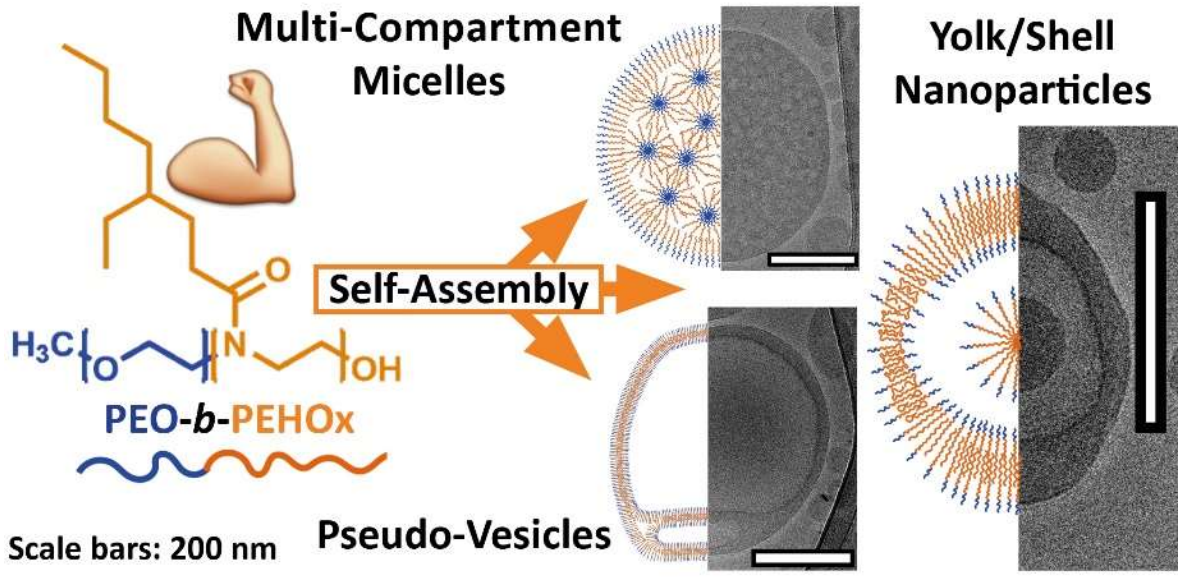


**Figure 11.** Graphical abstract of the complex Self-assembly of the amphiphilic PEO-*b*-PEHOx polymers into multicompartment micelles, pseudo-vesicles and yolk/shell nanoparticles

This study is published as **Davy Daubian**, Jens Gaitzsch and Wolfgang Meier. *Polymer Chemistry* (2020)**,** 11 (6), 1237-1248.

## 2.1 Introduction

In recent years, amphiphilic block copolymers have attracted a considerable amount of attention thanks to their ability to self-organize into various complex structures.[1, 11, 97] These structures formed by amphiphilic block copolymers can mimic complex structures found in nature (e.g. lipid bilayers) while exhibiting increased chemical and mechanical stability, which makes them interesting for different bio-inspired applications, like drug delivery or nanoreactors.[9, 98-103] Most investigated structures come from AB diblock copolymers (where A is an hydrophilic block and B is an hydrophobic block) or ABA triblock copolymers. Amphiphilic diblock copolymers have been the focus of numerous studies, like PSS-*b*-PAA,[14] PEO-*b*-PCL,[56] PEO-*b*-PMCL,[104] PEO-b-P(d)MCL,[105] or PEO-*b*-PDMS,[67], notably to form vesicles. Combining two different diblock copolymers AB and AC also leads to new exotic structures like multi-compartment micelles (MCMs)[106], vesicles with a patterned surface[7, 107] or Yolk/Shell nanoparticles.[108-109] Most of these studies use hydrophobic blocks with a short side chain to ensure mobility. There are only few works investigating AB diblock copolymers including a B block with a long side chain.[45, 110-111] This could lead to novel interactions during the self-assembly. The aim of this work is to shed some light on the self-assembly of such polymers and the AB diblock copolymer was designed accordingly.

Poly(2-oxazolines) have been extensively used to form amphiphilic block copolymers thanks to their biocompatibility and versatility.[49, 112-113] The water solubility of poly(2-oxazolines) can be precisely tailored by the length of the side chain as it becomes completely water insoluble with at least 4 carbons.[114] Moreover, its mechanical properties, notably its glass transition temperature ($T_g$) and crystallinity, can be modified significantly by branching its side chain on the right position.[115] Previously, Kempe et al. synthetized the first hydrophobic poly(2-

oxazoline) with a $T_g$ of -6°C, namely poly(2-(3-ethylheptyl)-2-oxazoline (PEHOx).[116] This polymer benefits from a purely hydrocarbon side chain of nine carbon atoms providing sufficient hydrophobicity and branching to supress crystallinity. PEHOx is thus perfectly suitable as a hydrophobic block in an amphiphilic block copolymer but has only been used so far to form polymer micelles to achieve a higher drug loading capacity.[117] The side chain of PEHOx with its ethyl branch and long length will generate additional hydrophobic-hydrophobic interactions. It will also prevent a compact order or strong entangling of the formed AB diblock copolymers in a membrane, potentially enabling more complex self-assembly structures. Combined with its backbone structure close to a peptide, these properties make PEHOx a compelling hydrophobic block to lead to new insights into self-assembled polymer nanoparticles.

In order to achieve a straightforward one-pot synthesis of our AB diblock copolymer, modified poly(ethylene oxide) (PEO) was used as a macroinitiator. A tosylated version has already been used as a macroinitiator for the polymerization of 2-oxazolines, but had significant disadvantages due to the low reactivity of tosylates.[118] We aimed to optimize this method by replacing tosylate with the more reactive nosylate.[119]

Herein, we report the one-pot synthesis of new poly(ethylene oxide)-*block*-poly(2-(3-ethylheptyl)-2-oxazoline (PEO-*b*-PEHOx) amphiphilic AB diblock copolymers using microwave-assisted polymerization of EHOx on a poly(ethylene oxide)-nosylate (PEO-Nos) macroinitiator. Using the obtained library of PEO-*b*-PEHOx, we then examined their thermal properties by differential scanning calorimetry (DSC) comparing it to the homopolymer PEHOx. Aqueous self-assembly of these diblock copolymers were examined by two different techniques: film rehydration and solvent switch. We studied the self-assemblies in depth by dynamic and static

light scattering (DLS/SLS), transmission electron microscopy (TEM) and cryogenic transmission electron microscopy (Cryo-TEM). The combined analysis proved the formation of a variety of potent self-assembly structures like multi-compartment micelles (MCMs) and pseudo-vesicles, amongst others. The new polymer was set to be a showcase example to elaborate which experiments are necessary to prove the existence of vesicles, notably the importance of Cryo-TEM insights into those complex structures.

## 2.2 Results and discussions part I: Synthesis of PEO-*b*-PEHOx

### 2.2.1 Choosing the right initiator

We started by selecting the best initiator and tested tosylated (Tos) and nosylated (Nos) PEO as macroinitiators for the synthesis of PEO-*b*-PEHOx diblock copolymers. Tosylated macroinitiators were already used for the polymerization of 2-oxazolines [34, 104, 120] but small molecule nosylates were shown to be advantageous over triflates and tosylates for polymerization of various 2-oxazolines.[119] Nosylates are more stable compared to triflates and result in faster initiation compared to tosylates. While PEO-Tos macroinitiator was commercially available, PEO-Nos was not reported previously and synthetized by adapting a procedure described for tosylation of PEO.[104] The reaction proceeded smoothly at 0 °C for 10 h resulting in 100% of nosylation of PEO. Purification of crude PEO-Nos via extraction in isopropanol and dialysis in acetonitrile resulted in a product of 96% purity (Figure 12). The residual 4% corresponded to non-nosylated PEO. Partial cleavage of the nosyl group during purification occurred because of its high reactivity and sensitivity towards protic solvents such as isopropanol and water traces in acetonitrile. Aprotic purification through precipitation in diethyl ether or using column chromatography were also conducted but proved to be ineffective as impurities were still present.

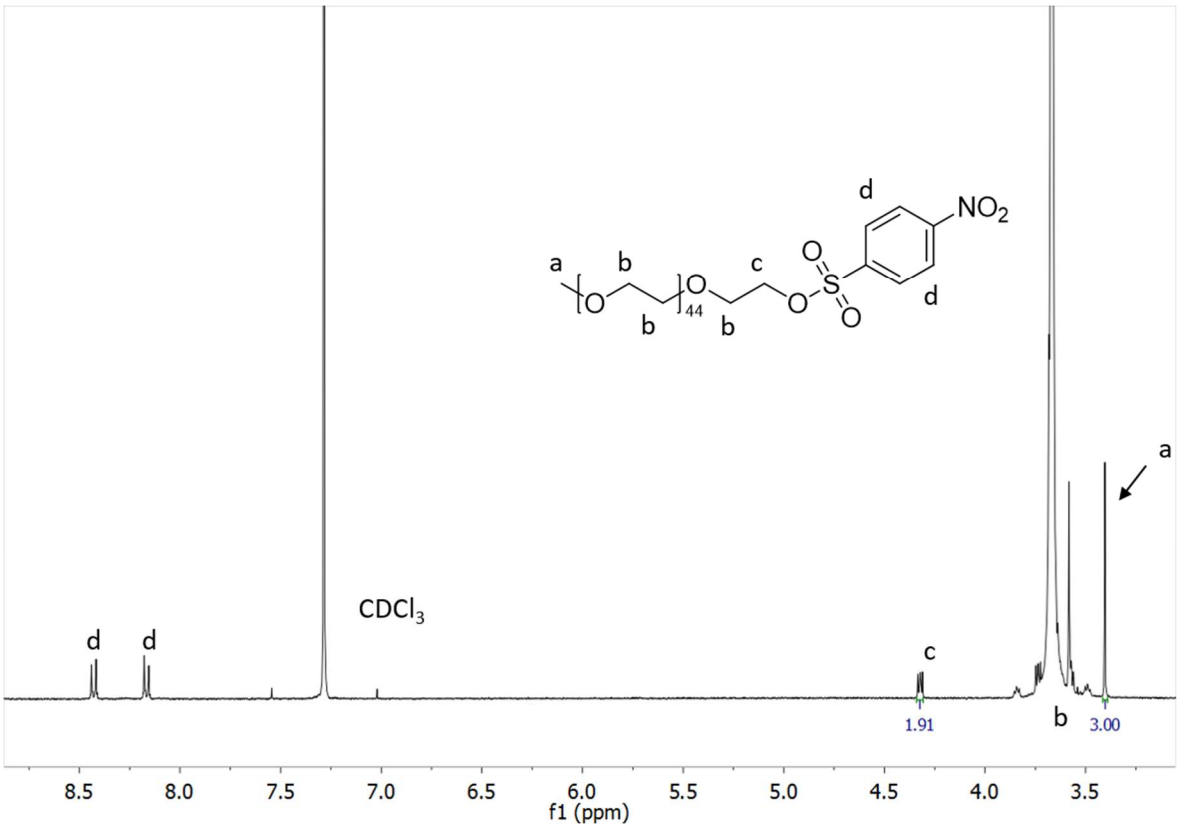


**Figure 12.** Representative $^{1}H$ NMR ($CDCl_3$) of PEO-Nos. Peak "a" is integrated as the reference to determine the integration of the peak "c" which should in value be equal to two if we had 100% nosylation. The difference between the theoretical value of 2 (100%) and the experimental integration of the peak "c" yield the nosylation ratio. Nosylation ratio (%) = 100 - ((2-1.91)/2)*100 = 96%

PEO-*b*-PEOHx polymers were synthesized via microwave-assisted polymerization of EHOx on a PEO macroinitiator (Figure 13). Using microwave-assisted polymerization, we were able to work with small volumes (as low as 0.5 mL), which was an advantage over conventional heating. Small volumes allowed for a kinetic study screening different parameters in triplicates while keeping the amount of reagents used to a bare minimum. It was especially advantageous considering that both the macroinitiator and monomer were self-synthetized. On top of that, the temperature was monitored precisely by the infrared sensor and kept constant by the microwave input. The synthesis was optimized by varying macroinitiator (PEO-Tos or PEO-Nos), solvent, and temperature.

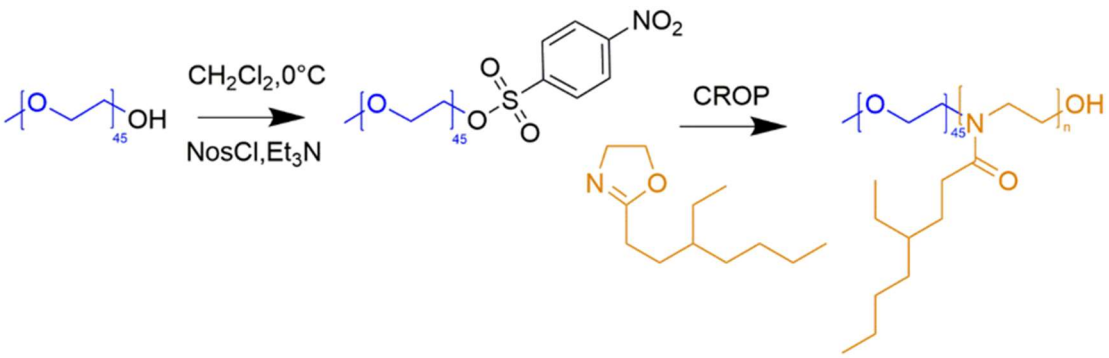


**Figure 13**. Schematic representation of the synthesis of poly (ethylene oxide)-nosylate followed by the synthesis of poly(ethylene oxide)-*b*-poly(2-(3-ethylheptyl)-2-oxazoline (PEO-*b*-PEHOx).

In line with previous reports, a PEO-Tos macroinitiator resulted in side reactions leading to the broadening of PEO-Tos elugram at various temperatures (Figure 14). PEO-Nos, on the other hand, did lead to polymerizations (Figure 15). Therefore, all further experiments were performed using PEO-Nos as a macroinitiator and keeping a constant ratio monomer-to-initiator of 100.

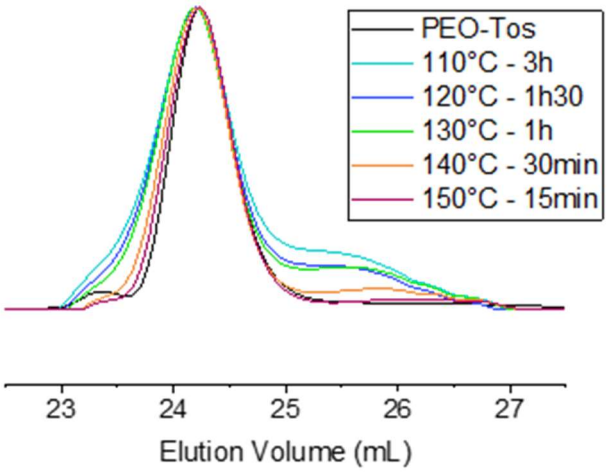


**Figure 14**. GPC traces ($CHCl_3$) of the microwave-assisted polymerization of EHOx on PEO-Tos in chlorobenzene at different temperatures. The monomer concentration was set to 1M and a monomer-to-initiator ratio of 100 was used. With increasing temperature, a shorter polymerization time was used to account for faster kinetics of the polymerization due the temperature increase.

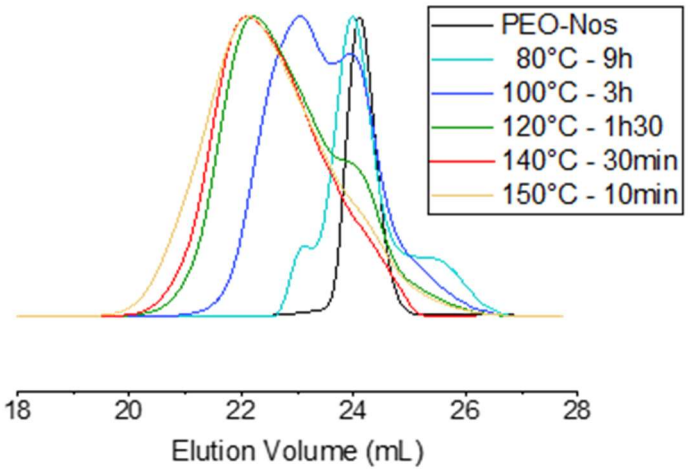


**Figure 15**. GPC traces ($CHCl_3$) of the microwave-assisted polymerization of EHOx on PEO-Nos in chlorobenzene at different temperatures. The monomer concentration was set to 1M and a monomer-to-initiator ratio of 100 was used. The different polymerization time at different temperature account for the decrease in reactivity with decreasing temperature.

### 2.2.2 Kinetics study: determining the right solvent and temperature

We then investigated three different solvents adequate for the CROP of 2-oxazolines: sulfolane, acetonitrile and chlorobenzene as they showed to solubilize the macroinitiatior PEO-Nos and the monomer EHOx. The correct choice of solvent is of utmost importance as it has to fully solubilize the initiator, the monomer and its growing polymer while having a high solvency power for cations (i.e., high Hildebrand solubility parameters) which is favourable for the CROP of 2-oxazolines.[121] Sulfolane was shown to accelerate the CROP of 2-oxazolines,[122] but was not suited for our system as PEO-*b*-PEHOx is not soluble in sulfolane. With a growing polymer and the already dense sulfolane, the polymerization mixture becomes very viscous to the point of obtaining two different phases, which lead to an uncontrolled polymerization (Figure 45 in the appendix). Acetonitrile and chlorobenzene were compared in a kinetic study. We monitored the monomer conversion by $^1$H NMR and stopped the polymerisation after 30 min as it was already showing that it reaches 80% in

chlorobenzene as compared to 52% in acetonitrile when polymerizing at 140 °C (Figure 13, B/C), proving that chlorobenzene is the better solvent for this system. Similarly to sulfolane, growing PEO-*b*-PEHOx decreases in solubility in acetonitrile. After 7 min (10 units of EHOx), the reactive solution becomes turbid, resulting in less control over the reaction from that point onwards as shown by the sharp increase in the dispersity. The change in solubility is due to the isomerization of the cyclic imino ether structure (EHOx) to a tertiary amide structure (PEHOx). The first order kinetic plot (Figure 13, A) illustrates this lack of control even further, revealing two different trends: a late initiation with a steady but irregular increase in concentration until 20 min where the polymerization reaches its limit and is slowed down dramatically. For chlorobenzene, the linear increase in the $\ln([M]_0/[M]_t)$ with time demonstrates a constant concentration of propagating species indicative of a living polymerization of the 2-oxazolines. In all further experiments, chlorobenzene was then chosen as the solvent for polymerization of EHOx. Assuming a 100% initiator efficiency, the polymerization rate ($k_p$) was determined from the slope of the graph. With a value of 60 ± 2 $L.mol^{-1}.s^{-1}$, the rate is lower than the homopolymerization rate of EHOx in acetonitrile using methyl tosylate as an initiator (106 ± 2 $L.mol^{-1}.s^{-1}$).[116] This decrease most probably come from the use of a PEO-modified macroinitiator and its decreased mobility compared to a small molecule initiator like methyl tosylate. This can also be explained by the lower Hildebrand solubility parameter of chlorobenzene (9.5) compared to acetonitrile (11.9).[122]

The used temperature (140 °C) was also carefully chosen. The temperatures investigated varied from 80 to 150 °C. For temperatures lower than 140 °C, there is an increased amount of side reactions like homopolymerization while 150 °C lead to a broadening of the peak (Figure 15). Hence, all other temperatures other than 140 °C proved to be inadequate for this system.

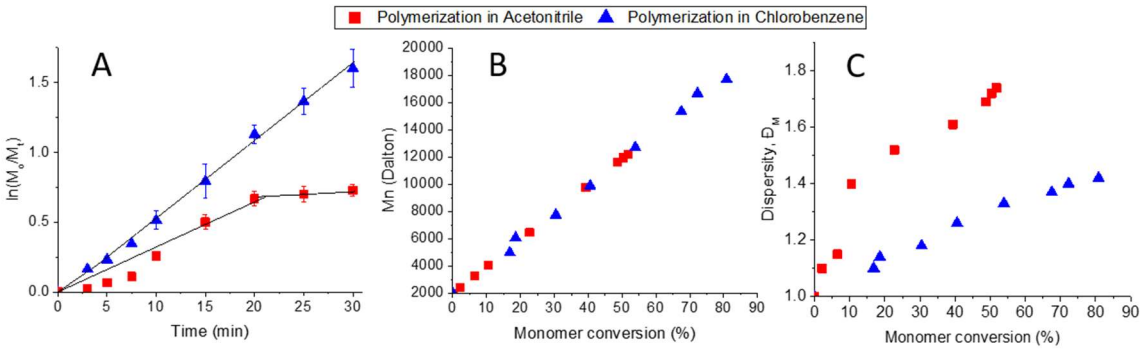


**Figure 16**. Microwave-assisted polymerization kinetics of EHOx in acetonitrile and chlorobenzene at 140 °C using PEO-Nos as macroinitiator. A - First-order Kinetic plot. B - $M_n$ values against monomer conversion. C - $Đ_M$ against monomer conversion.

The optimized conditions, i.e. PEO-Nos in chlorobenzene and 140 °C, were used to synthetize several PEO-*b*-PEHOx characterized by NMR and GPC. GPC showed a complete shift, indicating no left-over macroinitiator and $^1$H NMR allowed to assign all peaks for PEO-PEHOx, thus proving its formation (Figure 17).

| Polymers | Mn [Da][a] | ĐMb | f [%][c] |
|---|---|---|---|
| PEO45-b-PEHOx8 | 3500 | 1.14 | 56 |
| PEO45-b-PEHOx26 | 6000 | 1.20 | 28 |
| PEO45-b-PEHOx40 | 9900 | 1.27 | 20 |
| PEO45-b-PEHOx57 | 13200 | 1.32 | 15 |

**Table 2** comprises the library of synthetized PEO-*b*-PEHOx diblock copolymers with their respective average molecular weight $M_n$, dispersity $Đ_M$ and hydrophilic weight fraction, *f.* In order to reach a longer B block, we increased the monomer-to-initiator ratio to 200. To obtain a phase diagram of the self-assemblies formed with PEO-*b*-PEHOx, an extensive spectrum of different *f* was essential to obtain a holistic phase diagram of the self-assemblies formed with PEO-*b*-PEHOx; from the most hydrophilic $PEO_{45}$-*b*-$PEHOx_8$ (*f*=57%) to the most hydrophobic $PEO_{45}$-b-$PEHOx_{171}$ (*f*=6%).

| | | | |
|---|---|---|---|
| PEO45-b-PEHOx95 | 21000 | 1.35 | 10 |
| PEO45-b-PEHOx128 | 27600 | 1.37 | 7 |
| PEO45-b-PEHOx151 | 32200 | 1.4 | 6 |
| PEO45-b-PEHOx171 | 36200 | 1.41 | 6 |
| PEHOx60 | 11800 | 1.18 | - |

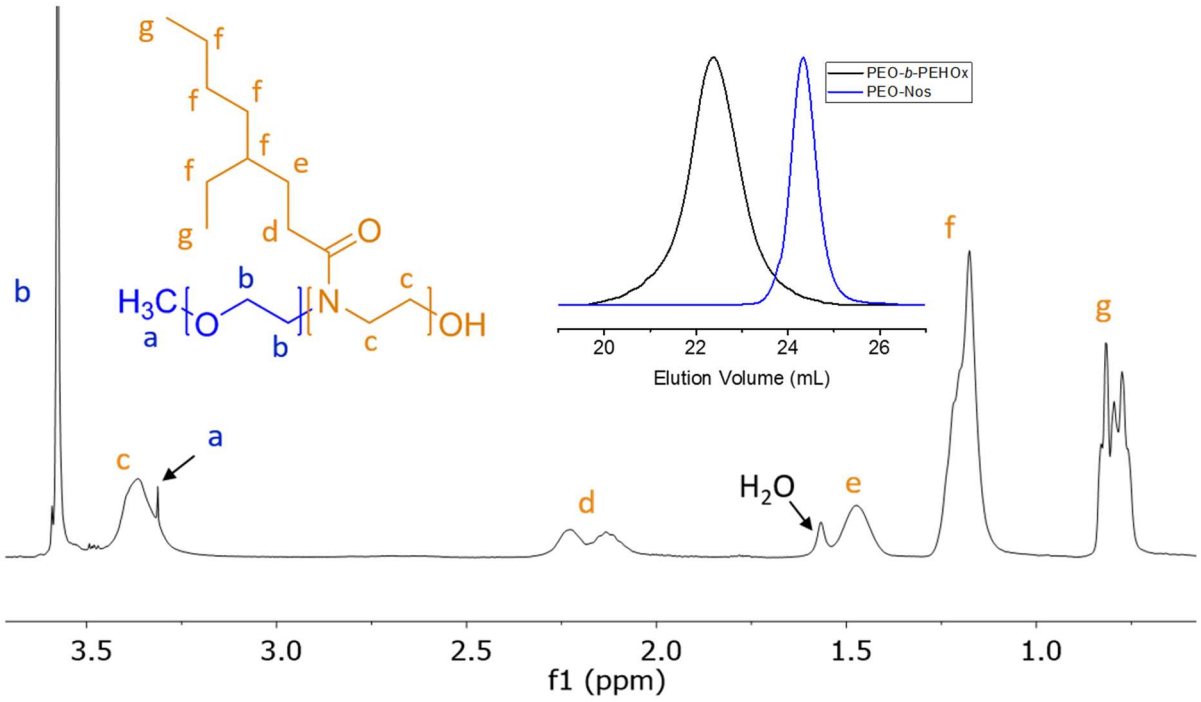


**Figure 17**. Representative NMR ($^1$H, 400 MHz, $CDCl_3$) of $PEO_{45}$-*b*-$PEHOx_{40}$. All peaks have been assigned to the chemical structure of the polymer with a representative GPC traces ($CHCl_3$) of $PEO_{45}$-b-$PEHOx_{40}$ and the macroinitiator PEO-Nos.

**Table 2**. Characterization of PEO-PEHOx diblock copolymers using $^1$H NMR, GPC ($CHCl_3$) and hydrophilic weight fraction, *f*. [a]obtained from $^1$H NMR, [b]obtained by GPC, [c]calculated by the equation *f* =($M_n$ of PEO)/($M_n$(PEO)+$M_n$(PEHOx)). For $PEO_{45}$-*b*-$PEHOx_{8\text{-}57}$, a ratio Monomer to Initiator of 100 was used. For $PEO_{45}$-*b*-$PEHOx_{95\text{-}171}$, a ratio Monomer to Initiator of 200 was used. For calculations of EHOx block length, see section 7.1.2 of the appendix.

| Polymers | $M_n$ [Da][a] | $Đ_M$[b] | f [%][c] |
|---|---|---|---|
| $PEO_{45}$-*b*-$PEHOx_8$ | 3500 | 1.14 | 56 |
| $PEO_{45}$-*b*-$PEHOx_{26}$ | 6000 | 1.20 | 28 |
| $PEO_{45}$-*b*-$PEHOx_{40}$ | 9900 | 1.27 | 20 |
| $PEO_{45}$-*b*-$PEHOx_{57}$ | 13200 | 1.32 | 15 |
| $PEO_{45}$-*b*-$PEHOx_{95}$ | 21000 | 1.35 | 10 |
| $PEO_{45}$-*b*-$PEHOx_{128}$ | 27600 | 1.37 | 7 |
| $PEO_{45}$-*b*-$PEHOx_{151}$ | 32200 | 1.4 | 6 |
| $PEO_{45}$-*b*-$PEHOx_{171}$ | 36200 | 1.41 | 6 |
| $PEHOx_{60}$ | 11800 | 1.18 | - |

### 2.2.3 Determination of the glass transition temperature ($T_g$)

The thermal properties were then assessed by differential scanning calorimetry (DSC) of the homopolymer PEHOx as well as of the diblock copolymers $PEO_{45}$-*b*-$PEHOx_8$ and $PEO_{45}$-*b*-$PEHOx_{171}$, the smallest and longest of the library (Figure 18, for the rest of the diblock copolymers DSC curves, Figure 46 in the appendix). The thermal properties of the homopolymer PEO were obtained from the literature.[123] A glass transition temperature ($T_g$) below room temperature is key for self-assembly with biological actives in mild conditions that does not harm enzyme activity for example.[124] Being in a flexible and rubbery state above the $T_g$ enables the amphiphilic block copolymers to reorganize readily in response to environmental changes and attain particular structures through self-assembly.[58, 125]

The homopolymer PEHOx revealed a $T_g$ of -7 °C and no melting point which is coherent with the value (-6°C) from Hoogenboom et al.[116] and the amorphous behaviour of this polymer. Interestingly, every diblock copolymers PEO-*b*-PEHOx revealed two glass transition temperatures and a melting peak. The broad melting peak of PEO starts at about 15 °C and passes its maximum around 45 °C. $PEO_{45}$-*b*-$PEHOx_8$ and $PEO_{45}$-*b*-$PEHOx_{171}$ both exhibit two $T_g$ values with the first one in the range of -40°C (PEO block) and a second one in the range of 3°C (PEHOx block). No significant difference in the glass transitions temperatures were observed with increasing block length of the EHOx. The fact that we have two independent visible $T_g$'s confirms a phase separation between PEO and PEHOx. In comparison to the $T_g$'s of the homopolymers (PEO: -73°C, PEHOx: -7°C), the increased values obtained for PEO-*b*-PEHOx can be explained by a decrease in flexibility of the polymers chains when part of a diblock copolymer. Nonetheless, the values remain well below room temperature and thus enable a

self-assembly process at room temperature with solvent-free technique like film rehydration, which is advantageous for incorporation of biological actives in the future.

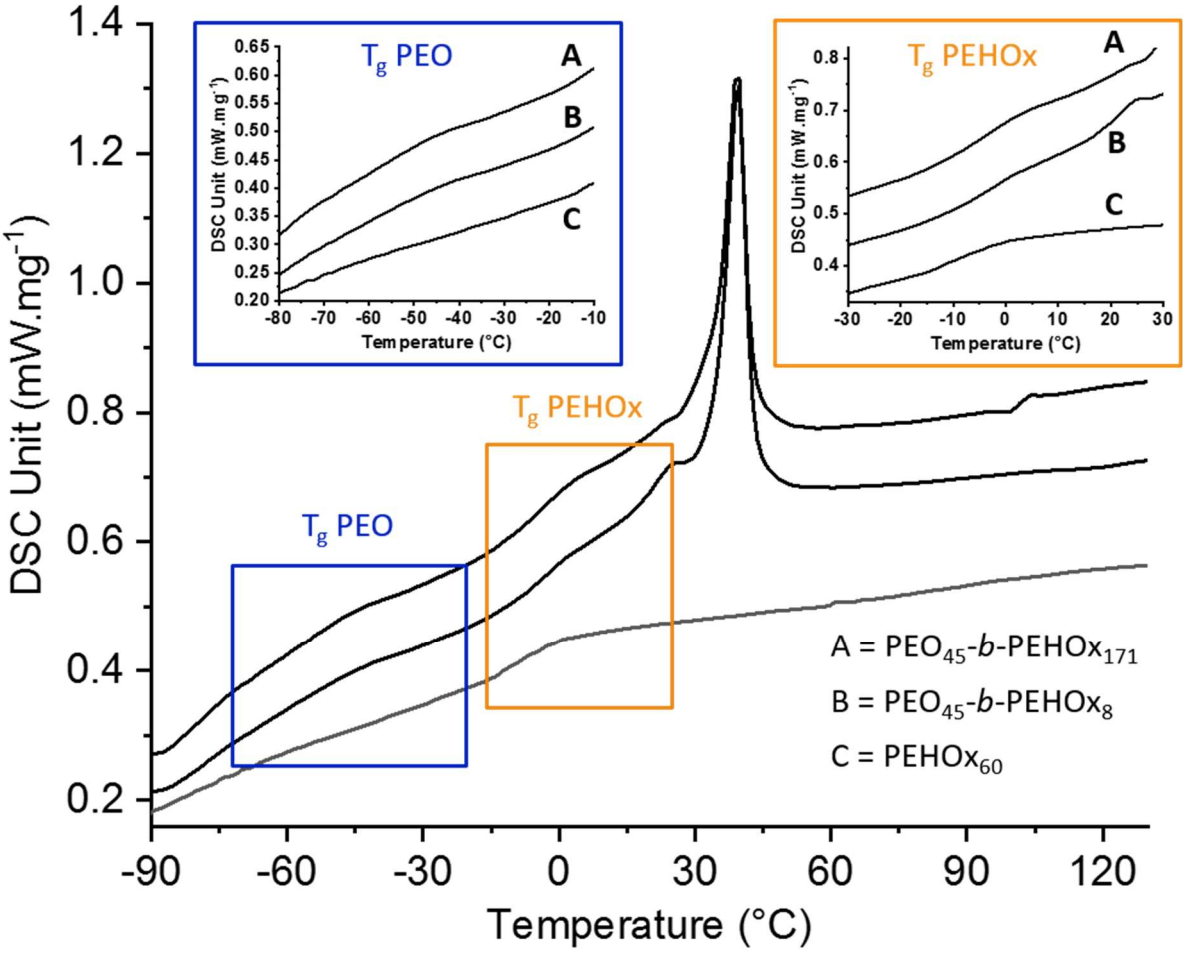


**Figure 18**. DSC measurements of diblock copolymers $PEO_{45}$-*b*-$PEHOx_8$ and $PEO_{45}$-*b*-$PEHOx_{171}$ and homopolymer $PEHOx_{60}$, highlighting the regions of the glass transition temperatures, in blue for PEO and in orange for PEHOx.

## 2.3 Results and discussions part II: Self-Assembly of PEO-*b*-PEHOx

### 2.3.1 Formation of the self-assemblies: film rehydration and solvent switch

We studied the self-assembly of PEO-*b*-PEHOx polymers in aqueous solution using two different techniques: film rehydration (FR) and solvent switch (SS). The final concentration of

self-assembled polymer was always set to 0.2 w/w%. For film rehydration, the polymer solutions were stirred extensively for one week as a stirring time of only one day only resulted in precipitated polymer. For solvent switch, the self-assemblies were formed much faster as they were completely formed at the end of the dialysis step after 2 days. Further stirring did not yield any change in the self-assemblies (Figure 19). All self-assemblies were then characterized extensively using SLS/DLS, TEM and Cryo-TEM. PEO-*b*-PEHOx$_{151}$ and PEO-*b*-PEHOx$_{171}$ were not investigated as they did not yield any self-assembly structures. With a hydrophilic weight fraction of 6% for those two diblock copolymers, they reached the limit in terms of hydrophobicity and cannot self-assemble.

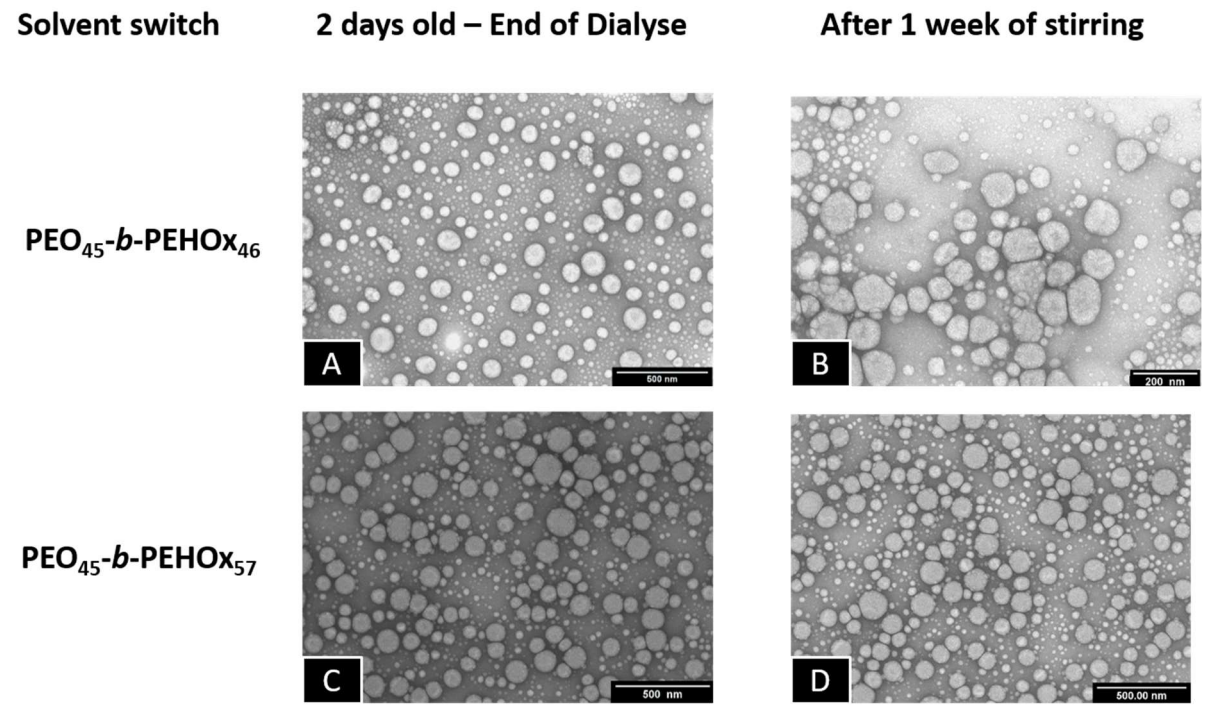


**Figure 19**. Representative TEM images of self-assemblies formed by solvent switch method of PEO$_{45}$-*b*-PEHOx$_{46}$ and PEO$_{45}$-*b*-PEHOx$_{57}$. after: (left) 2 days of dialysis and (right) 2 days of dialysis and 1 week of stirring. Scale bar 200 nm – D. Scale bars 500 nm – A, C, D.

### 2.3.2 Characterisation of the self-assemblies

Light scattering was conducted as the first step to assess the form factor $\rho$, which is the ratio of the radius of gyration ($R_g$) to the hydrodynamic radius ($R_h$). With dynamic light scattering (DLS), $R_h$ can be obtained while static light scattering (SLS) allows to obtain $R_g$. The form factor $\rho$ is a structure property that reflects the radial density distribution of the particle. Typical values for $\rho$ are $\rho$=0.78 for solid spheres and $\rho$=1.0 for hollow spheres with an infinitely thin shell and viewed typical for vesicles.[57, 126] The $R_g$, $R_h$ and $\rho$ for both self-assembly techniques are comprised in Table 3. For most polymers and both self-assembly techniques $\rho$ was close to 0.78 and thus indicated solid-filled particles as a common morphology but in different sizes. Among those, three results stood out: FR of $PEO_{45}$-*b*-$PEHOx_{26}$ and SS of $PEO_{45}$-*b*-$PEHOx_{95}$ showed values of $\rho$=0.93 and $\rho$=0.94 respectively, which indicated a hollow sphere with a thin shell, while for SS of $PEO_{45}$-*b*-$PEHOx_{128}$ with $\rho$=0.88 indicated a hollow sphere with a thicker shell.

TEM and Cryo-TEM images of all samples showed the various PEO-*b*-PEHOx self-assemblies obtained by FR and SS with increasing EHOx length (

Figure **20**). The nature of the self-assemblies formed was confirmed by combining the results from these images and the light scattering data.

**Table 3**. Light scattering data of self-assembled structures formed by PEO-*b*-PEHOx polymers by film rehydration and solvent switch techniques. dn/dc = 0.15 (Figure 49 in the appendix) for PEO-*b*-PEHOx in Milli-Q. For MIE plot study and DLS profiles of FR and SS of $PEO_{45}$-*b*-$PEHOx_{95}$ and $PEO_{45}$-*b*-$PEHOx_{128}$, Figure 21.

| | Film Rehydration (FR) | | | Solvent Switch (SS) | | |
|---|---|---|---|---|---|---|
| Diblock copolymers | $R_h$ [nm] | $R_g$[nm] | $\rho = R_g/R_h$ | $R_h$ [nm] | $R_g$[nm] | $\rho = R_g/R_h$ |
| $PEO_{45}$-*b*-$PEHOx_8$ | 19 ± 3 | 15 | 0.79 | 13 ± 2 | 10 | 0.77 |
| $PEO_{45}$-*b*-$PEHOx_{26}$ | 67 ± 20 | 62 | 0.93 | 21 ± 4 | 16 | 0.80 |
| $PEO_{45}$-*b*-$PEHOx_{40}$ | 80 ± 8 | 61 | 0.76 | 77 ± 14 | 58 | 0.75 |
| $PEO_{45}$-*b*-$PEHOx_{57}$ | 91 ± 12 | 73 | 0.80 | 93 ± 16 | 69 | 0.74 |
| $PEO_{45}$-*b*-$PEHOx_{95}$ | 139 ± 19 | 112 | 0.81 | 132 ± 6 | 124 | 0.94 |
| $PEO_{45}$-*b*-$PEHOx_{128}$ | 178 ± 21 | 120 | 0.67 | 101 ± 19 | 89 | 0.88 |

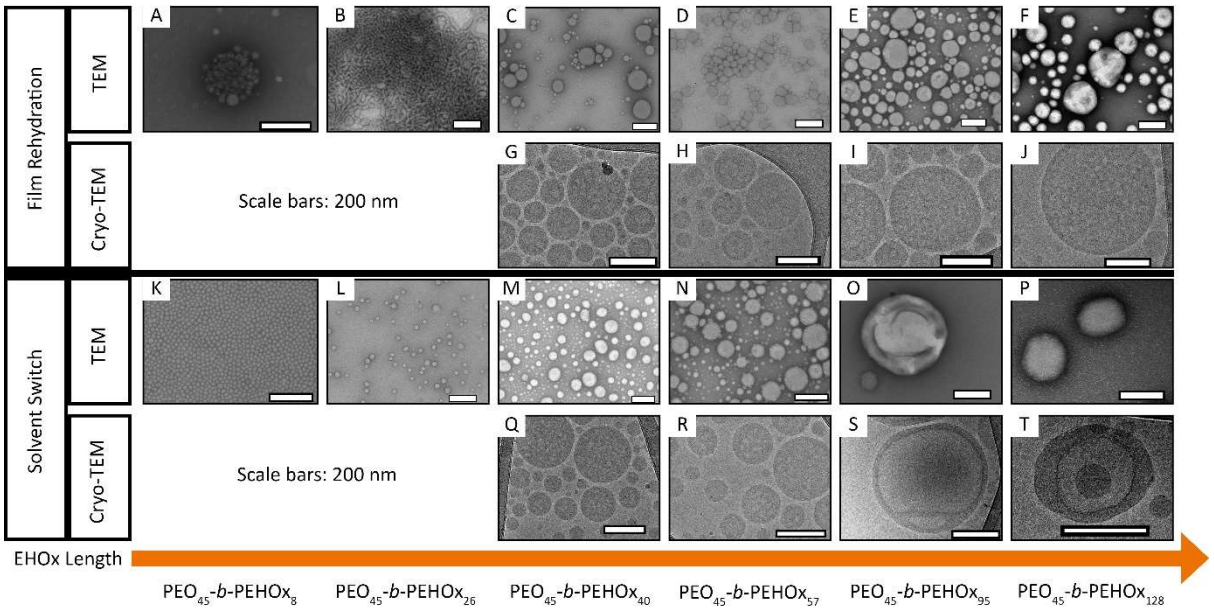


**Figure 20.** TEM and Cryo-TEM images of the self-assemblies by film rehydration and solvent switch of AB diblock PEO-b-PEHOx for increasing length of B block – EHOx. Scale bars 200 nm. Supplementary Cryo-TEM images of SS of $PEO_{45}$-*b*-$PEHOx_{95}$ (

Figure **20**.S) and $PEO_{45}$-b-$PEHOx_{128}$ (

Figure **20**.T) can be seen on Figure 47 and Figure 48 in the appendix, respectively.

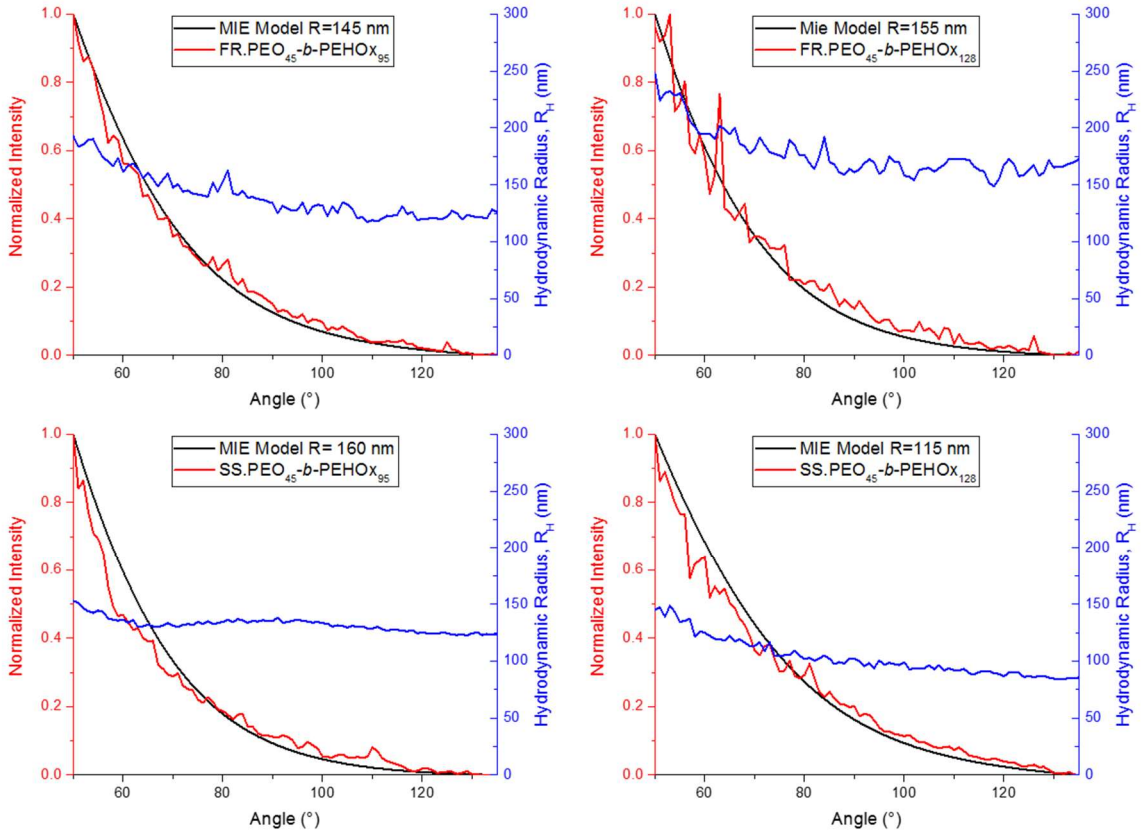


**Figure 21**. MIE plot and DLS profiles of FR and SS of $PEO_{45}$-*b*-$PEHOx_{95}$ and $PEO_{45}$-*b*-$PEHOx_{128}$.

### 2.3.3 Micelles and Worms

Starting with the smallest polymer, $PEO_{45}$-*b*-$PEHOx_{8,}$ a small size and $\rho$ values close to 0.78 were obtained by light scattering, for both FR ($R_h$= 19 ± 3 nm, $\rho$=0.79) and SS ($R_h$= 13 ± 2 nm, $\rho$=0.77). Both are typical values for spheres filled with polymers, hence for micelles, which were confirmed by TEM (

Figure **20**.A/K). TEM revealed that SS yielded in significantly more monodisperse and more numerous micelles than FR. With similar light scattering results, SS of $PEO_{45}$-*b*-$PEHOx_{26}$ ($R_h$= 21 ± 4 nm, $\rho$=0.80) was confirmed to also form micelles (

Figure **20**.L). However, the same polymer by FR yielded distinct results ($R_h$= 67 ± 20 nm, $\rho$=0.93) which would indicate a different morphology which was proved to be worms by TEM

(

Figure **20**.B). This explains why its $\rho$ was peculiar as Zimm plot is not valid for a complex cylinder-like shape of worms. Both polymers demonstrate the impact of using two self-assembly techniques which are fundamentally different in terms of approach: with FR, the AB diblock copolymer is forming the self-assembly structures top-down from a solid film. When the thin polymer film is formed, it is directly rehydrated with a large volume of water. The diblock copolymer then needs to reduce fast the contact with water and form a structure, which is kinetically stable like worms for $PEO_{45}$-*b*-$PEHOx_{26}$. While with SS, the AB diblock copolymer is forming the self-assembly structures bottom-up. It induces more flexibility to the single chains during self-assembly as they start from freely dissolved unimers rather than a bulk material, yielding thermodynamically favoured structures. Water is added very slowly which gives PEO-*b*-PEHOx enough time to be able to adapt to the growing volume of water and forms the most adapted and stable structure in this environment, like micelles for $PEO_{45}$-*b*-$PEHOx_{26}$.

### 2.3.4 Multicompartment Micelles (MCMs)

Increasing the length of the hydrophobic block further, we observed similar light scattering results and TEM images for both self-assembly techniques for $PEO_{45}$-*b*-$PEHOx_{46}$ ([FR]

Figure **20**.C, $R_h$= 80 ± 8 nm, $\rho$=0.76 / [SS]

Figure **20**.M, $R_h$= 77 ± 14 nm, $\rho$=0.75) and $PEO_{45}$-*b*-$PEHOx_{57}$ ([FR]

Figure **20**.D, $R_h$= 91 ± 12 nm, $\rho$=0.80 / [SS]

Figure **20**.N, $R_h$= 93 ± 16 nm, $\rho$=0.74). Both diblock copolymers self-assembled into nanoparticles consisting of spherical objects with radii ranging from 70 to 100 nm for SS and FR. Similarly, we observed spherical nanoparticles but with bigger radii in accordance with the light scattering data for the FR of $PEO_{45}$-*b*-$PEHOx_{95}$ (Fig 5.E, $R_h$= 139 ± 19 nm, $\rho$=0.81) and $PEO_{45}$-*b*-$PEHOx_{128}$ (Fig 5.F, $R_h$= 178 ± 21 nm, $\rho$=0.67).

All of these results are too big for normal micelles. In a stretched conformation, $PEO_{45}$-*b*-$PEHOx_{46}$ is 32 nm in length, which is in theory the largest possible radius for a micelle from this polymer (see section 5b of the SI). With 36 nm for $PEO_{45}$-*b*-$PEHOx_{57}$ and 50 nm for $PEO_{45}$-*b*-$PEHOx_{95}$, these polymers are also too short to form micelles of the size measured by DLS and the form factor is too small for vesicles. To clarify the type of nanoparticles formed, Cryo-TEM was conducted as it can visualize them in their native environment and discriminate between solid spherical particles, vesicles or other types of nanoparticles. Surprisingly, all spheres were filled with inverse micelles forming multi-compartment micelles (MCMs) as shown by the absence of any membrane and the presence of many compartments the size of micelles (

Figure **20**.G/H/Q/R/I/J, Figure 23.A, Figure 22 for a higher resolution).[127-130] It should also be noted that MCMs of $PEO_{45}$-*b*-$PEHOx_{46}$ and $PEO_{45}$-*b*-$PEHOx_{57}$ formed by SS are completely filled with monodisperse inverse micelles ($R_{micelles}$=12.3 ± 1.4 nm and $R_{micelles}$=12.3 ± 1.4 nm, respectively) compared to MCMs from $PEO_{45}$-*b*-$PEHOx_{46}$ and $PEO_{45}$-*b*-$PEHOx_{57}$ formed by FR which are more loosely filled with polydisperse inverse micelles ($R_{micelles}$=22.6 ± 6.3 nm). The different sizes of the inverse micelles can be explained by the random presence of a few small direct micelles in their center. Since FR does not give the PEO chains time to equilibrate the size of the micelles, a higher dispersity can be explained as observed for $PEO_{45}$-*b*-$PEHOx_{57}$.

The bigger MCMs observed for the FR for $PEO_{45}$-*b*-$PEHOx_{95}$ and PEO-*b*-$PEHOx_{128}$ are filled completely with monodisperse inverse micelles similar to the MCMs of smaller diblocks formed by SS ($R_{micelles}$=13.1 ± 1.3 nm and $R_{micelles}$=14.5 ± 1.7 nm, respectively,). The core of these inverse micelles is now composed of PEO and water as a solvent. It is likely that the PEO chains are present as a coil rather than a stretched conformation. R of the PEO block is 2.8 nm as a perfect random coil. In order to fill the volume of the internal micelles, solvent must be present either to hydrate the polymer chains or to fill the gaps between them (see section 7.1.7 of the appendix).

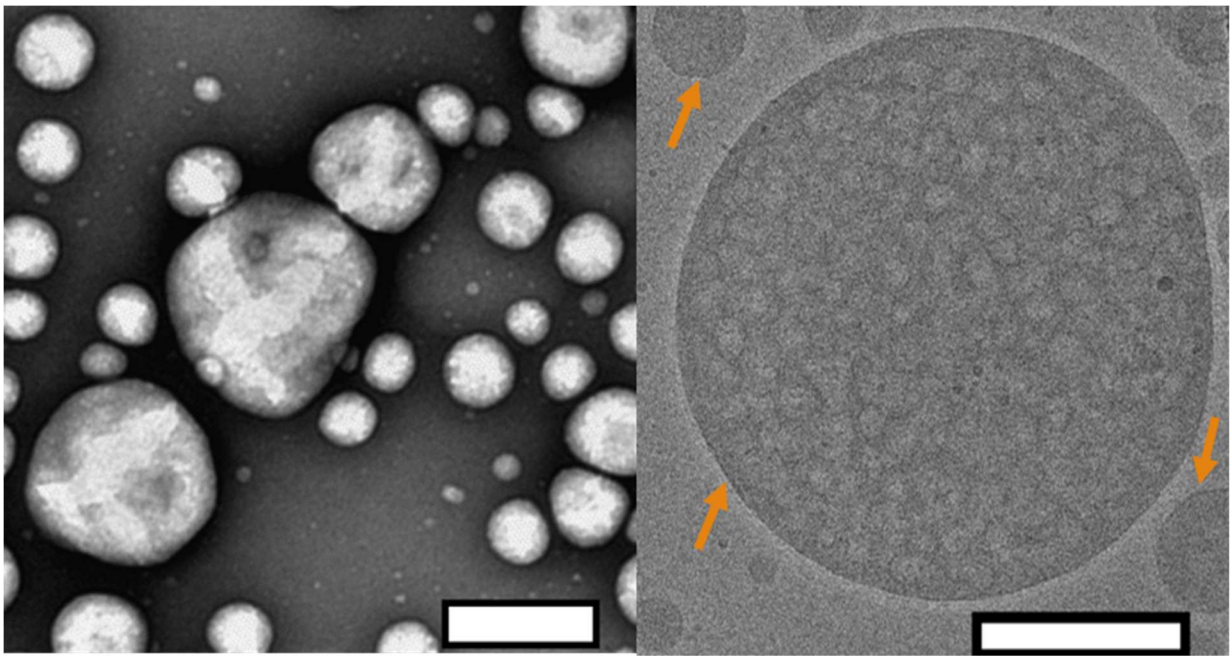

**Figure 22**. Representative TEM and Cryo-TEM images of a multicompartment micelle (MCM) formed by the FR of $PEO_{45}$-*b*-$PEHOx_{128}$. Scale bars 200 nm. The orange arrows highlight the black halo of PEO corona.

MCMs are composed of discrete and structured nanodomains within the core of the nanoparticles. This explains the form factor close to 0.78 as it is a myriad of inverse micelles that make the overall structure comparable to a solid sphere. The most common pathway to

induce the formation of MCMs is either by peptides[129-130] or by a terpolymer system in the presence of two mutually incompatible hydrophobic segments and one hydrophilic segment.[106] For PEO-*b*-PEHOx, there is only one hydrophobic block and to the best of our knowledge, this is the first synthetic amphiphilic AB diblock copolymer forming MCMs. We hypothesize that the self-assembly of the MCMs is driven by the hydrophobic interactions between the branched 2-ethyl-3-heptyl side chains of the PEHOx, while the backbone of the 2-oxazolines form discrete subdomains due to a certain incompatibility with the purely hydrocarbon side-chains. Consequently, the system contains PEO, the PEHOx main chain and the PEHOx side chains as three distinctly different contributors, which act like a terpolymer system when forming the MCMs. Moreover, those self-assembly structures are stable over months. Both, TEM and Cryo-TEM pictures were taken three months after the sample self-assembled and TEM images did not change over that period (Figure 50 in the appendix). Together with the fact that both film rehydration and solvent switch techniques yielded predominantly MCMs, we presume those structures to be near-equilibrium and thermodynamically favourable.

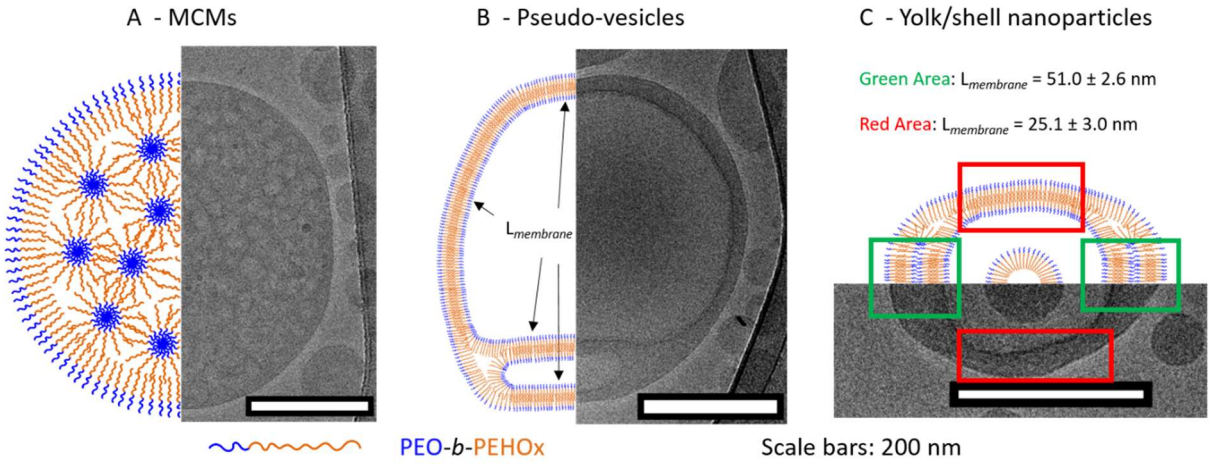


**Figure 23.** Representative cartoons with the corresponding model Cryo-TEM image of the various self-assemblies. A - Multi-compartment micelles (MCMs). B - Pseudo-vesicles. C - Yolk/Shell nanoparticles.

### 2.3.5 Pseudo-vesicles

SS of $PEO_{45}$-*b*-$PEHOx_{95}$, (

Figure **20**.O/S, $R_h$= 132 ± 6 nm, $\rho$=0.94) formed a new structure, which to the best of our knowledge has not been reported: pseudo-vesicles. In the TEM picture (

Figure **20**.O), the typical topology for vesicles in TEM is found as the vacuum of TEM compresses this kind of soft and hollow self-assemblies. Cryo-TEM (

Figure **20**.S, Figure 24 for a higher resolution) then revealed that the main conformation contains more than one hydrophobic core. If two cores are present, one is the dominant cavity and a small second one is also present. When three cavities are around, all of them are of a similar size (Figure 25 in the appendix). All of these structures are contained by an outer

shell which splits and separates the cavities from one another. It is in accordance with the light scattering data which foreshadowed a hollow sphere structure ($\rho$=0.94).

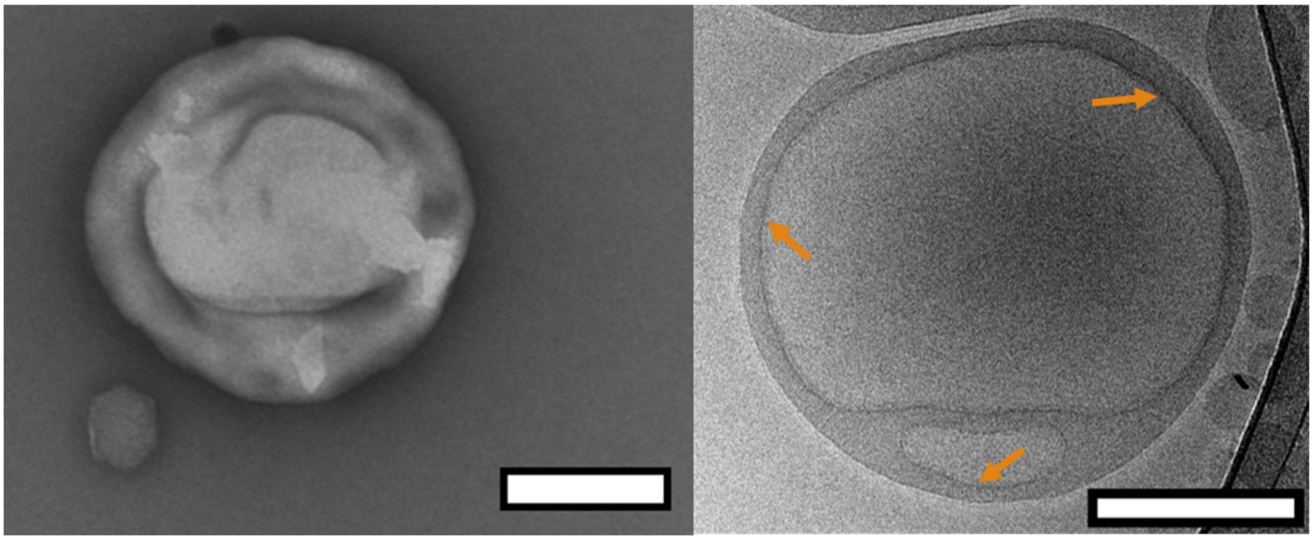

**Figure 24**. Representative TEM and Cryo-TEM images of a pseudo-vesicle formed by the SS of $PEO_{45}$-*b*-$PEHOx_{95}$. Scale bars 200 nm. The orange arrows highlight the black halo of PEO corona.

All of these structures represent a regular membrane with the same thickness between the compartments and the outer medium but also between compartments of 17.9 ± 1.5 nm (Figure 23.B). The membranes only increase significantly in thickness at the intersection between the outer shell and multiple compartments. An extensive comparison of all measurable membrane thicknesses of pseudo-vesicles was done and the data is presented in Table 4. We hypothesized that the differences observed can be explained by the dispersity of the diblock copolymers and the remaining traces of THF lingering in the hydrophobic domains due to the solvent switch method. We confirmed it by NMR (Figure 51 in the appendix). Moreover, the long and branched side chain of the PEHOx block can prevent the formation of a perfect bilayer, which results in a mix of bilayers within one structure. A compact bilayer,

stabilised by the proximity of the side chains and a stretched-out bilayer, stabilised by the impurities mentioned above, to stabilize a thicker membrane at the intersections. We would like to stress that THF is likely to be held in the self-assemblies by “dipole-dipole” interactions with the polymer, which is why it is still present despite the conducted extensive purification of the self-assembly structures.

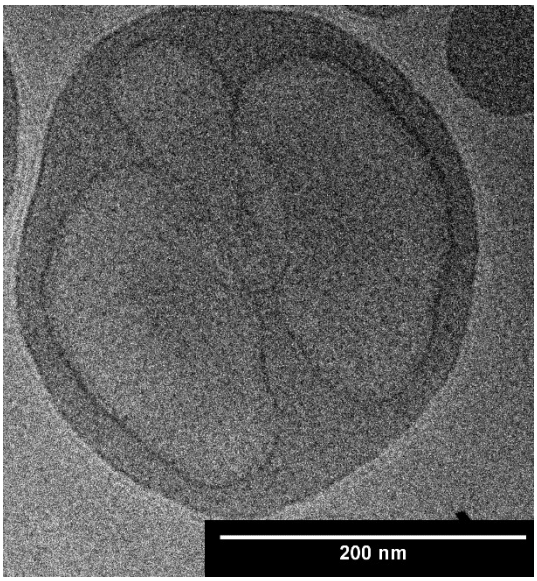


**Figure 25**. Representative Cryo-TEM images of SS of $PEO_{45}$-b-$PEHOx_{95}$ showing the other morphologie of the pseudo-vesicles. Scale bar 200 nm.

**Table 4**. Compilation of the membrane thicknesses of all observed pseudo-vesicles and yolk/shell nanoparticles determined by Cryo-TEM. For yolk/shell nanoparticles, each single nanoparticle is highlighted by the thicker border. [a] corresponds to the radius of the micellar core.

| $PEO_{45}$-b-$PEHOx_{95}$ | $l_{membrane}$ [nm] | $PEO_{45}$-*b*-$PEHOx_{128}$ | $l_{membrane}$ [nm] |
|---|---|---|---|
| Pseudo-vesicles | 18.4 ± 1.6 | Yolk/shell nanoparticles | 36.8 ± 1.6 |
| | 17.3 ± 1.9 | | 17.2 ± 1.1 |
| | 13.8 ± 1.4 | | 26.7 ± 1.2[a] |
| | 14.1 ± 2.2 | | 41.3 ± 5.0 |
| | 24.3 ± 5.3 | | 36.1 ± 1.1[a] |
| | 25.7 ± 6.7 | | 18.0 ± 3.3 |
| | 20.2 ± 4.1 | | 20.2 ± 5.1 |
| | 17.7 ± 3.9 | | 36.9 ± 2.3[a] |
| | 15.5 ± 2.5 | | 14.6 ± 2.1 |
| | 15.2 ± 1.9 | | 34.5 ± 0.7[a] |
| | 14.2 ± 1.6 | | 51.0 ± 3.6 |
| | 14.3 ± 2.5 | | 25.1 ± 3.0 |
| | 16.9 ± 2.2 | | 40.4 ± 0.8[a] |
| | 13.7 ± 1.9 | | 22.5 ± 2.3 |
| | 17.9 ± 2.7 | | 17.6 ± 0.4[a] |
| | 18.2 ± 3.1 | | 37.8 ± 3.7 |
| | 14.6 ± 1.9 | | 20.2 ± 2.0 |
| | 20.0 ± 4.5 | | 15.7 ± 0.4[a] |
| | 25.9 ± 14.0 | | 23.5 ± 2.1 |
| | 23.6 ± 7.4 | | 40.2 ± 4.1 |
| | 15.5 ± 2.0 | | 27.5 ± 0.9[a] |
| | 18.6 ± 4.1 | | 19.7 ± 3.0 |
| | 22.7 ± 4.8 | | 59.6 ± 5.2 |
| | 18.3 ± 4.4 | | 31.2 ± 1.1[a] |
| | 17.3 ± 3.4 | | |
| | 18.4 ± 3.0 | | |
| | 14.6 ± 2.3 | | |
| | 16.4 ± 3.4 | | |
| | 16.5 ± 3.8 | | |

### 2.3.6 Yolk/shell nanoparticles

SS of $PEO_{45}$-*b*-$PEHOx_{128}$ formed yolk/shell nanoparticles and is, to the best of our knowledge, the first synthetic amphiphilic AB diblock copolymer to do so. The general method for preparing such material is based on removing the intermediate sacrificial layer of the trilayer

nanoparticles by chemical dissolution or thermal decomposition.[109] To overcome some problems like the destruction of the encapsulated agents and tedious synthetic procedure, polymeric yolk/shell nanoparticles were formed by polymerization-induced self-assembly and reorganization using poly(4-vinylpyrodine)-polystyrene for the shell and homopolystyrene for the core. [108] This is a pseudo-triple-layer ellipsoid structure where an irregular bilayer membrane encloses a cavity which then hosts a micelle at its core (

Figure **20**.P/T,

Figure **20**.C, Figure 26 for a higher resolution). The core has a radius of 43 ± 3.6 nm which is now in line with a stretched length of $PEO_{45}$-*b*-$PEHOx_{128}$ of 62 nm. The polymer will be present at least somewhat coiled, making a radius of 43 nm completely reasonable. The bilayer forms two discrete domains defined by a certain thickness of the membrane. A narrow one with a thickness of 25.1 ± 3.0 nm (Red area in Figure 23.C) and a broad one with a thickness of 51.0 ± 2.6 nm (Green area in Figure 23.C).

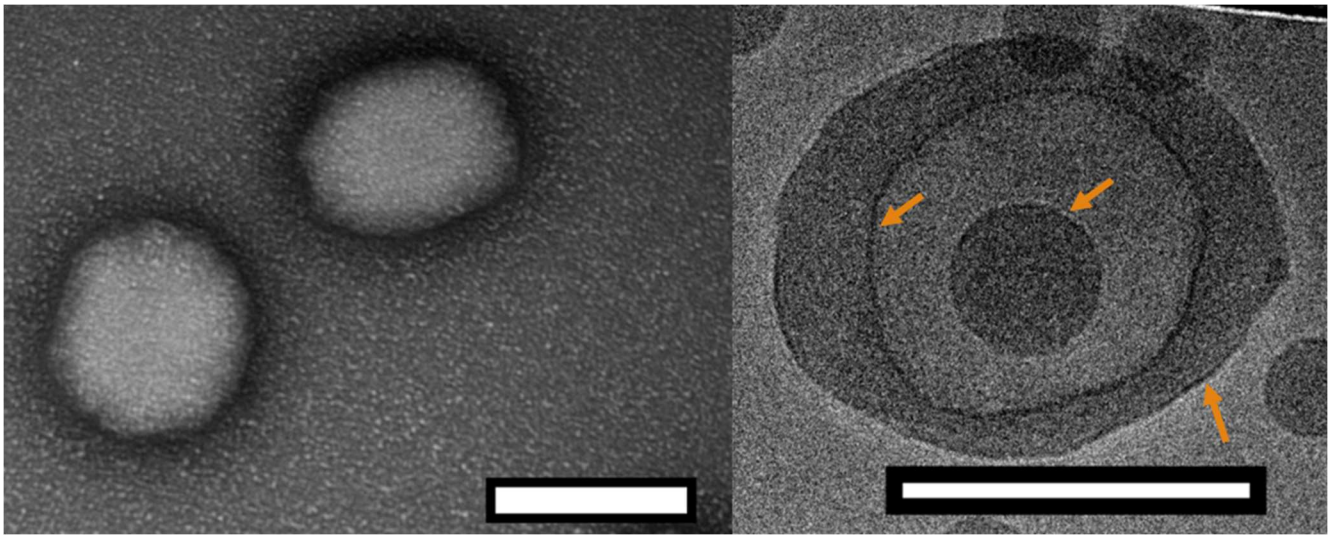

**Figure 26**. Representative TEM and Cryo-TEM images of a yolk/shell nanoparticle formed by the SS of $PEO_{45}$-*b*-$PEHOx_{128}$. Scale bars 200 nm. The orange arrows highlight the black halo of PEO corona.

We hypothesize that the broad bilayer is actually a double bilayers of diblock copolymers which dissociates and transition to a simple bilayer. Those compact bilayers and the transition between simple and double bilayer are stabilized by the hydrophobic interactions of the side chains. This yolk/shell nanoparticles present similarities to the pseudo-vesicles. The main differences are that the hydrophilic domain between bilayers remain minimal and is not an actual hollow cavity filled with water and that a micelle is encapsulated at its core. Just like for the pseudo-vesicles, an extensive comparison of all measurable membrane thicknesses of yolk/shell nanoparticles was conducted and the results are comprised in Table 4. We hypothesized that the differences observed can be explained by the dispersity of the diblock copolymers and the remaining traces of THF lingering in the hydrophobic domains due to the solvent switch method. We confirmed it by NMR (Figure 51 in the appendix). Additionally, by adopting a more coiled up conformation it maximizes the hydrophobic interactions between the side chains, which enables the formation of a compact bilayer of entangled side chains.

### 2.3.7 PEO Corona visible by Cryo-TEM on the self-assemblies

Interestingly, in all Cryo-TEM images of MCMs, pseudo-vesicles and yolk/shell nanoparticles, the PEO corona can be visualized and measured as it forms a clear black halo around all nanoparticles (see orange arrows in Figure 22 for MCMs, Figure 24 for pseudo-vesicles and Figure 26 for yolk/shell nanoparticles). It is 2.9 ± 0.3 nm thick across all Cryo-TEM images. This length is perfectly in line with the 2.8 nm of a $PEO_{45}$ as a random as coil mentioned earlier (see section A of 7.1.7 of the appendix).

### 2.3.8 Self-assembly phase diagram of PEO-*b*-PEHOx

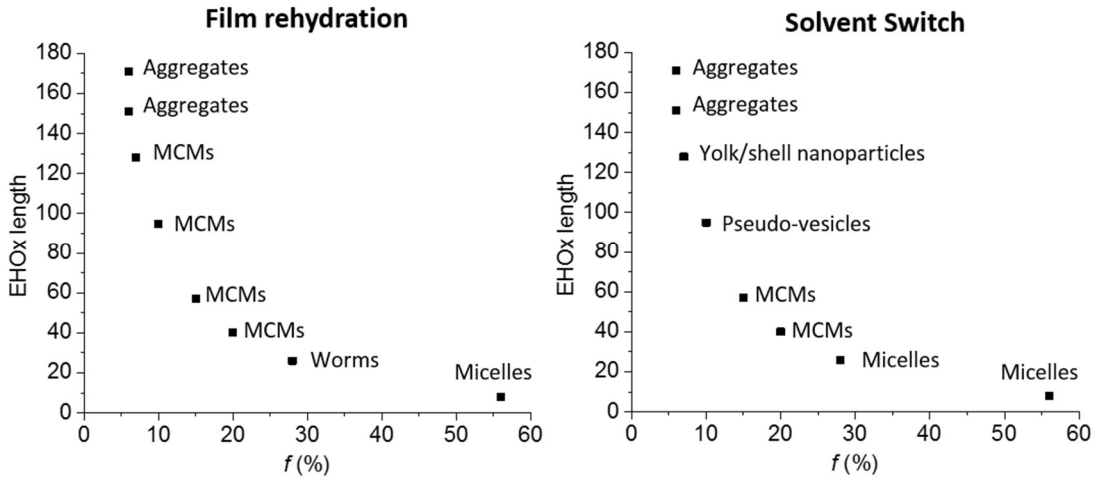


**Figure 27**. Self-assembly phase diagram of AB diblock PEO-*b*-PEHOx self-assemblies by film rehydration and solvent switch. MCMs = Multicompartment Micelles

All results were summarized in a self-assembly phase diagram (Figure 27), to emphasize the broad range of self-assembly structures possible with this AB diblock copolymer, which could only be proven using a combination of DLS, SLS, TEM and Cryo-TEM. Both film rehydration and solvent switch yield unique yet distinct self-assembly structures with a variety which is usually seen for ABC triblock copolymers.[1] This great variety reflects the unique influence of the side chain of PEHOx, as it is the first synthetic amphiphilic AB diblock copolymer to efficiently form such a variety of complex self-assemblies on its own. Further studies on the influence of THF or others solvents on the solvent switch might also elucidate how to form regular vesicles with this system.

## 2.4 Conclusions

We presented the synthesis of a new amphiphilic diblock copolymer PEO-*b*-PEHOx by cationic ring opening microwave-assisted polymerization using a previously unknown nosylate-based PEO macroinitiator. The choice of solvent proved to be as paramount as the choice of temperature, with chlorobenzene and 140°C being the best combination. A library of AB

diblock copolymers with different PEHOx was synthetized and designed for self-assembly into defined nanoparticles. DSC revealed that the resulting diblocks copolymers have a $T_g$ below 0°C ensuring a high flexibility of the system for the following self-assembly at room temperature. Using film rehydration and solvent switch, we showed that PEO-*b*-PEHOx predominantly self-assembles into multi-compartment micelles (MCMs). MCMs grow in size when the PEHOx becomes longer. As hydrophilic and hydrophobic molecules could be loaded in a same carrier, those MCMs could find applications in advanced drug delivery applications.

Solvent switch of PEO-*b*-PEHOx with a long PEHOx block also lead to pseudo-vesicles and yolk/shell nanoparticles. As organic solvent was trapped within the walls of those vesicles-like structures, further studies can focus on loading those distinct hydrophobic and hydrophilic domains with different catalysts in order to perform cascade reactions. All those complex structures were formed from a single AB diblock copolymer which show the potential of hydrophobic blocks with a long side chain to obtain complex nanoparticles from a single material. Further studies will be conducted to gain deeper insights into the influence of various side chains of the hydrophobic block on the self-assembly of block copolymers. Only an in-depth study using Cryo-TEM and SLS revealed these structures and should motivate the community to look deeper if regular TEM suggests the presence of vesicles as this might not always be the case. This work will also be used as a step-stone towards the one-pot synthesis of new self-assembling triblock amphiphilic copolymers based on this system using the sequential polymerization of oxazolines.[1, 118]

# 3. One-pot Synthesis of the Amphiphilic PEO-*b*-PEHOx-*b*-PEtOz Polymers and its Self-Assembly into Nanoscopic Asymmetric Polymersomes

Within this chapter, the synthesis and self-assembly of the ABC polymers PEO-*b*-PEHOx-*b*-PEtOz is presented. First, the full monomer conversion polymerization of EHOx on PEO-Nos is studied in order to synthetize in one-pot by adding EtOz a comprehensive library of PEO-*b*-PEHOx-*b*-PEtOz with different block lengths of PEHOx and PEtOz. Their self-assembly by film rehydration was thoroughly characterized. Among other self-assemblies like micelles or multicompartment vesicles (MCV), most ABC polymer self-assembled into polymersomes. Depending on the length of PEtOz compared to PEO, we managed to assess precisely by two independent methods which ABC polymer self-assemble into asymmetric polymersomes.

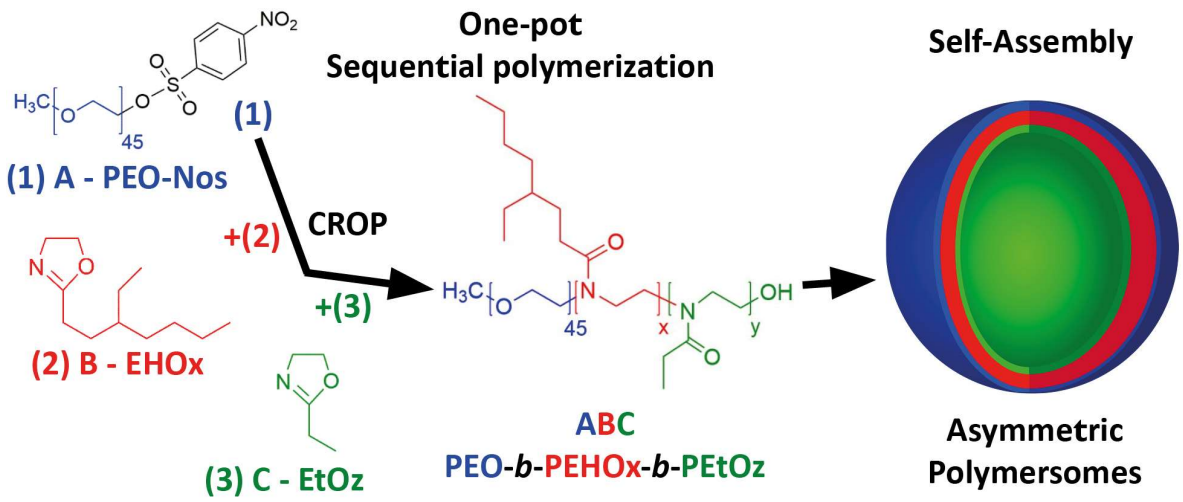


**Figure 28.** Graphical abstract of the one-pot synthesis of the amphiphilic PEO-*b*-PEHOx-*b*-PEtOz polymers and its self-assembly into nanoscopic asymmetric polymersomes

This study is published as **Davy Daubian**, Alexandra Fillion, Jens Gaitzsch and Wolfgang Meier. *Macromolecules.* (2020), 53, 11040-11050.

## 3.1 Introduction

Nature is a treasure trove of elaborate structures assembled from different bio(macro)molecules. One of those fascinating structures is the lipid bilayer, which forms the membrane around living cells, but also within them to construct cellular compartments based on lipid vesicles or liposomes. During the last decades, elaborating mimics of cell membranes from lipids, proteins and polymers have attracted significant interest especially in biomedical fields, like drug delivery or catalytic nanocompartments.[98, 102, 131-135] Artificial membranes self-assembled from amphiphilic block copolymers, are particularly interesting as these polymersomes show several advantages compared to liposomes. They exhibit an improved chemical and physical stability and a lower membrane permeability than liposomes since the thickness of their membrane can be engineered by modulating the molecular weight of the hydrophobic block. By changing the species and the lengths of individual segments of the block-copolymer, polymersomes can be functionalized and their membrane properties can be controlled and modulated.[136-138] Most of the polymersomes investigated are obtained from AB diblock and ABA triblock copolymers (with A = hydrophilic and B = hydrophobic block). The resulting polymersomes have a symmetric AB/BA bilayer membrane from diblock copolymers or an ABA monolayer membrane from triblock copolymers membrane, hence the same inner and outer leaflet.[139] However, this does not mimic one of the core characteristic of biological membranes: its asymmetry, which is expressed by the lipid composition, substitution and distribution. This characteristic is essential for the insertion and orientation of membrane proteins e.g. proton pumps and similar vectorial molecules.[140-141] It has been shown that the insertion of membrane proteins into symmetric artificial membranes leads to the loss of their preferred orientation and by extension to the loss of their function.[142] To overcome this issue, some studies attempted to break the symmetry of artificial membranes

by tailoring the chemical composition of the internal and external leaflet of the vesicle.[92, 143] A more straightforward strategy to obtain asymmetric polymeric membranes is by self-assembly of asymmetric amphiphilic ABC triblock copolymers (with C = 2nd hydrophilic block), which will be shortened to "ABC triblocks" in this manuscript. In order to obtain asymmetry, both hydrophilic blocks (A and C) should be different in size. Following spacial arguments, the longer hydrophilic segments segregate towards the outer leaflet due to a larger radius (curvature) and reduced steric hindrance whereas the smaller segments tend to remain on the inner leaflet the polymersome membrane. Therefore, for polymersomes from an ABC triblock where A is longer than C, A is predominantly on the outside while C is inside (Figure 29).[2, 34-35]

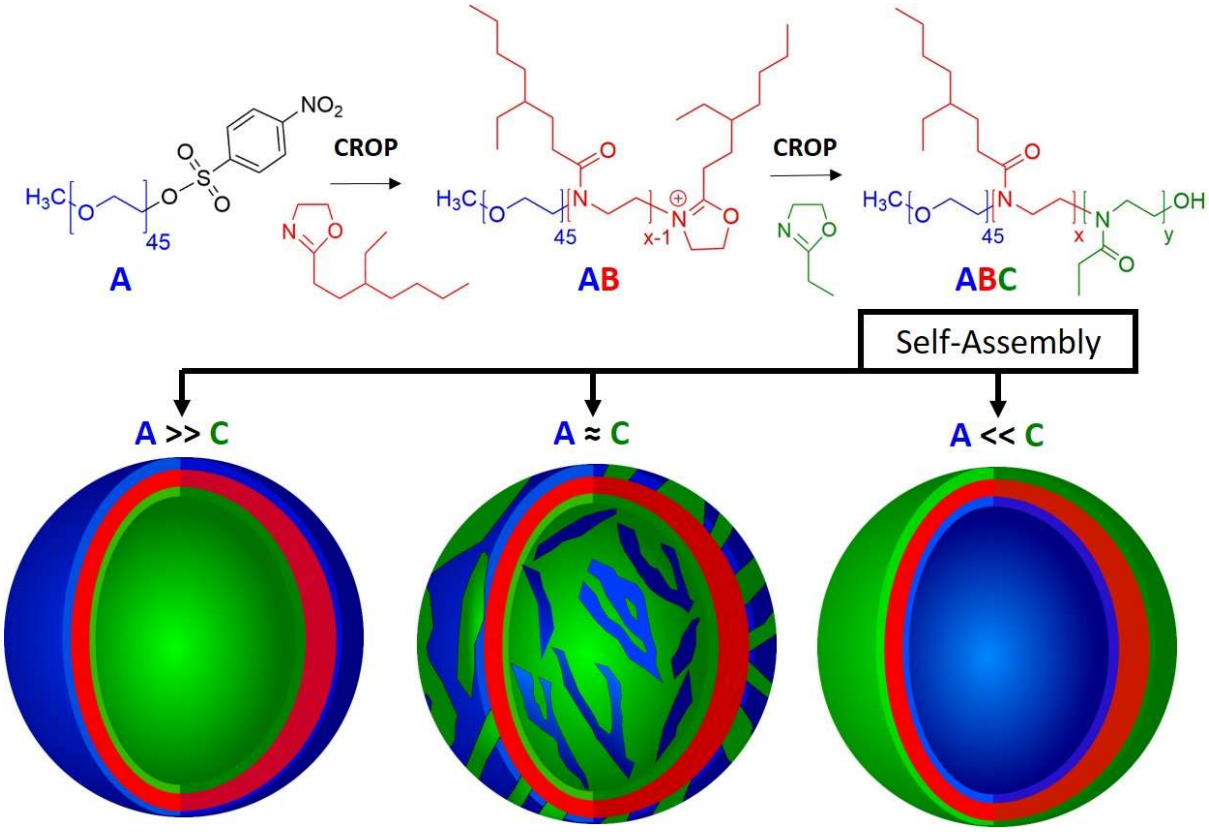


**Figure 29.** Schematic representation of the synthesis of poly(ethylene oxide)-*block*-poly(2-(3-ethylheptyl)-2-oxazoline-*block*-poly(2-ethyl-2-oxazoline) (PEO-*b*-PEHOx-*b*-PEtOz) and the resulting possible membrane orientations of the polymersomes formed by self-assembly.

Until now, only a few studies have reported the synthesis of such ABC triblock copolymers.[34, 36, 38, 55, 88, 103, 144] In most cases their syntheses are complex procedures as they involve the combination of different polymerization techniques. It means that intermediate products must be purified and sometimes end-groups need to be modified to serve as initiator for the next step. In order to reduce the number of synthetic steps, an interesting alternative is the use of sequential polymerization. In this approach, the same polymerization technique is employed to polymerize the monomers one after the other. Once a monomer is fully consumed, the polymerization continues with the next one in suitable conditions. It is a powerful stategy to obtain various ABC triblocks, for example poly(2-oxazolines) using the living character of cationic ring-opening polymerization (CROP).[31, 51, 145-146] The ABC triblock targeted in this paper continues our previous works on ABC triblocks: PEO-*b*-PDMS-*b*-PMOXA[35] and PEO-*b*-PCL-*b*-PMOXA[34], mainly replacing PDMS with poly(2-(3-ethylheptyl)-2-oxazoline) (PEHOx). The amphiphilic AB diblock copolymer PEO-*b*-PEHOx[65] already showed the great potential of PEHOx for self-assembly due to its branched side chain and is the basis for this work.

Herein, we present the one-pot synthesis of a novel amphiphilic ABC triblock copolymer consisting of biocompatible blocks: Poly(ethylene oxide)-*block*-poly(2-(3-ethylheptyl)-2-oxazoline)-*block*-poly(2-ethyl-2-oxazoline) (PEO-*b*-PEHOx-*b*-PEtOz). Starting from our previously published PEO-Nos macroinitiator (block A), PEHOx (block B) and PEtOz (block C) were added using sequential CROP [65]. A library of ABC triblocks with different PEHOx and PEtOz block lengths was obtained and their self-assembly was studied in depth. Depending on both PEHOx length and hydrophilic weight fraction (*f*), different self-assembly morphologies were obtained via film rehydration and characterized intensively. A combination of dynamic and static light-scattering (DLS/SLS), transmission electron

microscopy (TEM) and cryogenic transmission electron microscopy (Cryo-TEM) analysis proved the formation of a variety of nanoscale structures, notably polymersomes. Using two independent methods, namely bicinchoninic assay (BCA) and 2D-$^{1}$H-NOESY NMR, the surface composition of the polymersomes from the self-assembled ABC triblocks was thoroughly characterized.

## 3.2 Results and discussions part I: Synthesis of PEO-*b*-PEHOx-*b*-PEtOz

ABC triblocks with a structure of PEO-*b*-PEHOx-*b*-PEtOz represent a novel family of asymmetric triblock copolymers, which are based on the previously published on PEO-*b*-PEHOx AB diblock copolymers.[65] The polymers were synthetized *via* microwave-assisted sequential CROP of EHOx and EtOz on a PEO-Nos macroinitiatior (Figure 29).

### 3.2.1 Full monomer conversion kinetics

In order to leverage the power of sequential polymerization for the addition of the monomer EtOz for the third block PEtOz, any remaining traces of EHOx had to be eliminated. EtOz and EHOx have similar reactivities, thus in the presence of EHOx, both monomers would polymerize in those conditions and would then yield a statistical mixture C of EtOz and EHOx.[116] The polymerization kinetics of EHOx on PEO-Nos were performed in order to obtain the precise time at which the monomer EHOx is fully consumed to be able to pursue with the addition of EtOz. These polymerization kinetics were performed at 140°C in chlorobenzene with 1M total monomer concentration with PEO-Nos as a macroinitiator. The monomer conversion of EHOx was monitored by $^{1}$H NMR and the resulting kinetic plots are depicted in Figure 30. The linear increase of $\ln([M]_0/[M]_t)$ with time demonstrated a constant concentration of propagating species, indicative of a living polymerization of the 2-oxazolines. For monomer-to-initiator ratios of 30, 60, 90 and 140, it was determined that the

polymerization needed 30 min, 40 min, 50 min and 70 min, respectively, to reach a monomer conversion higher than 98%. Thanks to the use of microwave-assisted polymerization, it was possible to stop the reaction rapidly and precisely.

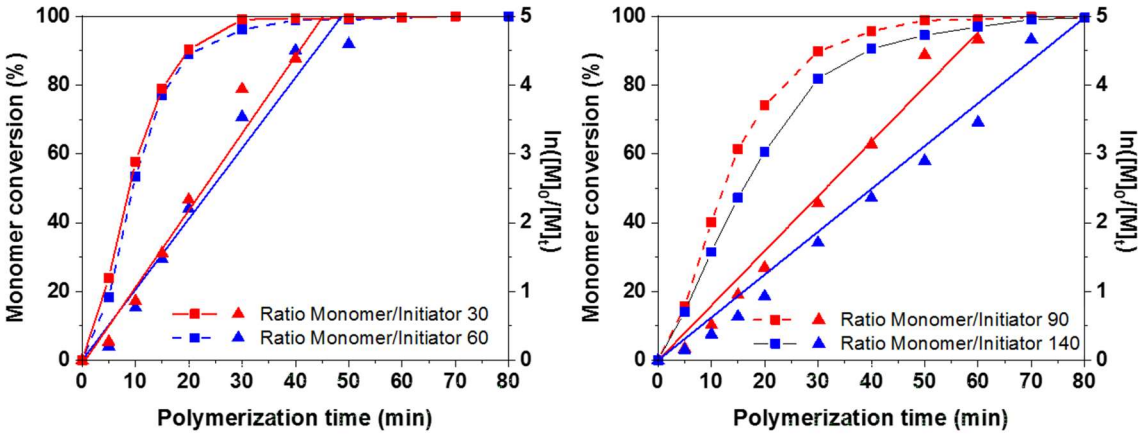


**Figure 30.** Microwave-assisted polymerization kinetics of EHOx in chlorobenzene at 140°C using various Monomer to Initiator ratios and PEO-Nos as macroinitiator. Left – Ratio monomer to initiator of 30 and 60. Right - Ratio monomer to initiator of 90 and 140. Dashed lines correspond to monomer conversion of EHOx (left Y-axis) in % in function of polymerization time in min. Straight lines correspond to first order kinetic plots (right Y -axis) in function of polymerization time in min.

### 3.2.2 Characterization of the library of PEO-*b*-PEHOx-*b*-PEtOz

With these optimized conditions, EtOz could now be added directly at a concentration of 0.5M to the still reactive diblock copolymer precursor PEO-*b*-PEHOx cleaned of any trace of EHOx monomer. To obtain the desired length of PEtOz, the polymerization was stopped when the necessary conversion was reached and took between 1 min and 20 min depending on the EtOz length. It was possible to produce a wide variety of ABC triblock copolymers with this one-pot synthesis in less than 2 hours per batch. By using ultrafiltration for purification, it only took an extra 3 hours to fully purify the crude mixture. All triblock copolymers were characterized by $^{1}$H NMR and GPC (Figure 31, Table 5). Figure 31 shows representative GPC

traces of the macroinitiator $PEO_{45}$-Nos, $PEO_{45}$-*b*-$PEHOx_{65}$ and $PEO_{45}$-*b*-$PEHOx_{65}$-*b*-$PEtOz_{19}$. After addition of PEHOx, the trace of $PEO_{45}$-Nos was shifted completely to higher molecular weights showing a successful synthesis of $PEO_{45}$-*b*-$PEHOx_{65}$ with no left-over macroinitiator. Further addition of EtOz resulted in a smaller shift of the trace of $PEO_{45}$-b-$PEHOx_{65}$ to higher molecular weight showing a successful chain-extension. The smaller shift after adding EtOz could be explained with the logarithmic dependency of retention times and molecular weights. All peaks of the $^1$H NMR spectrum of PEO-*b*-PEHOx-*b*-PEtOz (Figure 31) could be assigned to the polymer. The peak at 1.1 ppm could be attributed to the characteristic methyl group of PEtOz, thus proving the successful addition of EtOz. Table 5 comprises the library of synthesized PEO-*b*-PEHOx-*b*-PEtOz with their respective average molecular weight $M_n$, dispersity $Đ_M$ and the total hydrophilic weight fraction, *f,* determined by taking both hydrophilic blocks PEO and PEtOz into account (See formula in Table 5).

As the concentration of monomer got lower and the system was more susceptible to side reactions like chain extension, the linear growth of the polymer disappeared for monomer conversion of higher than 90%. This limited the lowest dispersity obtainable with the investigated systems but it still remained satisfactory between 1.3 and 1.4.

Investigating a broad range of different *f* was essential to obtain a comprehensive self-assembly phase diagram formed with PEO-*b*-PEHOx-*b*-PEtOz: from the most hydrophilic $PEO_{45}$-*b*-$PEHOx_{53}$-*b*-$PEtOz_{56}$ (*f* = 42%) to the most hydrophobic $PEO_{45}$-*b*-$PEHOx_{139}$-*b*-$PEtOz_{10}$ (*f* = 10%).

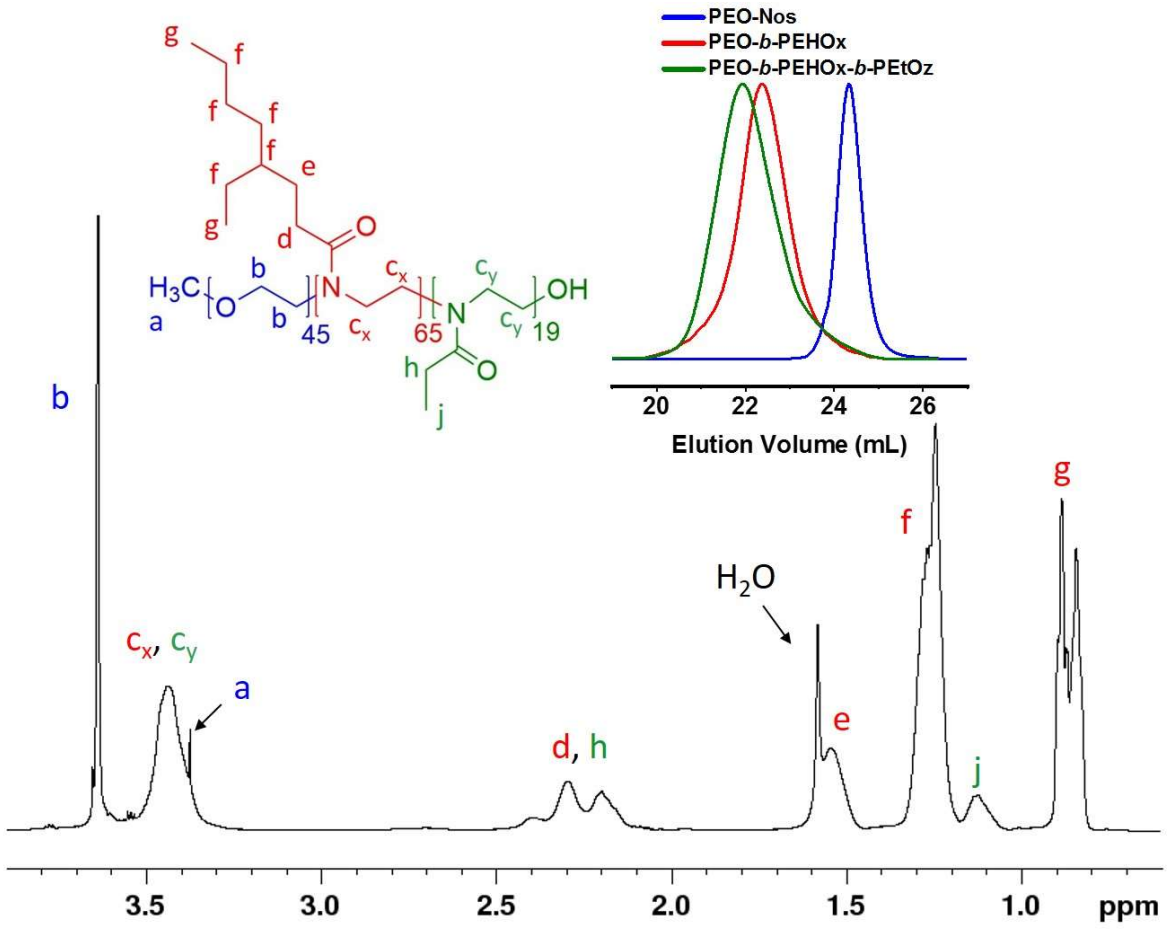


**Figure 31**. Representative NMR ($^1$H, 500 MHz, $CDCl_3$) of $PEO_{45}$-*b*-$PEHOx_{65}$-*b*-$PEtOz_{19}$. All peaks have been assigned to the chemical structure of the polymer with a representative GPC trace ($CHCl_3$) of the starting macroinitiator $PEO_{45}$-Nos (blue), the precursor $PEO_{45}$-*b*-$PEHOx_{65}$ (red) and the resulting triblock $PEO_{45}$-b-$PEHOx_{65}$-b-$PEtOz_{19}$ (green).

**Table 5.** Characterization of PEO-*b*-PEHOx-*b*-PEtOz triblock copolymers using $^1$H NMR, GPC ($CHCl_3$) and hydrophilic weight fraction, *f*. [a]Obtained from $^1$H NMR. [b]Obtained by GPC. [c]Calculated by the equation $f = (M_n(PEO)+M_n(PEtOz))/(M_n(PEO)+M_n(PEHOx)+M_n(PEtOz))$. [d]Ratio Monomer (EHOx) to Initiator (PEO-Nos). [e]SLS not possible for non-monodisperse samples (tubes and polymersomes). For calculations of PEHOx and PEtOz block length, see section A of 7.2.1 in the appendix. The remaining triblock copolymers can be seen in the section B of 7.2.1 in the appendix. For calculations of the length of the polymers segments and their stretching factor, see section 7.2.2 in the appendix.

| $PEO_t$-*b*-$PEHOx_i$-*b*-$PEtOz_g$ | $M_n$ [Da][a] | $Đ_M$[b] | *f* [%][c] | Ratio (Mono/Ini)[d] | $R_h$ [nm] | $R_g$ [nm][e] | $\rho = R_g / R_h$ | $l_{membrane}$ vesicles [nm] (stretching factor) |
|---|---|---|---|---|---|---|---|---|
| $A_{45}B_{30}C_{14}$ | 9300 | 1.31 | 36 | 30 | 79 ± 23 | - | - | - |
| $A_{45}B_{55}C_{8}$ | 13600 | 1.33 | 20 | 50 | 109 ± 14 | 108 ± 5 | 0.99 | - |
| $A_{45}B_{48}C_{10}$ | 12400 | 1.33 | 23 | 50 | 95 ± 10 | 97 ± 4 | 1.02 | 6.3 ± 1.0 (25%) |
| $A_{45}B_{62}C_{12}$ | 15400 | 1.30 | 21 | 60 | 102 ± 9 | 99 ± 5 | 0.97 | - |
| $A_{45}B_{55}C_{13}$ | 14000 | 1.33 | 23 | 60 | 99 ± 11 | 101 ± 5 | 1.02 | - |
| $A_{45}B_{48}C_{14}$ | 12900 | 1.32 | 26 | 50 | 105 ± 16 | 105 ± 4 | 1.00 | - |
| $A_{45}B_{49}C_{17}$ | 12800 | 1.37 | 28 | 50 | 112 ± 11 | 108 ± 6 | 0.96 | - |
| $A_{45}B_{65}C_{19}$ | 16700 | 1.36 | 23 | 60 | 111 ± 13 | 108 ± 7 | 0.97 | 7.8 ± 0.8 |
| $A_{45}B_{54}C_{24}$ | 14900 | 1.39 | 29 | 50 | 106 ± 11 | 109 ± 6 | 1.03 | - |
| $A_{45}B_{56}C_{32}$ | 16200 | 1.41 | 32 | 60 | 98 ± 8 | 96 ± 5 | 0.98 | - |
| $A_{45}B_{62}C_{35}$ | 17700 | 1.37 | 31 | 60 | 104 ± 14 | 102 ± 4 | 0.98 | 8.2 ± 1.0 (23%) |
| $A_{45}B_{53}C_{56}$ | 18000 | 1.38 | 42 | 50 | 21 ± 7 | - | - | - |
| $A_{45}B_{87}C_{10}$ | 20100 | 1.39 | 15 | 90 | 108 ± 19 | 103 ± 6 | 0.95 | 9.9 ± 0.9 (22%) |
| $A_{45}B_{96}C_{11}$ | 22000 | 1.39 | 14 | 90 | 114 ± 28 | 106 ± 7 | 0.93 | - |
| $A_{45}B_{138}C_{14}$ | 30500 | 1.47 | 11 | 140 | 476 ± 175 | -[e] | -[e] | - |
| $A_{45}B_{139}C_{10}$ | 30300 | 1.45 | 10 | 140 | 568 ± 156 | -[e] | -[e] | 12.9 ± 1.5 (18%) |

## 3.3 Results and discussions part II: Self-assembly of PEO-*b*-PEHOx-*b*-PEtOz

### 3.3.1 Formation of the self-assemblies: film rehydration and solvent switch

The self-assembly of PEO-*b*-PEHOx-*b*-PEtOz polymers in aqueous solution was studied using two different techniques: film rehydration (FR) and solvent switch (SS). The final concentration of the self-assembled polymer was always set to 0.2 w/w%. For film rehydration, the polymer solutions were stirred extensively for one week as a stirring time of only one day only resulted mostly in a precipitated polymer. For solvent switch, the self-assemblies were completely formed at the end of the dialysis step after 2 days. Further stirring did not yield any change in the self-assemblies.[65] All self-assemblies were analysed via TEM and DLS and polymersomes were further characterized by SLS and Cryo-TEM (Figure 34 and Table 5).

Using solvent switch, monodisperse micelles ($R_h$= 13 ± 1 nm, Figure 32) were obtained for all triblock copolymers but $A_{45}B_{87}C_{10}$, $A_{45}B_{96}C_{11}$, $A_{45}B_{138}C_{10}$ and $A_{45}B_{139}C_{10}$. With hydrophilic weight fractions, *f*, between 10% and 15%, they could not self-assemble with this method, forming only aggregates and polymer film as observed by TEM (Figure 33). The study was then focused on film rehydration as it yielded more diverse and interesting structures, most notably polymersomes.

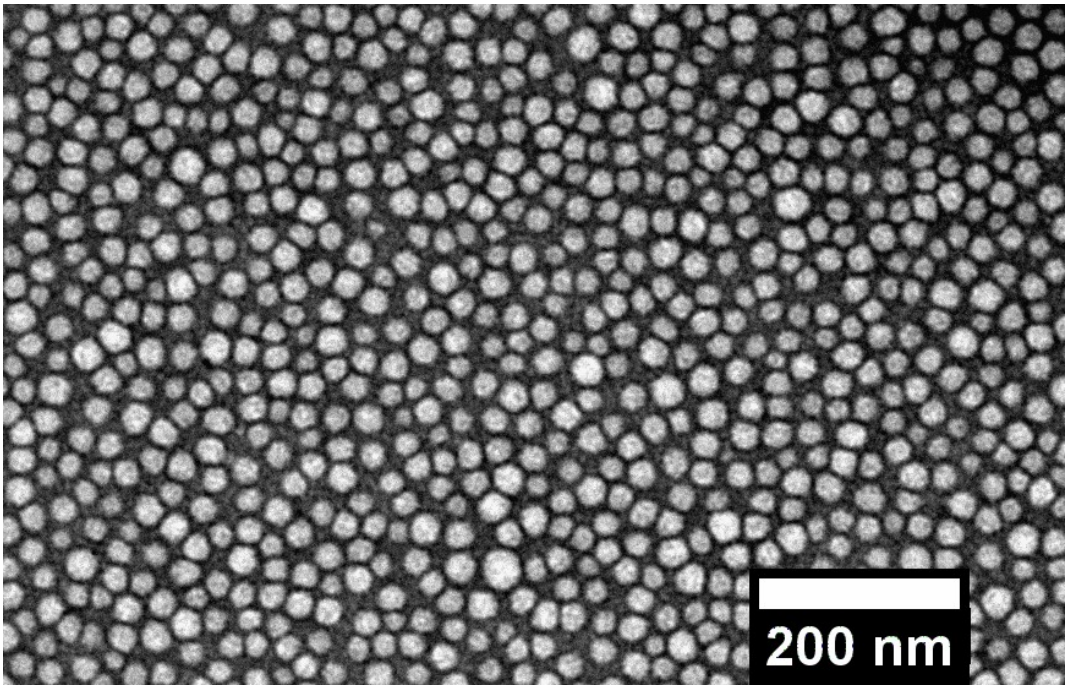


**Figure 32.** Representative TEM image of micelles formed by solvent switch of $PEO_{45}$-*b*-$PEHOx_{65}$-*b*-$PEtOz_{19}$.

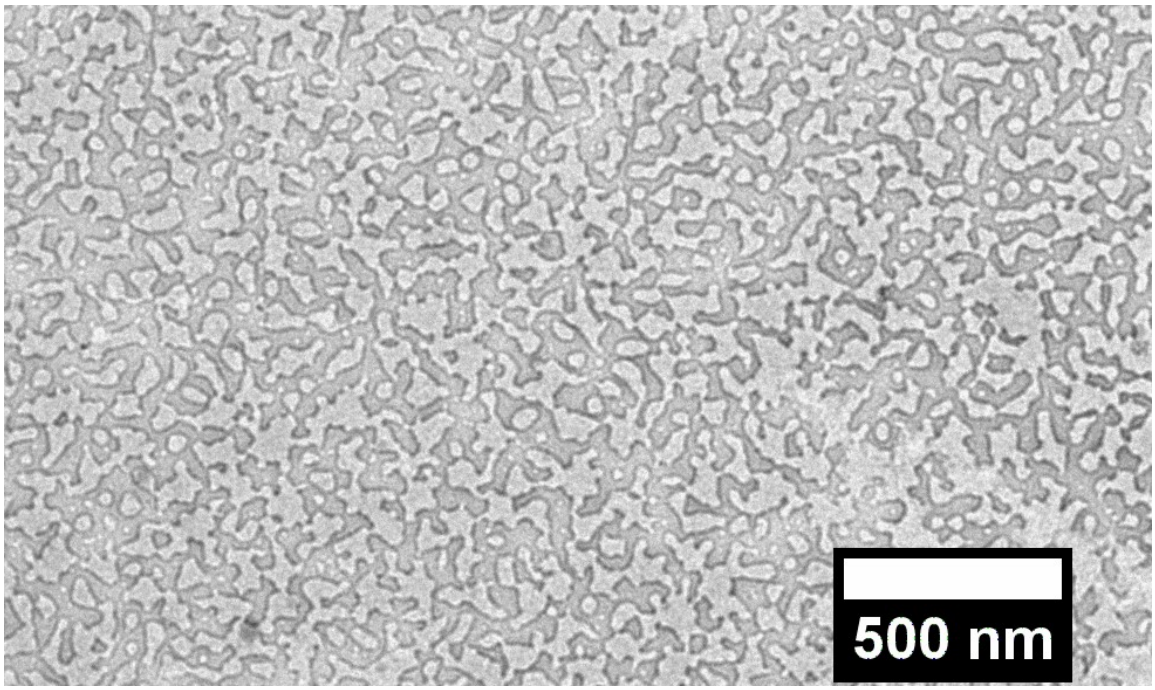


**Figure 33**. Representative TEM image of polymer films observable after solvent switch of $PEO_{45}$-*b*-$PEHOx_{138}$-*b*-$PEtOz_{14}$.

### 3.3.2 Micelles and worms

The self-assembly of $A_{45}B_{53}C_{56}$ ($f$ = 42%) also led to the formation of micelles (Figure 34.E, $R_h$= 21 ± 7 nm) when film rehydration was used. Those micelles exhibited a higher dispersity in size than the one formed by solvent switch ($R_h$= 11 ± 1 nm). This is in accordance with the differences highlighted previously in our previous work between film rehydration and solvent switch.[65] Film rehydration is a top-down approach which leads to kinetically stable structures while solvent switch, a bottom-up approach which yields more thermodynamically favoured structures. The copolymer $A_{45}B_{30}C_{14}$ ($f$ = 36%) self-assembled into worms, which are elongated micelles, as revealed by TEM (Figure 34.D). This explained the surprisingly high $R_h$ determined by DLS which also indicated a high polydispersity in sizes ($R_h$= 79 ± 23). Indeed, the hydrodynamic radius measurements are based on spherical models and are not adapted to complex cylinder-like shapes. This led to a discrepancy to the dimensions observed in several TEM images, revealing an average worm thickness of 13.9 ± 1.8 nm and typical worm's lengths between 50 and 400 nm.

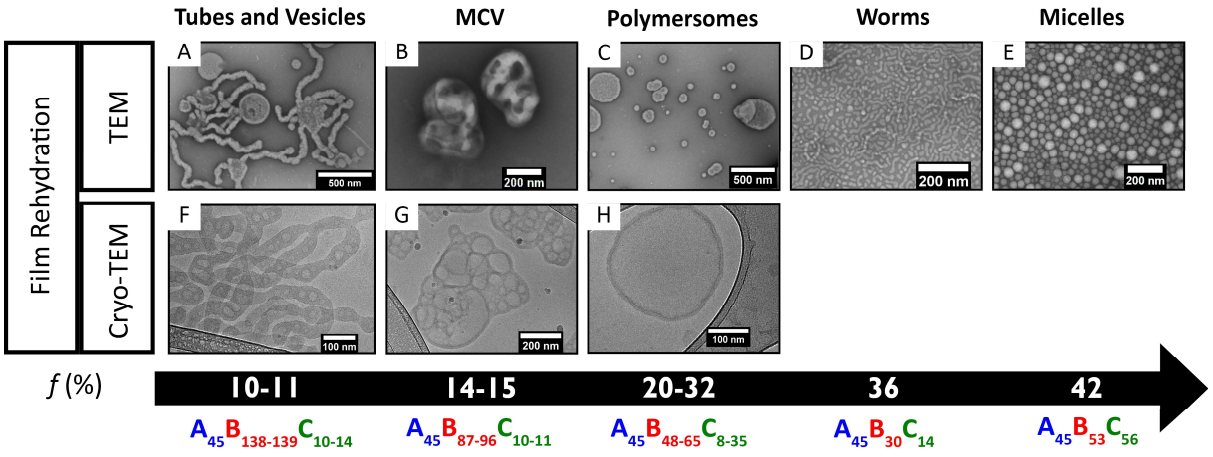


**Figure 34**. TEM (A-E) and Cryo-TEM (F-H) images of the self-assemblies formed by film rehydration of ABC triblock copolymers PEO-*b*-PEHOx-*b*-PEtOz for increasing hydrophilic weight fraction, *f*. MCV= Multicompartment Vesicles. Supplementary and in higher resolution Cryo-TEM images can be seen for polymersomes in Figure 52, for MCV in Figure 53 and in Figure 54 for tubes and vesicles in the appendix.

### 3.3.3 Polymersomes

Nanoscopic polymersomes were formed using self-assembly by film rehydration with a wide range of ABC triblock copolymers, $A_{45}B_{48\text{-}65}C_{8\text{-}35}$ ($f$ = 20-32%). The vesicles were formed in homogenous phases but showed a large dispersity in sizes. DLS measurements revealed $R_h$ values between 200 and 400 nm. In order to narrow down the size distribution and obtain a reliable characterization by SLS, the samples were extruded through a 200 nm membrane. By combining data from SLS with data from DLS, it was possible to confirm the suspected morphology of self-assembled structures, i.e. polymersomes. As an example, self-assemblies from $A_{45}B_{49}C_{17}$, exhibited an $R_h$ after extrusion of 112 ± 11 nm. Following a SLS experiment exploiting the MIE model, a radius of gyration ($R_g$) of 108 ± 6 nm was calculated (Figure 35). When dividing $R_g$ by $R_h$, the form factor $\rho$ was obtained. This structure property reflected the radial density distribution of a particle. The typical value for hollow spheres with an infinitely thin membrane, i.e. polymersomes, is 1.0.[57, 126] For $A_{45}B_{49}C_{17}$, a resulting $\rho$ of 0.97 indicated the formation of polymersomes. For the other ABC triblocks, similar results were obtained as $\rho$ values oscillated around 1.0, from 0.96 for $A_{45}B_{49}C_{17}$ to 1.03 for $A_{45}B_{54}C_{24}$.

The presence of polymersomes was further confirmed by TEM as the typical topology for vesicles in TEM was found (Figure 34.C and Figure 36 for higher resolution). Under the vacuum of TEM, this kind of soft and hollow self-assembly is flattened and folds onto itself displaying a characteristic wrinkled structure.[66] On top of that, a white halo was observable at the edge of the structures and suggested the presence of a membrane (Figure 37).

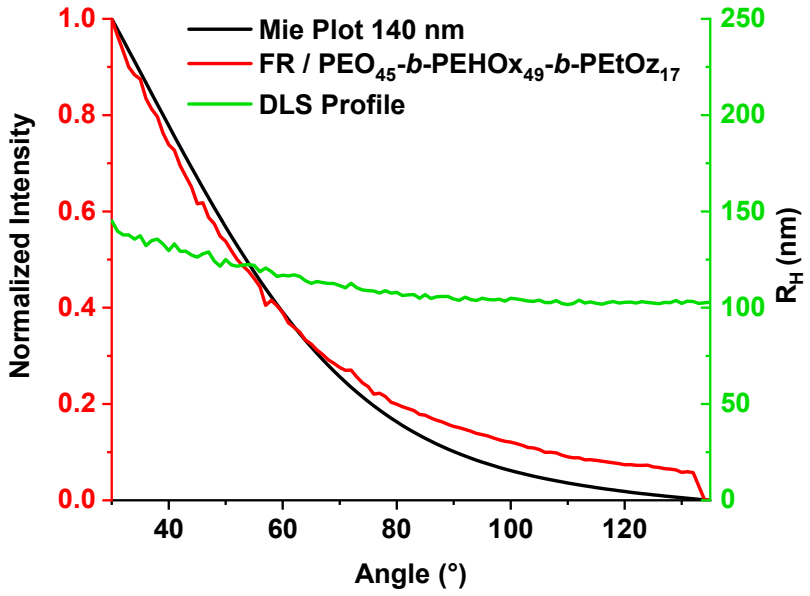


**Figure 35.** Representative MIE plot and DLS profile of ABC triblock, here $PEO_{45}$-*b*-$PEHOx_{49}$-*b*-$PEtOz_{17}$. $R_g$ of 108 nm was calculated from the MIE Plot fit at 140 nm.

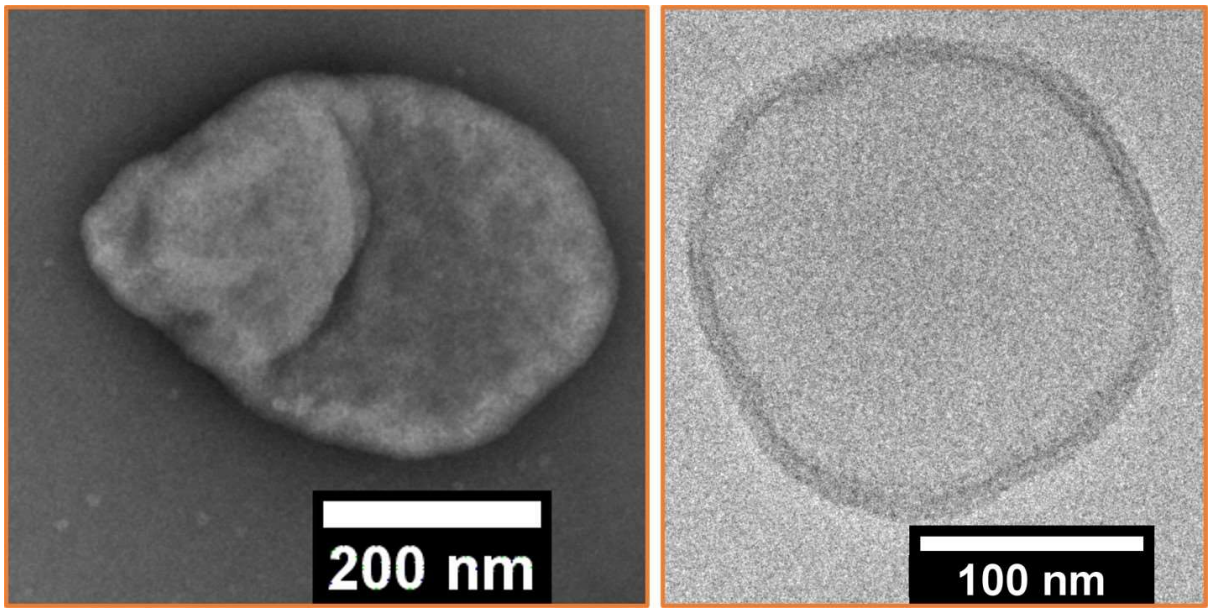


**Figure 36**. Representative TEM and Cryo-TEM images of polymersomes formed by film rehydration of $PEO_{45}$-*b*-$PEHOx_{48\text{-}65}$-*b*-$PEtOz_{8\text{-}35}$.

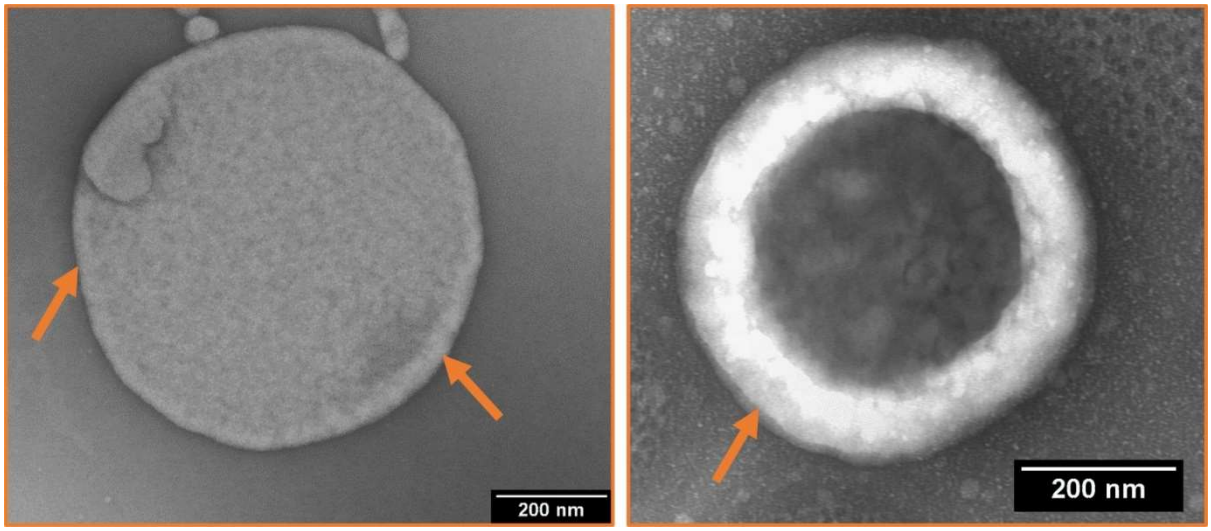


**Figure 37**. Representative TEM images of polymersomes formed by film rehydration of $PEO_{45}$-*b*-$PEHOx_{48\text{-}65}$-*b*-$PEtOz_{8\text{-}35}$ (left) and $PEO_{45}$-*b*-$PEHOx_{138\text{-}139}$-*b*-$PEtOz_{10\text{-}14}$ (right). The orange arrows highlight the white halo of contrast that suggests the presence of a membrane.

Due to the negative staining, it was not possible to determine the membrane thickness. To measure the membrane thickness, visualize the polymersomes in their native environment and ultimately prove their formation, Cryo-TEM was conducted on self-assemblies of selected ABC triblocks, namely $A_{45}B_{48}C_{10}$, $A_{45}B_{65}C_{19}$ and $A_{45}B_{62}C_{35}$ (Figure 34.H, Figure 36 and Figure 52 for supplementary Cryo-TEM images in the appendix). $A_{45}B_{48}C_{10}$ and $A_{45}B_{65}C_{19}$ were chosen to compare the membrane thicknesses of their resulting polymersomes, 48 units of PEHOx being the shortest PEHOx block forming polymersomes and 65 units of PEHOx being the longest. $A_{45}B_{62}C_{35}$ was chosen as it has the longest PEtOz block while having a comparable PEHOx length to $A_{45}B_{65}C_{19}$. Cryo-TEM confirmed hollow spheres (polymersomes) from all of these ABC triblocks. Using several Cryo-TEM images, the membrane thicknesses were determined, $A_{45}B_{48}C_{10}$ - $l_{membrane}$= 6.3 ± 1.0 nm, $A_{45}B_{65}C_{19}$ - $l_{membrane}$= 7.8 ± 0.8. It suggested a dependency between the block of length of the hydrophobic block, EHOx, and the membrane thickness. $A_{45}B_{62}C_{35}$ had a membrane thickness of 8.2 ± 1.0, which was comparable to the membrane thickness of $A_{45}B_{65}C_{19}$ and showed that a longer block of PEtOz neither significantly influenced

the thickness of the membrane nor prevented the formation of polymersomes. Due to the values on membrane thickness from Cryo-TEM, these values could not be put in perspective to the hydrophobic polymer PEHOx segments of the polymer chains. Comparing the theoretical length of PEHOx as a random coil and in a stretched conformation, both polymersomes had a mixed conformation due to the branched side chain of PEHOx. The polymers were stretched by a similar percentage (25% for $A_{45}B_{48}C_{10}$ and 23% for $A_{45}B_{65}C_{19}$, see section 7.2.2 in the appendix) in both instances. This is also reflected by the small difference in membrane thickness measured by Cryo-TEM. Hence, the hydrophobic polymer PEHOx showed a similar overall conformation on both ends of polymersome-forming triblocks and by extension in all the studied polymersomes. The lower amount of stretching for the longer polymer was noted, but could easily be due to statistical deviations.

### 3.3.4 Multicompartment vesicles

The self-assembly of $A_{45}B_{87}C_{10}$ and $A_{45}B_{96}C_{11}$ formed multicompartment vesicles (MCV). With DLS and SLS measurements indicating that those self-assemblies were hollow spheres ($R_h$ = 108 ± 19, $\rho$ = 0.95, $R_h$= 114 ± 28, $\rho$ = 0.93, respectively), those structures were at initially presumed to be regular polymersomes. But the TEM images revealed a more complex structure (Figure 34.B and Figure 38 for higher resolution). Besides being non-spherical, compared to the characteristic morphology of polymersomes, the images showed more irregular contrast and wrinkles which hinted at the presence of more than one hollow cavity as it was previously observed for PEO-*b*-PEHOx forming pseudo-vesicles structures.[65] Cryo-TEM images unveiled these structures to be multicompartment vesicles (Figure 34.G, Figure 38 for higher resolution and Figure 53 for supplementary Cryo-TEM images in the appendix). A regular membrane of constant thickness ($l_{membrane}$ = 9.9 ± 0.9 for $A_{45}B_{87}C_{10}$) in between numerous cavities could be observed. Following the same calculations as for the

polymersomes, the PEHOx in the self-assembled $A_{45}B_{87}C_{10,}$ showed a conformation which was 22% stretched. Similar to the polymersomes, the yet longer PEHOx segments leaned more towards the random coil and were less stretched, and yielded a small increase in membrane thickness. However, the differences were still too small to act as proof and only hinted a possible tendency.

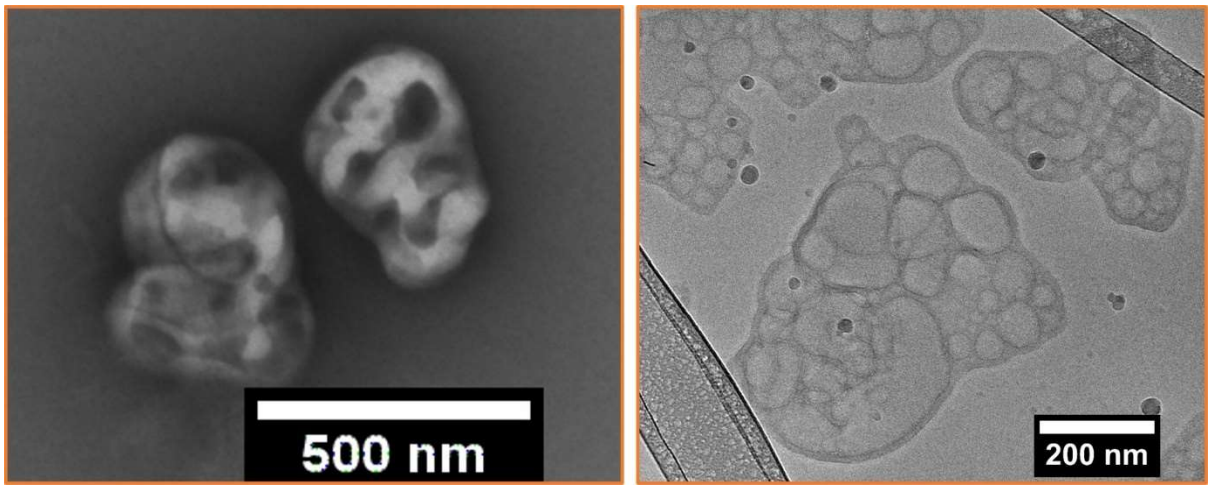


**Figure 38.** Representative TEM and Cryo-TEM images of multicompartment vesicles formed by film rehydration of $PEO_{45}$-*b*-$PEHOx_{87\text{-}96}$-*b*-$PEtOz_{10\text{-}11}$.

### 3.3.5 Polymersomes and Tubes

$A_{45}B_{138}C_{14}$ and $A_{45}B_{139}C_{10}$ were the only copolymers to not form pure phases by self-assembly. Both of them formed polymersomes and tubes, which are elongated polymersomes. TEM images confirmed both by showing the presence of typical structures resembling tubes and polymersomes (Figure 34.A and Figure 39). The tubes showed a typical length being between 1000 and 3000 nm. Polymersomes of these ABC triblocks showed a white halo on the edge, which was the same difference of contrast as previously observed for shorter ABC triblocks like $A_{45}B_{65}C_{19}$. However, it appeared to be significantly bigger for the longer ABC triblocks which already suggested polymersomes with thicker membranes (Figure 37). Due to the

presence of two distinct populations, polymersomes and tubes, and the subsequent inhomogeneity, only DLS and not SLS was conducted ($A_{45}B_{138}C_{14}$, $R_h$ = 476 ± 175 nm and $A_{45}B_{139}C_{10,}$ $R_h$ = 568 ± 156 nm). The large polydispersity in sizes prohibited the use of SLS on these samples. With Cryo-TEM, the formation of the polymersomes with a thicker membrane ($l_{membrane}$=12.9 ± 1.5) was proven. Similar to above, this allowed for a calculation on the conformation of the PEHOx segments with the polymersome membranes. The polymers were 18% stretched for $A_{45}B_{139}C_{10}$, which finally confirmed the suggested trend that longer PEHOx chains were more densely packed than shorter ones. Cryo-TEM also allowed for a visualisation of the inner structure of the tubes. Their width vary (Overall thickness = 43 ± 12 nm) and they were all filled with a myriad of spherical hollow cavities which are homogenous in sizes (R = 12.6 ± 2.2 nm). This is very much in between the stretched conformations of PEO-45 (16.0 nm, 74% stretched at 12.6 nm) and PEtOz (3.5 nm), suggesting that these cavities were filled with hydrated and mostly stretched hydrophilic polymer segments of both kinds.

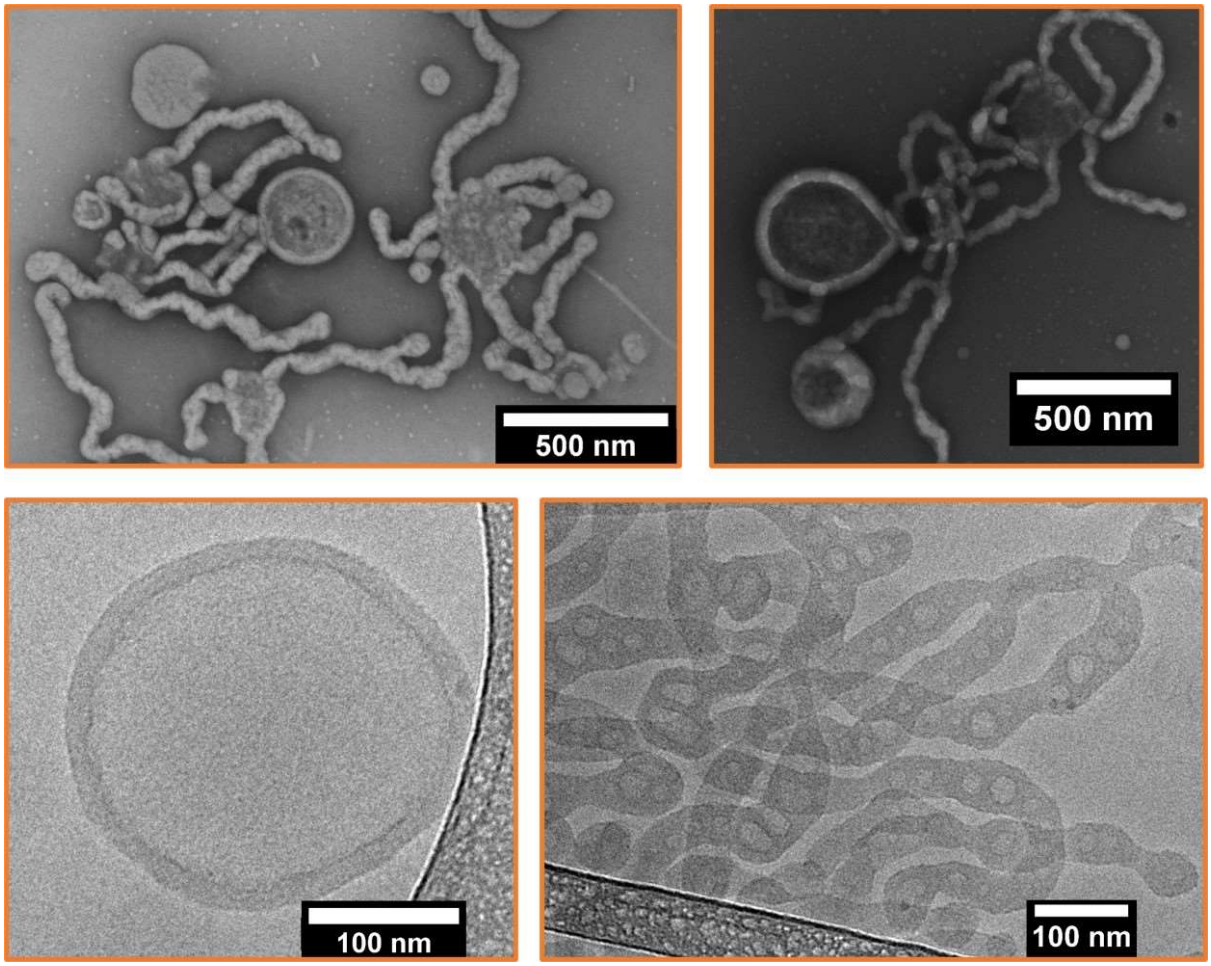


**Figure 39**. Representative TEM and Cryo-TEM images of tubes and vesicles formed by film rehydration of $PEO_{45}$-*b*-$PEHOx_{138\text{-}139}$-*b*-$PEtOz_{10\text{-}14}$.

### 3.3.6 Self-assembly phase diagram of PEO-*b*-PEHOx-*b*-PEtOz

All results for film rehydration were summarized in a self-assembly phase diagram (Figure 40). The diagram emphasizes the wide range of self-assembled structures which were possible with this ABC triblock copolymer and could only be proven using a combination of DLS, SLS, TEM and Cryo-TEM as complimentary analytical methods. Furthermore, solvent switch produced micelles which are much more monodisperse in terms of size compared to ones from film rehydration. Solvent switch allowed for targeting an additional self-assembly structure with the same copolymer, for example for $A_{45}B_{65}C_{19}$ which resulted either in micelles

(solvent switch) or in polymersomes (film rehydration). This showed the importance of using various self-assembly techniques to unlock more potential applications of amphiphilic block copolymers. As previously shown[65], the branched side chain of PEHOx allowed for unique and distinct structures like the multicompartment vesicles reported in here. They confirmed the intriguing influence of the side chain of PEHOx to form such complex self-assemblies.

Among the obtained self-assembled structures formed, polymersomes were of interest due to the ability of their membrane to confine aqueous media. ABC polymersomes were especially intriguing because their membrane can be asymmetric and therefore can mimic the natural orentiation of cell membrane[34-35, 103]. To probe the asymmetry in the case of PEO-*b*-PEHOx-*b*-PEtOz polymersomes, this study focused on $A_{45}B_{48\text{-}65}C_{8\text{-}35}$, as they produce pure phases of polymersomes and the dependence of the asymmetry on PEtOz block length could be studied in detail.

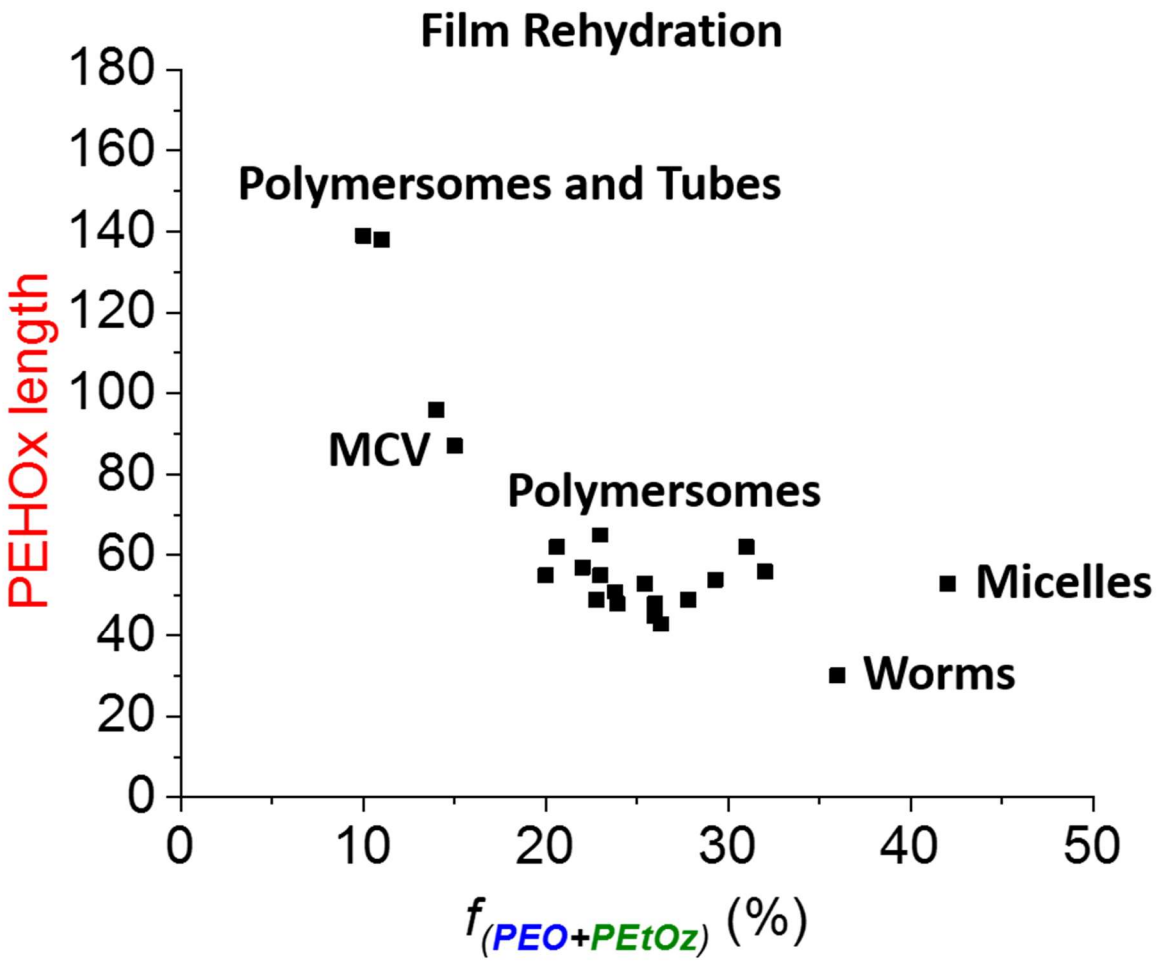


**Figure 40.** Self-Assembly Phase diagram of PEO-b-PEHOx-*b*-PEtOz using film rehydration. MCV=Multicompartment Vesicles.

## 3.4 Results and discussions part III: Orientation of PEO-b-PEHOx-b-PEtOz chains in the membrane of polymresomes

Polymersomes formed by ABC copolymers with two different hydrophilic blocks (A, C) can result in polymersomes with 3 different scenarios with respect to the orientation of their hydrophilic blocks: either A is outside, C is outside or there is a mix of A and C on the inside and outside (Figure 29). One way to have a preferred orientation and create an asymmetric membrane, is to tailor the length of the A and C blocks. If one is significantly longer, it would

prefer to segregate on the outer surface of the membrane due to a larger radius of curvature and steric hindrance while the shorter segment would remain inside. This approach proved to be successful for the ABC triblocks PEO-*b*-PDMS-*b*-PMOXA[55] and PEO-*b*-PCL-*b*-PMOXA[34] where the orientation could even be flipped by modifying one block with a large molecule.[2]

### 3.4.1 First method: BCA assay

To show the presence of a longer PEtOz block on the surface of PEO-*b*-PEHOx-*b*-PEtOz polymersomes, the composition on the surface was tested using a difference in the chemical composition of PEO and PEtOz. Bicinchoninic acid assay (BCA), an assay to measure peptide concentration, was used to detect only PEtOz since polyoxazolines as quasi-polypeptides, contain amide bonds while the polyether PEO does not. This assay is based on the reduction of $Cu^{2+}$ to $Cu^{+}$ by a peptide bond in alkaline medium and its further complexation with bicinchoninic acid yielding a purple complex with a maximum absorbance at 562 nm. All results for each category of polymers are summed up in Figure 41. $PEO_{45}$(2kDa) yielded a small base signal (0.105 ± 0.003) due to the lack of peptide-like bonds and the results were coherent with Konishcheva *et al.*[34] AB diblock copolymers $PEO_{45}$-*b*-$PEHOx_{40}$, $PEO_{45}$-*b*-$PEHOx_{46}$, $PEO_{45}$-*b*-$PEHOx_{57}$ and $PEO_{45}$-*b*-$PEHOx_{62}$ were selected to have similar repeating units of EHOx to the ABC triblock copolymer forming polymersomes. AB diblock copolymer yielded a signal higher than $PEO_{45}$ (0.163 ± 0.009) due to a small reactivity of PEHOx. Despite being hydrophobic PEHOx was still able to react mildly to the BCA assay as the PEHOx block is not completely covered. This control signal of a pure PEO outer leaflet was similar to all polymersomes from ABC triblocks with a block length of C(EtOz) inferior to 32 units (0.167 ± 0.010). These comparable signals (0.163 ± 0.009 and 0.167 ± 0.010), were a strong indicator that polymersomes formed from these ABC triblocks had an outer leaflet purely of PEO and no PEtOz. This was further confirmed by a sharp increase in absorbance for all triblocks with

C(EtOz) superior or equal to 32 units (0.458 ± 0.072). This sharp increase for self-assemblies from ABC triblocks like $A_{45}B_{56}C_{32}$ indicated that the orientation transitioned from asymmetric (A outside and C inside) to either a mixed phase between A and C or a reverse asymmetric orientation with purely C on the outer leaflet. In an effort to shed more light on this orientation, a BC diblock copolymer, $PEHOx_{60}$-*b*-$PEtOz_{34}$, was synthetized to compare with a control signal of a pure EtOz outer leaflet for similar repeating units of EHOx. This BC diblock copolymer yielded a signal significantly higher (0.935 ± 0.107). Both polymersomes from triblocks with C(EtOz) superior or equal to 32 units can be estimated to be about 40%. Taking the signal from $PEHOx_{60}$-*b*-$PEtOz_{34}$ as the reference when 100% of PEtOz is outside and the signal AB diblock copolymers as the reference when 0% of PEtOz is outside, the percentage of PEtOz outside could be calculated and was rounded to the next 5% to respect measurements errors.

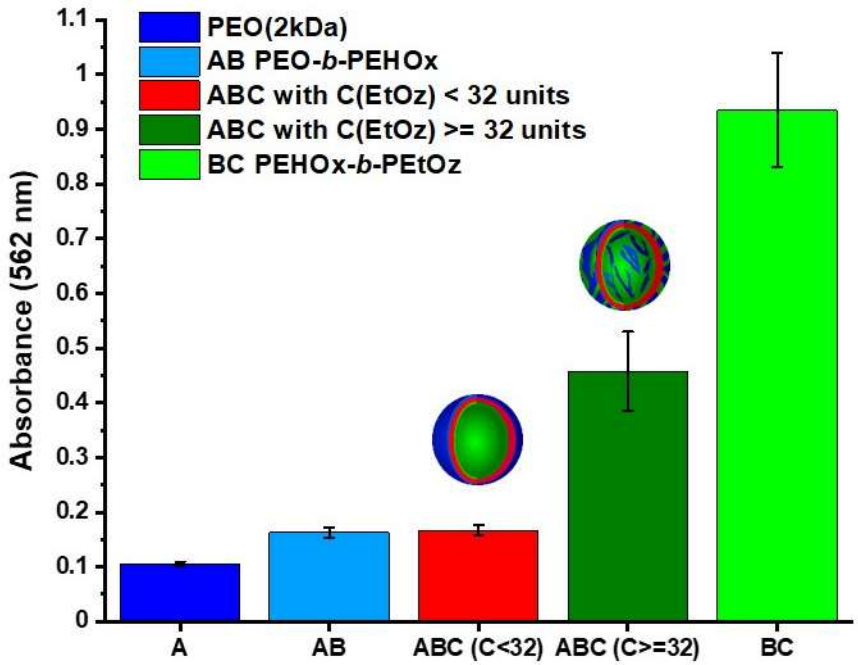


**Figure 41.** Absorbance (562 nm) of the supernatant after conducting BCA assay on PEO(2kDA) (A block only), PEO-*b*-PEHOx (AB diblock copolymers), PEHOx-*b*-PEtOz (BC diblock copolymer) and PEO-*b*-PEHOx-*b*-PEtOz (ABC triblocks). The graphs represent mean values measured over various samples. For AB: $A_{45}B_{40\text{-}62}$. For ABC(C<32): $A_{45}B_{48\text{-}65}C_{8\text{-}24}$. For ABC (C≥32): $A_{45}B_{56\text{-}62}C_{32\text{-}35}$. For BC: $B_{60}C_{34}$.

### 3.4.2 Second method: 2D-$^{1}$H-NOESY NMR in $D_2O$ of polymersomes

In addition to the approach discussed above, $^{1}$H-NMR and 2D-$^{1}$H-NOESY-NMR was used to determine the 3D spatial correlations and hydrogen bonding interactions between the two hydrophilic blocks A and C in polymersomes.[89-90] The NMR spectra were recorded in $D_2O$ of polymersomes from a representative ABC triblock with C(EtOz) inferior to 32 units in length, $A_{45}B_{54}C_{24}$, and with C(EtOz) equal or superior to 32 units in length, $A_{45}B_{56}C_{32}$ (Figure 42). The peaks of interest in the $^{1}$H NMR spectra were the ones at 3.60 ppm of the backbone of PEO (b in Figure 42, 3.60 ppm) and the overlapping peaks at 0.96 ppm of the methyl group of the side chain of PEtOz (j in Figure 42, 0.96 ppm) and the protons of the side chain of PEHOx (f in Figure 42, 0.96 ppm).

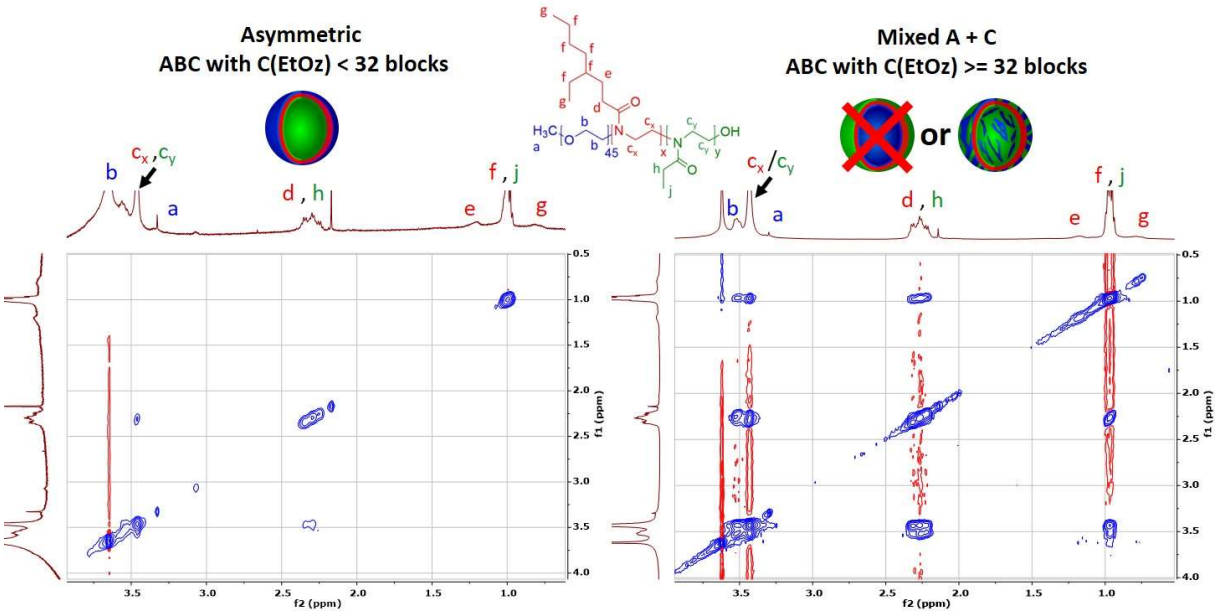


**Figure 42.** Representative 2D-$^{1}$H-NOESY NMR in $D_2O$ of (left) asymmetric polymersomes from ABC triblock copolymers PEO-*b*-PEHOx-*b*-PEtOz with EtOz length less than 32 blocks, here $PEO_{45}$-*b*-$PEHOx_{54}$-*b*-$PEtOz_{24}$ and (right) mixed A and C polymersomes from ABC triblock copolymers PEO-*b*-PEHOx-*b*-PEtOz with EtOz length equal or superior to 32 units of PEtOz, here $PEO_{45}$-*b*-$PEHOx_{56}$-*b*-$PEtOz_{32}$.

Comparing the intensity of both peaks (Figure 43), the ratio for $A_{45}B_{54}C_{24}$ ($I_{PEO}/I_{PEHOx+PEtOz}$= 13) was significantly higher than for $A_{45}B_{56}C_{32}$ ($I_{PEO}/I_{PEHOx+PEtOz}$=1.86). It suggested that PEO was located at the outside of the polymersomes in the case of $A_{45}B_{54}C_{24}$ while both PEHOx and PEtOz were shielded, which was very much in line with the results from the BCA assay. As for $A_{45}B_{56}C_{32}$, it hinted a mixture of PEO and PEtOz on the outer leaflet of the polymersome membrane. Considering that the polymer had similar amount of PEHOx and PEO but an increased amount of PEtOz, the difference observed in the NMR spectra could be associated with PEtOz and not PEHOx although it contributed to the signal at 0.96 ppm. PEtOz was thus not shielded anymore, suggesting it was now also located outer leaflet of the polymersome membrane. Since the PEO signal was still present, a mixed surface of both polymers could be assumed.

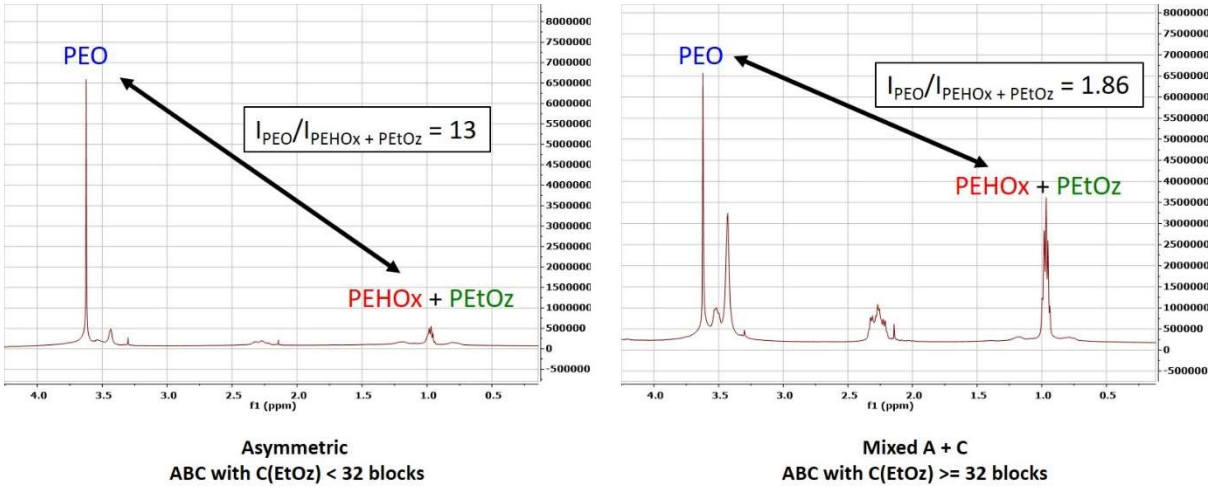


**Figure 43**. Representative $^1$H NMR Spectra in $D_2O$ of polymersomes formed by film rehydration with ABC triblock with C(EtOz) inferior to 32 blocks, here $PEO_{45}$-*b*-$PEHOx_{54}$-*b*-$PEtOz_{24}$ (left) and with ABC triblock with C(EtOz) superior or equal to 32 blocks, here $PEO_{45}$-*b*-$PEHOx_{54}$-*b*-$PEtOz_{32}$ (right). The ratio of the intensity of the peak at 3.60 ppm of the backbone of PEO (3.60 ppm) and the intensity of the overlapping peaks at 0.96 ppm of the methyl group of the side chain of PEtOz (0.96 ppm) and the protons of the side chain of PEHOx (0.96 ppm) is calculated and compared.

The 2D-$^{1}$H-NOESY NMR confirmed this assumption as it showed cross signals between the methylene protons of the side chain of PEtOz (j in Figure 42, 0.96 ppm) and the backbone of PEO (b in Figure 42, 3.60 ppm) for $A_{45}B_{56}C_{32}$ but not for $A_{45}B_{54}C_{24}$. This proved that PEO and PEtOz were able to interact with each other for $A_{45}B_{56}C_{32}$. Further cross signals between the methyl protons of the side chain of PEtOz (j in Figure 42, 0.96 ppm), the protons of the backbone of PEtOz ($c_y$ in Figure 42, 3.43 ppm) and the methylene protons of the side chain of PEtOz (h in Figure 42, 2.24 ppm) were again exclusive to $A_{45}B_{56}C_{32}$. This was the final confirmation that both, PEtOz and PEO, were located on the outer leaflet of the membrane in the case of $A_{45}B_{56}C_{32}$ forming a mixed surface with about 40% of PEtOz estimated outside. For $A_{45}B_{54}C_{24}$, however, PEtOz was located inside and remained shielded while PEO was located outside thus forming an asymmetric polymersome.

These results were even more striking as they overlap with previous research on asymmetric polymersomes from PEO-*b*-PCL-*b*-PMOXA. Polymersomes from that ABC triblock also showed either a pure PEO phase on the outer leaflet on the membrane, or a mixed one with PEO and PMOXA. A pure PMOXA surface was not observed when screening several unmodified PEO-*b*-PCL-*b*-PMOXA ABC triblocks.[2, 34]

## 3.5 Conclusions

A library of novel amphiphilic asymmetric PEO-*b*-PEHOx-*b*-PEtOz ABC triblock copolymers with different PEHOx and PEtOz block lengths were synthetized in a one-pot synthesis. The sequential polymerisation started from a PEO-Nos macroinitiator where EHOx and EtOz were added one after the other. The synthesis was well-controlled, producing a large array of ABC triblocks with 45 units of PEO, PEHOx up to 139 units and PEtOz with up to 56 units in less

than 2 hours. Self-assembly by solvent switch predominantly led to the formation of monodisperse micelles. Using film rehydration, the formed nanostructures followed the established self-assembly theory. With decreasing hydrophilic weight fraction *f,* the self-assembly structures started from micelles, followed by worms as elongated micelles then polymersomes and then multicompartment vesicles (MCV). Finally, tubes as elongated vesicles finished this textbook series of self-assembly structures. However, no pure phases of tubes were formed, but also polymersomes with notably thicker membrane. All those structures were analysed in-depth using dynamic and static light scattering, TEM and Cryo-TEM. MCVs formed by PEO-*b*-PEHOx-*b*-PEtOz echoed to its diblock precursor PEO-*b*-PEHOx which could also form complex structures like multicompartment micelles and yolk/shell nanoparticles. This confirmed the potential of PEHOx in self-assembly to obtain complex nanoparticles from a single material as it is a hydrophobic block with a long branched side chain. Comparing the measured membrane thickness with the theoretical length of the PEHOx segments, it became evident that PEHOx was predominantly in a random coil state and only partially stretched to the special requirements of the side chain. With growing chain length, this stretching decreased from 25% for 48 repeating units to 18 % for 138 units. Nanoscale polymersomes assembled from $PEO_{45}$-*b*-$PEHOx_{48\text{-}65}$-*b*-$PEtOz_x$ exhibited an asymmetric orientation of the membrane for a PEtOz length lower than 32 units as proven by two independent methods, namely BCA assay and 2D-$^1$H-NOESY NMR. The same methods proved that a mixed phase of PEO and PEtOz was located outside of the polymersomes for PEtOz longer or equal to 32 units. Coupled with the peptide-like nature of the membrane formed with PEHOx as an oxazoline, this preferred orientation opens new opportunities toward directed insertion of transmembrane proteins into asymmetric polymersomes.

# 4. Conclusions

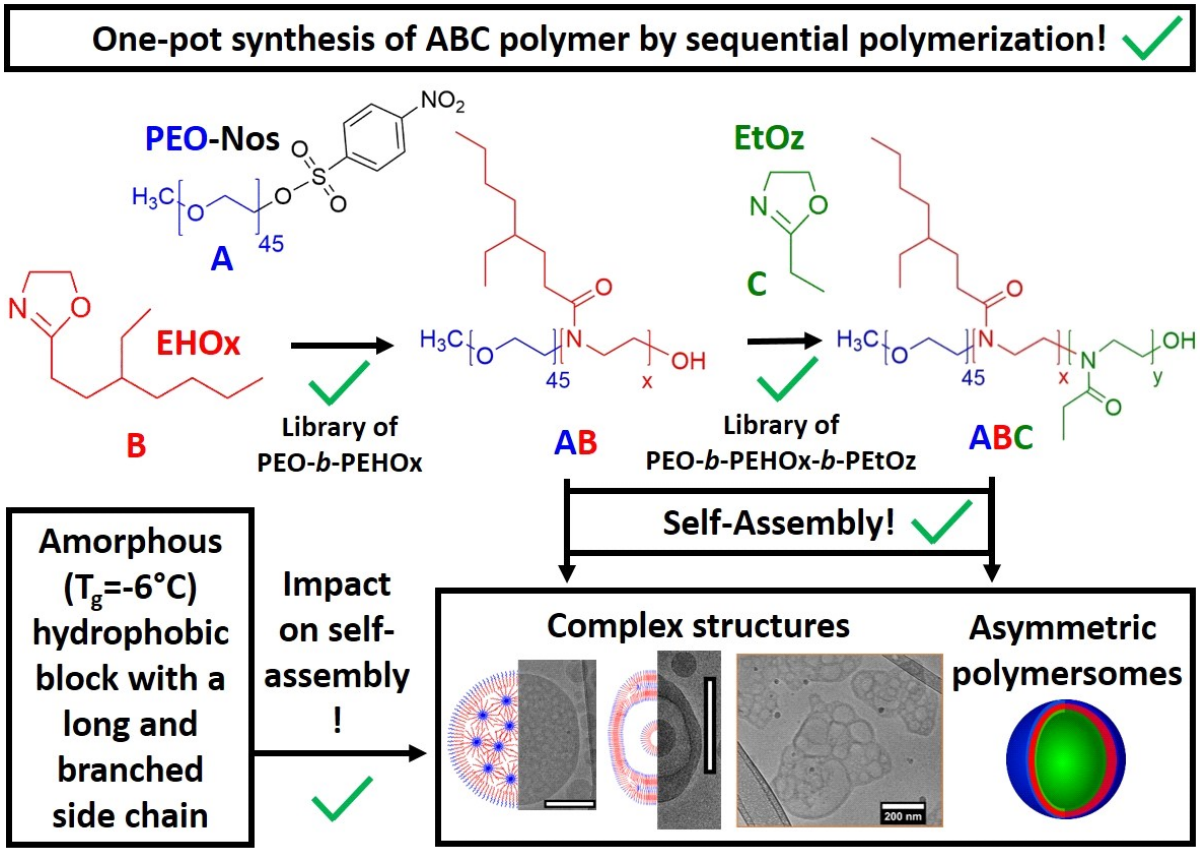


**Figure 44**. Graphical abstract of the conclusion of this thesis.

Using a new nosylate-based PEO macroinitiatior, novel amphiphilic diblock copolymers PEO-*b*-PEHOx with different PEHOx block length were synthetized efficiently *via* microwave-assisted polymerization. Their self-assembly in aqueous solutions was studied in-depth by two different methods: film rehydration and solvent switch. PEO-*b*-PEHOx design with a long and branched hydrophobic block, PEHOx, proved to be very impactful on its self-assembly. We managed to show one of the rare examples of various complex structures self-assembled from a single AB polymer: multicompartment micelles (MCMs), pseudo-vesicles and yolk/shell nanoparticles. This showed the potential of such hydrophobic blocks to obtain complex nanoparticles from a single material.

Building upon our previous work on PEO-*b*-PEHOx to reach a higher level of complexity, a library of novel amphiphilic ABC triblock copolymers PEO-*b*-PEHOx-*b*-PEtOz with different PEHOx and PEtOz was obtained *via* a controlled one-pot synthesis. The characterization of their self-assembly in aqueous solutions led us to the following conclusions. By solvent switch PEO-*b*-PEHOx-*b*-PEtOz predominantly form monodisperse micelles while by film rehydration it forms nanostructures that follows the established self-assembly theory. With decreasing hydrophilic weight fraction *f,* the self-assembly structures started from micelles, followed by worms as elongated micelles then polymersomes and then multicompartment vesicles (MCV). The formation of those MCV confirmed the unique ability of PEHOx in self-assembly to facilitate the creation of complex nanoparticles from a single material. Polymersomes formed from a wide range of PEO-*b*-PEHOx-*b*-PEtOz proved to be asymmetric, with PEO (long) located outside and PEtOz (short) located inside the polymersomes. When a critical length of PEtOz is reached and its length is comparable to PEO, the polymersomes then exhibited a mixed phase of PEO and PEtOz located outside of the polymersomes.

In comparison to the established ABC triblocks self-assembling into asymmetric polymersomes in aqueous solutions: PEO-*b*-PDMS-*b*-PMOXA[35] and PEO-*b*-PCL-*b*-PMOXA[34], PEO-*b*-PEHOx-*b*-PEtOz provide significant advantageous in synthesis thanks to its fast and reproducible one-pot synthesis. PEO-*b*-PDMS-*b*-PMOXA and PEO-*b*-PCL-*b*-PMOXA synthesis are robust and takes several days with the various intermediates, i.e, diblock copolymer polymerization, its purification and its modification with an initiator for the polymerization of the third block. PEO-*b*-PCL-*b*-PMOXA remains overall the most controlled polymerization and provides lower dispersity triblock copolymers. Due to the semi-crystalline nature of its hydrophobic block, PCL, the self-assembly of PEO-*b*-PCL-*b*-PMOXA is only possible with film rehydration at 60°C ($T_g$(PCL) = 60°C) which is incompatible with biomolecules. It also only

self-assembles into microscale polymersomes whereas PEO-*b*-PDMS-*b*-PMOXA can self-assemble into nanoscale and microscale polymersomes and PEO-*b*-PEHOx-*b*-PEtOz is limited to nanoscale polymersomes. Microscale polymersomes are well-suited as models for cell-like structure whereas nanoscale polymersomes are more adapted for direct biomedical applications like drug delivery. This is why in the following paragraphs we will now focus on comparing only PEO-*b*-PDMS-*b*-PMOXA and PEO-*b*-PEHOx-*b*-PEtOz having in mind protein insertion related biomedical applications.

Both PEO-*b*-PDMS-*b*-PMOXA and PEO-*b*-PEHOx-*b*-PEtOz can self-assemble via film rehydration into asymmetric polymersomes in mild conditions, under room temperature and fast in one day. PEHOx with a $T_g$ of – 6 °C remains less flexible than PDMS with a $T_g$ of -125 °C which means that PEO-*b*-PEHOx-*b*-PEtOz need a strong magnetic stirring (i.e 1000 rpm) to self-assemble whereas PEO-*b*-PDMS-*b*-PMOXA self-assemble already efficiently with a mild magnetic stirring (i.e 300 rpm). This difference in flexibility might also play a role in the fluidity of the membrane formed from PEO-*b*-PEHOx-*b*-PEtOz. PEO-*b*-PDMS-*b*-PMOXA polymersomes have been extensively studied for protein insertion.[61, 67] The asymmetric polymersomes from PEO-*b*-PEHOx-*b*-PEtOz revealed to have a membrane thickness between 6 and 10 nm. Such a membrane thickness is known to be favourable for the insertion of transmembrane proteins (TMPs) while keeping their functionality intact in polymersomes from PMOXA-*b*-PDMS-*b*-PMOXA.[147] TMPs are usually in the range of 3 to 4 nm like the outer membrane protein F (OmpF) or AquaporinZ. The hydrophobic mismatch is low between those membrane proteins and the membrane thicknesses of those polymersomes. This can lead to promising applications with protein insertions.

Our results show that PEO-*b*-PEHOx and PEO-*b*-PEHOx-*b*-PEtOz are a meaningful addition to the canon of self-assembling block copolymers. As an outlook, to capitalize on this newly developed system, a few questions can be envisioned which could be answered in two main future possible studies: the directed insertion of transmembrane proteins and studying the membrane properties using a 3D approach (polymersomes) and a 2D approach (planar membranes).

# 5. Outlook

**Can transmembrane proteins be inserted with a preferred orientation into the asymmetric polymersomes from PEO-*b*-PEHOx-*b*-PEtOz?**

After successful insertion of established TMPs like OmPF, the asymmetric polymersomes could be employed to have a directed-insertion of more complex vectorial TMP like proton pumps.[103, 143]

**How does the quasi-polypeptide nature of poly(2-oxazoline) and the long and branched side chain of PEHOx influence the properties of the membrane formed from it?**

In this present work, only a 3D approach was used, by making self-assemblies in solution. It can be combined with a 2D approach by studying directly polymeric planar membranes to systematically study the membrane properties of both AB polymer PEO-*b*-PEHOx and ABC polymer PEO-*b*-PEHOx-*b*-PEtOz, as it was done previously for PMOXA-*b*-PDMS / PMOXA-*b*-PDMS-*b*-PMOXA.[61, 63, 147] It could lead to interesting insights (molecular organisation and dynamics in the membrane) to support various applications of this new system, in particular, the insertion of proteins.

# 6. Materials & Methods

## 6.1 Materials

Glassware for polymerization was dried overnight at 120°C prior to use. Isopropanol, sulfolane, 2-ethylhexyl bromide, n-butyllithium, N,N,N',N'-tetramethylenediamine (TMEDA), triethylamine, *p*-nitrobenzenesulfonyl chloride, anhydrous chlorobenzene, 2-methyl-2-oxazoline, barium oxide, methyl p-toluenesulfonate, deuterated chloroform ($CDCl_3$) and water ($D_2O$), a BCA assay kit, poly(ethylene oxide) monomethyl ether (PEO, 2000 $g.mol^{-1}$) and poly(ethylene oxide) monomethyl ether tosylate (PEO-Tos, 2000 $g.mol^{-1}$) were obtained from Sigma-Aldrich (CH) and used as received. 2-methyl-2-oxazoline and 2-ethyl-2-oxazoline was distilled over barium oxide (BaO) and stored under argon. Poly(ethylene oxide) monomethyl ether (PEO, 2000 $g.mol^{-1}$) was dissolved in water and then lyophilized. Sulfolane was dried over $CaH_2$ for 24h under reduced pressure at 40 °C, distilled, and stored in the glovebox. Milli-Q water (18.2 MΩ cm) was used from a Purelab Option-R 7/15 system (ELGA LabWater, UK). Anhydrous dichloromethane (DCM), tetrahydrofuran (THF) and acetonitrile were obtained from an inert solvent purification system PureSolv MD 5 (Inert, USA).

## 6.2 Microwave synthesis

Microwave polymerization was conducted on a Biotage Initiator System (Biotage, Sweden) equipped with Robot Eight. The microwave synthesizer operated at a constant set temperature (mentioned in results and discussion) monitored by the Infrared (IR) sensor.

## 6.3 Synthesis of PEO-Nos Macroinitiator

Poly(ethylene oxide) monomethyl ether (PEO, 2000 $g.mol^{-1}$) (4 g, 2 mmol, 1 eq) was dissolved in 80 mL dry DCM and chilled to 0 °C. Triethylamine (2.8 mL, 20 mmol, 10 eq) and p-

nitrobenzenesulfonyl chloride (4.4362 g, 20 mmol, 10 eq) were then added. The reaction was allowed to stir for 10 h at 0 °C under argon atmosphere. The reaction mixture was concentrated under vacuum and the high excess of unreacted reagents was then extracted 3 times with 400 mL of isopropanol at RT exploiting the poor solubility of PEO at RT in Isopropanol. It was then placed into a dialysis membrane (regenerated cellulose, MWCO 3.5 kDa, RC6, Spectra Por, USA)) and dialyzed against acetonitrile for 2 days (solution was exchanged 4 times, at least 8 hours in between exchanges). The purified product was stored under argon atmosphere and was stable over 12 months, as was confirmed by $^{1}$H NMR. The resulting ω-nosylation (96%) was determined by integrating the peak from terminal group of PEO at 3.38 ppm and the peak of the methylene group next to nosylate at 4.32 ppm (Figure 12). $^{1}$H NMR (400 MHz, $CDCl_3$, 295K, δ, ppm): 3.38 (s, 3H, -$OCH_2CH_2O$-C$H_3$), 3.65 (m, 180H, OC$H_2$C$H_2$O), 4.32 (t, J=4.6 Hz, 2H, Ar-O-C$H_2$-), 8.15 (m, 2H, Ar-$NO_2$), 8.41 (m, 2H, Ar-$NO_2$).

## 6.4 Synthesis of 2-(3-ethylheptyl)-2-oxazoline (EHOx)

The monomer was prepared by using the synthetic procedure described by Kempe et al.[116] Briefly, TMEDA (10.32 mL, 69 mmol, 1 eq) was dissolved in 300 mL THF at -78°C under argon. N-butyllithium (2.5M in hexane, 26 mL, 65 mmol, 0.96 eq) was then added and after 60 min stirring, 2-methyl-2-oxazoline (5.8 mL, 68 mmol, 1 eq) was added. The stirring was continued for 2 hours at -78°C and was concluded by the addition of 2-ethylhexyl bromide (10.13 mL, 57 mmol, 0.83 eq). The solution was allowed to warm to room temperature overnight and was then terminated after 25 hours with 150 mL of methanol and the solvents were evaporated under reduced pressure. The residue was dissolved in 200 mL of a biphasic solution 1:1 CHCl3/ $NaHCO_{3\,(sat)}$. The aqueous phase was extracted twice with 75 mL of chloroform. The combined

organic phases were washed with water and brine. After drying over $MgSO_4$, the solvent was removed under reduced pressure, and the crude product was purified by distillation. The purified product was confirmed to be EHOx by $^1$H NMR. It was then stored under argon atmosphere. $^1$H NMR (400 MHz, $CDCl_3$, 295K, δ, ppm): 0.86 (m, 6H, C*H*$_3$), 1.27 (m, 9H, C*H*(C*H*$_2$CH$_3$)-C*H*$_2$C*H*$_2$C*H*$_2$CH$_3$)), 1.60 (m, 2H, NCOCH$_2$C*H*$_2$), 2.25 (t, J=8.2 Hz, 2H, NCOC*H*$_2$CH$_2$), 3.82 (t, J=9.5Hz, 2H, CNC*H*$_2$), 4.2 (t, J=9.4 Hz, 2H, COC*H*$_2$).

## 6.5 Homopolymerization of EHOx

We used the procedure from Kempe et al.[116] Briefly, a microwave vial was prepared containing methyl p-toluenesulfonate, EHOx and acetonitrile. The monomer concentration was adjusted to 2M and a monomer-to-initiatior ratio of 60 was used. The microwave vial was then heated to 140°C for 30 min to reach full monomer conversion. To remove the solvent and residual components, the polymerization mixture was placed into a dialysis membrane (regenerated cellulose, MWCO 3.5 kDa, RC6, Spectra Por, USA) and dialyzed against THF for 3 days (solvent was exchanged 6 times). $^1$H NMR (400 MHz, $CDCl_3$, 295K, δ, ppm): 0.86 (m, 6H, C*H*$_3$), 1.24 (m, 9H, C*H*(C*H*$_2$CH$_3$)-C*H*$_2$C*H*$_2$C*H*$_2$CH$_3$)), 1.54 (m, 2H, N(COCH$_2$C*H*$_2$)), 2.24 ppm (m, 2H, N(COC*H*$_2$CH$_2$)), ), 3.43 ppm (m, 4H, N(COCH$_2$CH$_2$)-C*H*$_2$C*H*$_2$). $Đ_M$ (GPC)= 1.18. $M_n$= 11800 Da.

## 6.6 Synthesis of PEO-*b*-PEHOx diblock copolymers

PEO-*b*-PEHOx was synthetized via cationic ring-opening polymerization of EHOx in a microwave reactor using PEO-Nos as a macroinitiator. In a glovebox, a stock solution containing the initiator PEO-Nos, monomer EHOx, and the solvent (sulfolane, acetonitrile or chlorobenzene, see in main paper) was prepared. The monomer concentration was set to 1M for all experiments. A monomer-to-initiator ratio of 100 was used for the synthesis of $PEO_{45}$-*b*-$PEHOx_{8\text{-}57}$ and a monomer-to-initiator of 200 for $PEO_{45}$-*b*-$PEHOx_{95\text{-}171}$. The desired volume

of the solution was transferred into the microwave vials. The vials were sealed in the glovebox under argon atmosphere prior to the transfer into the microwave reactor.

To study the kinetics of EHOx polymerization at 140°C, reactions were performed three times. The kinetics were monitored by $^1$H NMR and GPC analysis of the crude polymerization mixture. The final PEO-*b*-PEHOx polymers were purified by dialyzing (regenerated cellulose, MWCO 3.5 kDa, RC6, Spectra Por, USA) the polymerization mixture against THF for 3 days (solvent was exchanged 6 times, at least 8 hours in between exchanges). The block ratio was determined by integrating the PEO backbone peak at 3.60 ppm and peaks of PEHOx side chain at 1.24 and 0.86 ppm. $^1$H NMR (400 MHz, $CDCl_3$, 295K, δ, ppm): 0.86 (m, 6H, C*H*$_3$), 1.24 (m, 9H, C*H*(C*H*$_2$CH$_3$)-C*H*$_2$C*H*$_2$C*H*$_2$CH$_3$)), 1.54 (m, 2H, N(COCH$_2$C*H*$_2$)), 2.24 (m, 2H, N(COC*H*$_2$CH$_2$)), ), 3.38 (s, 3H, -OCH$_2$CH$_2$O-C*H*$_3$), 3.43 (m, 4H, N(COCH$_2$CH$_2$)-C*H*$_2$C*H*$_2$), 3.65 (m, 180H, OC*H*$_2$C*H*$_2$O).

## 6.7 Synthesis of PEHOx-*b*-PEtOz diblock copolymer

Based on our work[65], we added a sequential polymerization step of EtOz to the homopolymerization of EHOx. A microwave vial was prepared containing methyl *p*-toluenesulfonate, EHOx and acetonitrile. The monomer concentration was adjusted to 2 M and a monomer-to-initiator ratio of 60 was used. The microwave vial was then heated to 140°C for 30 min to reach full monomer conversion. In the glovebox, EtOz was then added to the diblock copolymer mixture and its concentration adjusted to 1M. This second copolymerization was then carried out as well at 140°C for 12 min. After the microwave-irradiation, the polymerization mixture was cooled down to room temperature. The mixture was then dissolved in 50 mL of EtOH. To remove chlorobenzene, homopolymers and residual monomers, the solution was placed into an ultrafiltration reactor (from Millipore Corporation, 3.5 kDa RC membrane). To achieve a total purification, 5 cycles (30 min) with 50 mL of EtOH

and under a pressure of 5 bar, were carried out. To dissolve the polymer, 30 mL of EtOH was added into the reactor for 30 min without applying any pressure. After removal of the solution, 2 other cycles of 30 min and 30 mL EtOH were conducted. The solvent of the combined solutions was removed under reduced pressure. Products were characterized by $^1$H NMR. Peaks of PEO-*b*-PEHOx spectrum were attributed according to chemical shifts of EHOx monomers. Block length of EHOx was calculated using peak integrations with PEO peak at 3.60 ppm as standard (See section 7.1.2 in the appendix, Table 6). $^1$H NMR (500 MHz, $CDCl_3$, 295K, δ, ppm): 0.86 (m, 6H, C*H*$_3$), 1.1 (m, 3H, N(COCH$_2$CH$_3$)-CH$_2$CH$_2$), 1.24 (m, 9H, C*H*(C*H*$_2$CH$_3$)-C*H*$_2$C*H*$_2$C*H*$_2$CH$_3$)), 1.54 (m, 2H, N(COCH$_2$C*H*$_2$)), 2.24 (m, 4H, N(COC*H*$_2$CH$_2$)), 3.38 (s, 3H, -OCH$_2$CH$_2$O-C*H*$_3$), 3.43 (m, 4H, N(COCH$_2$CH$_2$)-C*H*$_2$C*H*$_2$). PEHOx$_{60}$-b-PEtOz$_{34}$. $Đ_M$ =1.22. $M_n$ = 15200 Da. *f* = 22%.

## 6.8 Synthesis of PEO-*b*-PEHOx-*b*-PEtOz triblock copolymers

In a 2 mL vial, a solution containing PEO-Nos macroinitiator (1 eq., 0,171 g, 0.09 mmol), chlorobenzene (1.57 mL) and EHOx (22 eq., 0,394 g, 2 mmol) was prepared in the glovebox. The copolymerization was carried out in a microwave at 140 °C for 40 min. In the glovebox, 0.104 g of EtOz (0.5 M, 1.1 mmol) was added to the diblock copolymer mixture. The second copolymerization was carried out again in a microwave at 140 °C. To get the desired EtOz length, the reaction time in the microwave was varied from 1 to 20 min. After the microwave-irradiation, the polymerization mixture was cooled down to room temperature. The mixture was then dissolved in 50 mL of EtOH. To remove chlorobenzene, homopolymers and residual monomers, the solution was placed into an ultrafiltration reactor (from Millipore Corporation, 5 kDa RC membrane). To achieve a total purification, 5 cycles (30 min), with 50 mL of EtOH and under a pressure of 5 bar, were carried out. To dissolve the polymer, 30 mL of EtOH was

added into the reactor for 10 min without applying any pressure. After removal of the solution, 2 other cycles of 10 min were proceeded. The solvent of the combined solutions was removed under reduced pressure. Products were characterized by $^{1}$H NMR. Peaks of PEO-*b*-PEHOx-*b*-PEtOz spectrum were attributed according to chemical shifts of EHOx and EtOz monomers. Block lengths were calculated using peak integrations with PEO peak at 3.60 ppm as standard (See section 7.2.1 in the appendix, Table 7). $^{1}$H NMR (500 MHz, $CDCl_3$, 295K, δ, ppm): 0.86 (m, 6H, C*H*$_3$), 1.1 (m, 3H, N(COCH$_2$CH$_3$)-CH$_2$CH$_2$), 1.24 (m, 9H, C*H*(C*H*$_2$CH$_3$)-C*H*$_2$C*H*$_2$C*H*$_2$CH$_3$)), 1.54 (m, 2H, N(COCH$_2$C*H*$_2$)), 2.24 (m, 4H, N(COC*H*$_2$CH$_2$)), 3.38 (s, 3H, -OCH$_2$CH$_2$O-C*H*$_3$), 3.43 (m, 4H, N(COCH$_2$CH$_2$)-C*H*$_2$C*H*$_2$), 3.65 (m, 180H, OC*H*$_2$C*H*$_2$O).

## 6.9 Gel Permeation Chromatography (GPC)

GPC traces were analysed and recorded in WinGPC Unichrom software (v 8.20 build 8251, PSS polymer, Germany). Traces of the diblock copolymers or of the reaction mixtures were recorded using an Agilent based system composed of a 1200 series pump and autosampler. The GPC system was equipped with a series of linear-S SDV columns (pre-column (5cm), three analytical columns (30 cm) all 5 µm particles and 0.8 cm in diameter, PSS polymer, Germany), followed by a Variable Wavelength Detector (VWD) (1100 series) and a Refractive Index Detector (RI) (1100 series). Detectors and columns were kept at 35°C. $CHCl_3$, stabilized with EtOH, was used as the eluent at a flow rate of 1 mL·min$^{-1}$. The system was calibrated against narrowly distributed polystyrene (PS) standards.

## 6.10 Nuclear magnetic resonance spectroscopy (NMR) and 2D-$^{1}$H-NOESY NMR analysis of polymersomes in $D_2O$

In order to perform NMR measurements in $D_2O$, polymersomes were prepared by film rehydration. In brief, 4 mg of a polymer was dissolved in 200 µL of EtOH and placed in a 5 mL

glass round-bottom flask. EtOH was removed by rotary evaporation, and then 2 mL of $D_2O$ was added. The samples were then stirred at 600 rpm for 7 days at room temperature. The resulting polymersomes solution with a concentration of 0.2 w/w % was analyzed by 2D-$^1$H-NOESY NMR. On a Bruker Avance III NMR spectrometer (500.13 MHz) at 295 K, 2D-$^1$H-NOESY were recorded in $D_2O$ while $^1$H NMR spectra were recorded in $CDCl_3$ (0.05% tetramethylsilane). To buffer any possible acidity, $CDCl_3$ was saturated with $K_2CO_3$. The instrument was equipped with a direct observe 5-mm BBFO smart probe. The experiments were performed at 295 K and the temperature was calibrated using a methanol standard showing accuracy within ±0.2 K. Spectra were processed with MestReNova software, and chemical shifts were reported in ppm.

## 6.11 Differential scanning calorimetry (DSC)

Thermal transitions were measured using 10 mg of polymer for each measurement on a DSC 214 Polyma (Netzsch GmbH, Austria) under a nitrogen atmosphere from -120 °C to 190 °C with a heating and cooling rate of 40 K·min$^{-1}$. The DSC curves shown correspond to the third heating curve.

## 6.12 Self-assembly

The self-assembly of PEO-*b*-PEHOx and PEO-b-PEHOx-*b*-PEtOz block copolymers were done using two different techniques: film rehydration and solvent switch. In all experiments, the final concentration of self-assembled polymer was 0.2 w/w%.

### 6.12.1 Film rehydration

4 mg of a polymer was dissolved in 200 µL of EtOH and placed in a 5 mL glass round-bottom flask. EtOH was removed by rotary evaporation, and then 2 mL of Milli-Q water was added. The samples were then stirred at 600 rpm for 7 days at room temperature.

### 6.12.2 Solvent switch

4 mg of a polymer was dissolved in 200 µL of THF and placed in a 5 mL glass round bottom flask. 1.8 mL of Milli-Q water was then added using a syringe pump (AL-1000, WPI, USA) at a rate of 0.01 mL·min$^{-1}$ under magnetic stirring (300 rpm). To remove THF, the resulting mixture was placed into a regenerated cellulose dialysis membrane (MWCO 1 kDa, Spectra Por, USA) and dialyzed against Milli-Q water for 2 days (solvent was exchanged 4 times, at least 8 hours in between exchanges).

## 6.13 Dynamic and static light scattering (DLS/SLS)

SLS and DLS experiments were performed on a light scattering spectrometer (LS instruments, Switzerland), equipped with a He-Ne 21 mW laser (λ = 632.8 nm) at scattering angles from 30° to 150° at 25 °C. All samples were diluted in order to suppress multiple scattering. For samples with a radius smaller than 100 nm, that satisfy the Rayleigh-Gans-Debye (RGD) scattering model, the radius of gyration ($R_g$) was obtained from the SLS data using Zimm plots. For samples with a radius superior to 100 nm, $R_g$ was obtained from the SLS data using MIE scattering models (MiePlot, UK). The intensity versus angle curve of samples were fit using Mie scattering models for $\eta$=1.35 and 5% polydispersity. $R_g$ is then calculated using the obtained R and the formula for a spherical structure: $R_g^2 = (3/5)R^2$. In the case of DLS, second order cumulant analysis of the data for various angles was performed to obtain the hydrodynamic radius ($R_h$).

## 6.14 Determination of the refractive Index increment

SLS experiments required the refractive index increment value, d*n*/d*c*, of the analyte in the respective solvent. It was obtained using an automatic refractometer Reichert AR7 series (Reichert, USA) at 25°C. After being calibrated with Milli-Q water (18.2 MΩ.cm), the self-

assemblies of PEO-*b*-PEHOx were analysed and d*n*/dc =0.15 obtained (Figure 49 in the appendix).

## 6.15 Transmission electron microscopy (TEM)

5 mL of solution containing self-assembled polymers (0.2 w/w %.) was left adsorbing on a formvar-coated and glow discharged 200 mesh copper grid and blotted off after 1 min. A drop of 5 µL of water was placed on the grid and blotted off immediately. The action was repeated two times. This procedure was repeated with 5 µL of 2% aqueous uranyl acetate, where the solution was left for 10 s in the second step ensuring sufficient staining of the assemblies. Prepared grids were left drying in air for at least 10 min before imaging them at an acceleration voltage of 80 kV on a Philipps CM100 (Netherlands) transmission electron microscope.

## 6.16 Cryogenic transmission electron microscopy (Cryo-TEM)

A 4 µL aliquot of a sample was adsorbed onto holey carbon-coated grid (Lacey, Tedpella, USA), blotted off with Whatman 1 filter paper and vitrified into liquid ethane at -178 °C using a Leica GP plunger (Leica, Austria). Frozen grids were transferred onto a Talos electron microscope (FEI, USA) using a Gatan 626 cryo-holder. Electron micrographs were recorded at an accelerating voltage of 200 kV and a nominal magnification of 57000 x, using a low-dose system (20 $e^-/Å^2$) and keeping the sample at low temperature. Micrographs were recorded on a CETA camera. Images were then processed using ImageJ (NIH, USA) to measure notably micelles sizes and membrane thicknesses.

## 6.17 Bicinchoninic acid assay (BCA)

100 µL of self-assembly solution (0.2 w/w %) was incubated with 800 µL in a 2.5 mL vial at 25°C (500 rpm). After incubating for 2 hours, the samples were centrifugated at 13000 rpm

for 10 min. Then 200 µL of the supernatant was transferred into a 96-well plate. This was repeated 3 times. The absorbance at 562 nm was measured using a Spectramax M5 microplate reader (Molecular Devices, USA). The resulting absorbance was the mean value of the triplicates. Each sample was analyzed 10 times for reproducibility.

# Bibligography


1. Konishcheva, E.; Daubian, D.; Gaitzsch, J.; Meier, W., Synthesis of Linear ABC Triblock Copolymers and Their Self-Assembly in Solution. *Helvetica Chimica Acta* **2018,** *101* (2), e1700287-n/a.
2. Konishcheva, E. V.; Daubian, D.; Rigo, S.; Meier, W. P., Probing membrane asymmetry of ABC polymersomes. *Chemical Communications* **2019**.
3. Adams, M. L.; Lavasanifar, A.; Kwon, G. S., Amphiphilic block copolymers for drug delivery. *Journal of pharmaceutical sciences* **2003,** *92* (7), 1343-55.
4. Gunkel-Grabole, G.; Sigg, S.; Lomora, M.; Lörcher, S.; Palivan, C. G.; Meier, W. P., Polymeric 3D nano-architectures for transport and delivery of therapeutically relevant biomacromolecules. *Biomaterials Science* **2015,** *3* (1), 25-40.
5. Garni, M.; Wehr, R.; Avsar, S. Y.; John, C.; Palivan, C.; Meier, W., Polymer membranes as templates for bio-applications ranging from artificial cells to active surfaces. *European Polymer Journal* **2019,** *112*, 346-364.
6. Pack, D. W.; Hoffman, A. S.; Pun, S.; Stayton, P. S., Design and development of polymers for gene delivery. *Nature reviews. Drug discovery* **2005,** *4* (7), 581-93.
7. Messager, L.; Gaitzsch, J.; Chierico, L.; Battaglia, G., Novel aspects of encapsulation and delivery using polymersomes. *Current Opinion in Pharmacology* **2014,** *18*, 104-111.
8. Najer, A.; Wu, D.; Vasquez, D.; Palivan, C. G.; Meier, W., Polymer nanocompartments in broad-spectrum medical applications. *Nanomedicine (Lond)* **2013,** *8* (3), 425-447.
9. Najer, A.; Wu, D.; Nussbaumer, M. G.; Schwertz, G.; Schwab, A.; Witschel, M. C.; Schafer, A.; Diederich, F.; Rottmann, M.; Palivan, C. G.; Beck, H. P.; Meier, W., An amphiphilic graft copolymer-based nanoparticle platform for reduction-responsive anticancer and antimalarial drug delivery. *Nanoscale* **2016,** *8* (31), 14858-69.
10. Bates, C. M.; Bates, F. S., 50th Anniversary Perspective: Block Polymers—Pure Potential. *Macromolecules* **2017,** *50* (1), 3-22.
11. Mai, Y.; Eisenberg, A., Self-assembly of block copolymers. *Chemical Society Reviews* **2012,** *41* (18), 5969-5985.
12. Jain, S.; Bates, F. S., On the Origins of Morphological Complexity in Block Copolymer Surfactants. *Science* **2003,** *300* (5618), 460-464.
13. Jain, S.; Bates, F. S., Consequences of Nonergodicity in Aqueous Binary PEO−PB Micellar Dispersions. *Macromolecules* **2004,** *37* (4), 1511-1523.
14. Zhang, L.; Eisenberg, A., Multiple Morphologies and Characteristics of "Crew-Cut" Micelle-like Aggregates of Polystyrene-b-poly(acrylic acid) Diblock Copolymers in Aqueous Solutions. *Journal of the American Chemical Society* **1996,** *118* (13), 3168-3181.
15. Terreau, O.; Bartels, C.; Eisenberg, A., Effect of poly(acrylic acid) block length distribution on polystyrene-b-poly(acrylic acid) block copolymer aggregates in solution. 2. A partial phase diagram. *Langmuir* **2004,** *20* (3), 637-45.
16. Braun, J.; Bruns, N.; Pfohl, T.; Meier, W., Phase Behavior of Vesicle-Forming Block Copolymers in Aqueous Solutions. *Macromolecular Chemistry and Physics* **2011,** *212* (12), 1245-1254.
17. Dionzou, M.; Morère, A.; Roux, C.; Lonetti, B.; Marty, J. D.; Mingotaud, C.; Joseph, P.; Goudounèche, D.; Payré, B.; Léonetti, M.; Mingotaud, A. F., Comparison of methods for the fabrication and the characterization of polymer self-assemblies: what are the important parameters? *Soft Matter* **2016,** *12* (7), 2166-2176.

18. Hadjichristidis, N.; Iatrou, H.; Pitsikalis, M.; Pispas, S.; Avgeropoulos, A., Linear and non-linear triblock terpolymers. Synthesis, self-assembly in selective solvents and in bulk. *Progress in Polymer Science* **2005,** *30* (7), 725-782.
19. Fustin, C. A.; Abetz, V.; Gohy, J. F., Triblock terpolymer micelles: A personal outlooka. *The European Physical Journal E* **2005,** *16* (3), 291-302.
20. Konishcheva, E. V.; Zhumaev, U. E.; Kratt, M.; Oehri, V.; Meier, W., Complex Self-Assembly Behavior of Bis-hydrophilic PEO-b-PCL-b-PMOXA Triblock Copolymers in Aqueous Solution. *Macromolecules* **2017,** *50* (18), 7155-7168.
21. Chambon, P.; Blanazs, A.; Battaglia, G.; Armes, S. P., Facile Synthesis of Methacrylic ABC Triblock Copolymer Vesicles by RAFT Aqueous Dispersion Polymerization. *Macromolecules* **2012,** *45* (12), 5081-5090.
22. Gaitzsch, J.; Messager, L.; Morecroft, E.; Meier, W., Vesicles in Multiple Shapes: Fine-Tuning Polymersomes' Shape and Stability by Setting Membrane Hydrophobicity. *Polymers* **2017,** *9* (10), 483.
23. Vaughn, T. H.; Suter, H. R.; Lundsted, L. G.; Kramer, M. G., Properties of some newly developed nonionic detergents. *Journal of the American Oil Chemists' Society* **1951,** *28* (7), 294-299.
24. Mankowich, A. M., Micellar Molecular Weights of Selected Surface Active Agents. *The Journal of Physical Chemistry* **1954,** *58* (11), 1027-1030.
25. Pitto-Barry, A.; Barry, N. P. E., Pluronic® block-copolymers in medicine: from chemical and biological versatility to rationalisation and clinical advances. *Polymer Chemistry* **2014,** *5* (10), 3291-3297.
26. Herzberger, J.; Niederer, K.; Pohlit, H.; Seiwert, J.; Worm, M.; Wurm, F. R.; Frey, H., Polymerization of Ethylene Oxide, Propylene Oxide, and Other Alkylene Oxides: Synthesis, Novel Polymer Architectures, and Bioconjugation. *Chem Rev* **2016,** *116* (4), 2170-243.
27. Skandalis, A.; Pispas, S., PDMAEMA-b-PLMA-b-POEGMA triblock terpolymers via RAFT polymerization and their self-assembly in aqueous solutions. *Polym. Chem.* **2017,** *8* (31), 4538-4547.
28. Jin, J.; Tian, J.; Lian, X.; Sun, P.; Zhao, H., Reactive triblock copolymer micelles induced by click reaction: A platform for RAFT polymerization. *Soft Matter* **2011,** *7* (23).
29. Löbling, T. I.; Hiekkataipale, P.; Hanisch, A.; Bennet, F.; Schmalz, H.; Ikkala, O.; Gröschel, A. H.; Müller, A. H. E., Bulk morphologies of polystyrene-block-polybutadiene-block-poly(tert-butyl methacrylate) triblock terpolymers. *Polymer* **2015,** *72*, 479-489.
30. Barthel, M. J.; Mansfeld, U.; Hoeppener, S.; Czaplewska, J. A.; Schacher, F. H.; Schubert, U. S., Understanding and tuning the self-assembly of polyether-based triblock terpolymers in aqueous solution. *Soft Matter* **2013,** *9* (13).
31. Kempe, K.; Baumgaertel, A.; Hoogenboom, R.; Schubert, U. S., Design of new amphiphilic triblock copoly(2-oxazoline)s containing a fluorinated segment. *Journal of Polymer Science Part A: Polymer Chemistry* **2010,** *48* (22), 5100-5108.
32. Wang, H.; Yao, Y.; Han, L.; Che, S. a., Amphiphilic ABC triblock terpolymer templating for mesoporous silica. *Chem. Res. Chin. Univ.* **2014,** *30* (5), 863-867.
33. Petrova, S.; Venturini, C. G.; Jäger, A.; Jäger, E.; Černoch, P.; Kereïche, S.; Kováčik, L.; Raška, I.; Štěpánek, P., Novel thermo-responsive double-hydrophilic and hydrophobic MPEO-b-PEtOx-b-PCL triblock terpolymers: Synthesis, characterization and self-assembly studies. *Polymer* **2015,** *59*, 215-225.

34. Konishcheva, E. V.; Zhumaev, U. E.; Meier, W. P., PEO-b-PCL-b-PMOXA Triblock Copolymers: From Synthesis to Microscale Polymersomes with Asymmetric Membrane. *Macromolecules* **2017,** *50* (4), 1512-1520.
35. Stoenescu, R.; Meier, W., Vesicles with asymmetric membranes from amphiphilic ABC triblock copolymers. *Chemical Communications* **2002,** (24), 3016-3017.
36. Bian, J.; Hao, Y.; He, J.; Zhang, W.; Zhang, M.; Ni, P., Synthesis and characterization of a biodegradable ABC triblock terpolymer as co-delivery carrier of doxorubicin and DNA. *Journal of Polymer Science Part A: Polymer Chemistry* **2014,** *52* (21), 3005-3016.
37. Matter, Y.; Enea, R.; Casse, O.; Lee, C. C.; Baryza, J.; Meier, W., Amphiphilic PEG-b-PMCL-b-PDMAEMA Triblock Copolymers: From Synthesis to Physico-Chemistry of Self-Assembled Structures. *Macromolecular Chemistry and Physics* **2011,** *212* (9), 937-949.
38. He, X.; Liang, L.; Xie, M.; Zhang, Y.; Lin, S.; Yan, D., Synthesis of Novel Linear PEO-b-PS-b-PCL Triblock Copolymers by the Combination of ATRP, ROP, and a Click Reaction. *Macromolecular Chemistry and Physics* **2007,** *208* (16), 1797-1802.
39. Moad, G.; Rizzardo, E.; Thang, S. H., RAFT polymerization and some of its applications. *Chem Asian J* **2013,** *8* (8), 1634-44.
40. Davaran, S.; Ghamkhari, A.; Alizadeh, E.; Massoumi, B.; Jaymand, M., Novel dual stimuli-responsive ABC triblock copolymer: RAFT synthesis, "schizophrenic" micellization, and its performance as an anticancer drug delivery nanosystem. *J Colloid Interface Sci* **2017,** *488*, 282-293.
41. Wang, W.; Lin, L.; Lu, J.; Liang, H.; Feng, H.; Hu, L., Synthesis, self-assembly, and formation of photo-crosslinking-stabilized fluorescent micelles covalently containing zinc(II)-bis(8-hydroxyquinoline) for ABC triblock copolymer bearing cinnamoyl and 8-hydroxyquinoline side groups. *Journal of Polymer Science Part A: Polymer Chemistry* **2016,** *54* (8), 1056-1064.
42. Hadasha, W.; Klumperman, B., Atom transfer radical polymerization as a powerful tool in the synthesis of molecular brushes. *Polymer International* **2014,** *63* (5), 824-834.
43. Siegwart, D. J.; Oh, J. K.; Matyjaszewski, K., ATRP in the design of functional materials for biomedical applications. *Prog. Polym. Sci.* **2012,** *37* (1), 18-37.
44. Gaynor, S.; Qiu, J.; Matyjaszewski, K., Using Atom Transfer Radical Polymerization in Environmentally Benign Processes. In *Advancing Sustainability through Green Chemistry and Engineering*, American Chemical Society: 2002; Vol. 823, pp 113-126.
45. Lomas, H.; Canton, I.; MacNeil, S.; Du, J.; Armes, S. P.; Ryan, A. J.; Lewis, A. L.; Battaglia, G., Biomimetic pH Sensitive Polymersomes for Efficient DNA Encapsulation and Delivery. *Advanced Materials* **2007,** *19* (23), 4238-4243.
46. Baskaran, D.; Müller, A. H. E., Anionic Vinyl Polymerization. In *Controlled and Living Polymerizations*, Wiley-VCH Verlag GmbH & Co. KGaA: 2010; pp 1-56.
47. Penczek, S.; Cypryk, M.; Duda, A.; Kubisa, P.; Slomkowski, S., Living ring-opening polymerizations of heterocyclic monomers. *Progress in Polymer Science* **2007,** *32* (2), 247-282.
48. Lecomte, P.; Jérôme, C., Recent Developments in Ring-Opening Polymerization of Lactones. In *Synthetic Biodegradable Polymers*, Rieger, B.; Künkel, A.; Coates, G. W.; Reichardt, R.; Dinjus, E.; Zevaco, T. A., Eds. Springer Berlin Heidelberg: Berlin, Heidelberg, 2012; pp 173-217.
49. Verbraeken, B.; Monnery, B. D.; Lava, K.; Hoogenboom, R., The chemistry of poly(2-oxazoline)s. *European Polymer Journal* **2017,** *88* (Supplement C), 451-469.
50. Hoogenboom, R.; Wiesbrock, F.; Huang, H.; Leenen, M. A. M.; Thijs, H. M. L.; van Nispen, S. F. G. M.; van der Loop, M.; Fustin, C.-A.; Jonas, A. M.; Gohy, J.-F.; Schubert, U. S.,

Microwave-Assisted Cationic Ring-Opening Polymerization of 2-Oxazolines: A Powerful Method for the Synthesis of Amphiphilic Triblock Copolymers. *Macromolecules* **2006,** *39* (14), 4719-4725.
51. Kempe, K.; Hoogenboom, R.; Hoeppener, S.; Fustin, C.-A.; Gohy, J.-F.; Schubert, U. S., Discovering new block terpolymer micellar morphologies. *Chemical Communications* **2010,** *46* (35), 6455-6457.
52. Fetsch, C.; Luxenhofer, R., Highly Defined Multiblock Copolypeptoids: Pushing the Limits of Living Nucleophilic Ring-Opening Polymerization. *Macromolecular Rapid Communications* **2012,** *33* (19), 1708-1713.
53. Barthel, M. J.; Schacher, F. H.; Schubert, U. S., Poly(ethylene oxide) (PEO)-based ABC triblock terpolymers – synthetic complexity vs. application benefits. *Polymer Chemistry* **2014,** *5* (8).
54. Sun, J.; Černoch, P.; Völkel, A.; Wei, Y.; Ruokolainen, J.; Schlaad, H., Aqueous Self-Assembly of a Protein-Mimetic Ampholytic Block Copolypeptide. *Macromolecules* **2016,** *49* (15), 5494-5501.
55. Stoenescu, R.; Graff, A.; Meier, W., Asymmetric ABC-triblock copolymer membranes induce a directed insertion of membrane proteins. *Macromol Biosci* **2004,** *4* (10), 930-5.
56. Konishcheva, E.; Häussinger, D.; Lörcher, S.; Meier, W., Key aspects to yield low dispersity of PEO- b -PCL diblock copolymers and their mesoscale self-assembly. *Eur. Polym. J.* **2016,** *83*, 300-310.
57. Hotz, J.; Meier, W., Vesicle-Templated Polymer Hollow Spheres. *Langmuir* **1998,** *14* (5), 1031-1036.
58. Nardin, C.; Hirt, T.; Leukel, J.; Meier, W., Polymerized ABA Triblock Copolymer Vesicles. *Langmuir* **2000,** *16* (3), 1035-1041.
59. Czajka, A.; Armes, S. P., In situ SAXS studies of a prototypical RAFT aqueous dispersion polymerization formulation: monitoring the evolution in copolymer morphology during polymerization-induced self-assembly. *Chemical Science* **2020**.
60. Lomora, M.; Itel, F.; Dinu, I. A.; Palivan, C. G., Selective ion-permeable membranes by insertion of biopores into polymersomes. *Physical Chemistry Chemical Physics* **2015,** *17* (24), 15538-15546.
61. Itel, F.; Chami, M.; Najer, A.; Lörcher, S.; Wu, D.; Dinu, I. A.; Meier, W., Molecular Organization and Dynamics in Polymersome Membranes: A Lateral Diffusion Study. *Macromolecules* **2014,** *47* (21), 7588-7596.
62. Jalmar, O.; François-Moutal, L.; García-Sáez, A.-J.; Perry, M.; Granjon, T.; Gonzalvez, F.; Gottlieb, E.; Ayala-Sanmartin, J.; Klösgen, B.; Schwille, P.; Petit, P. X., Caspase-8 Binding to Cardiolipin in Giant Unilamellar Vesicles Provides a Functional Docking Platform for Bid. *PLOS ONE* **2013,** *8* (2), e55250.
63. Belluati, A.; Mikhalevich, V.; Yorulmaz Avsar, S.; Daubian, D.; Craciun, I.; Chami, M.; Meier, W. P.; Palivan, C. G., How Do the Properties of Amphiphilic Polymer Membranes Influence the Functional Insertion of Peptide Pores? *Biomacromolecules* **2020,** *21* (2), 701-715.
64. Karayianni, M.; Pispas, S., Self-Assembly of Amphiphilic Block Copolymers in Selective Solvents. In *Fluorescence Studies of Polymer Containing Systems*, Procházka, K., Ed. Springer International Publishing: Cham, 2016; pp 27-63.
65. Daubian, D.; Gaitzsch, J.; Meier, W., Synthesis and complex self-assembly of amphiphilic block copolymers with a branched hydrophobic poly(2-oxazoline) into

multicompartment micelles, pseudo-vesicles and yolk/shell nanoparticles. *Polymer Chemistry* **2020,** *11* (6), 1237-1248.
66. Wehr, R.; Gaitzsch, J.; Daubian, D.; Fodor, C.; Meier, W., Deepening the insight into poly(butylene oxide)-block-poly(glycidol) synthesis and self-assemblies: micelles, worms and vesicles. *RSC Advances* **2020,** *10* (38), 22701-22711.
67. Wu, D.; Spulber, M.; Itel, F.; Chami, M.; Pfohl, T.; Palivan, C. G.; Meier, W., Effect of Molecular Parameters on the Architecture and Membrane Properties of 3D Assemblies of Amphiphilic Copolymers. *Macromolecules* **2014,** *47* (15), 5060-5069.
68. Njikang, G.; Han, D.; Wang, J.; Liu, G., ABC Triblock Copolymer Micelle-Like Aggregates in Selective Solvents for A and C. *Macromolecules* **2008,** *41* (24), 9727-9735.
69. Du, J.; Armes, S. P., Patchy multi-compartment micelles are formed by direct dissolution of an ABC triblock copolymer in water. *Soft Matter* **2010,** *6* (19), 4851-4857.
70. Fang, B.; Walther, A.; Wolf, A.; Xu, Y.; Yuan, J.; Müller, A. H. E., Undulated Multicompartment Cylinders by the Controlled and Directed Stacking of Polymer Micelles with a Compartmentalized Corona. *Angew. Chem., Int. Ed.* **2009,** *48* (16), 2877-2880.
71. Schmalz, H.; Schmelz, J.; Drechsler, M.; Yuan, J.; Walther, A.; Schweimer, K.; Mihut, A. M., Thermo-Reversible Formation of Wormlike Micelles with a Microphase-Separated Corona from a Semicrystalline Triblock Terpolymer. *Macromolecules* **2008,** *41* (9), 3235-3242.
72. Walther, A.; Millard, P.-E.; Goldmann, A. S.; Lovestead, T. M.; Schacher, F.; Barner-Kowollik, C.; Müller, A. H. E., Bis-Hydrophilic Block Terpolymers via RAFT Polymerization: Toward Dynamic Micelles with Tunable Corona Properties. *Macromolecules* **2008,** *41* (22), 8608-8619.
73. Walther, A.; Barner-Kowollik, C.; Müller, A. H. E., Mixed, Multicompartment, or Janus Micelles? A Systematic Study of Thermoresponsive Bis-Hydrophilic Block Terpolymers. *Langmuir* **2010,** *26* (14), 12237-12246.
74. Erhardt, R.; Böker, A.; Zettl, H.; Kaya, H.; Pyckhout-Hintzen, W.; Krausch, G.; Abetz, V.; Müller, A. H. E., Janus Micelles. *Macromolecules* **2001,** *34* (4), 1069-1075.
75. Saito, R.; Fujita, A.; Ichimura, A.; Ishizu, K., Synthesis of microspheres with microphase-separated shells. *J. Polym. Sci., Part A: Polym. Chem.* **2000,** *38* (11), 2091-2097.
76. Hoppenbrouwers, E.; Li, Z.; Liu, G., Triblock Nanospheres with Amphiphilic Coronal Chains. *Macromolecules* **2003,** *36* (3), 876-881.
77. Dag, A.; Zhao, J.; Stenzel, M. H., Origami with ABC Triblock Terpolymers Based on Glycopolymers: Creation of Virus-Like Morphologies. *ACS Macro Lett.* **2015,** *4* (5), 579-583.
78. Walther, A.; Müller, A. H. E., Janus Particles: Synthesis, Self-Assembly, Physical Properties, and Applications. *Chem. Rev.* **2013,** *113* (7), 5194-5261.
79. Du, J.; O'Reilly, R. K., Anisotropic particles with patchy, multicompartment and Janus architectures: preparation and application. *Chem. Soc. Rev.* **2011,** *40* (5), 2402-2416.
80. Zupancich, J. A.; Bates, F. S.; Hillmyer, M. A., Aqueous Dispersions of Poly(ethylene oxide)-b-poly(γ-methyl-ε-caprolactone) Block Copolymers. *Macromolecules* **2006,** *39* (13), 4286-4288.
81. Adams, D. J.; Butler, M. F.; Weaver, A. C., Effect of Block Length, Polydispersity, and Salt Concentration on PEO−PDEAMA Block Copolymer Structures in Dilute Solution. *Langmuir* **2006,** *22* (10), 4534-4540.
82. Yu, K.; Eisenberg, A., Multiple Morphologies in Aqueous Solutions of Aggregates of Polystyrene-block-poly(ethylene oxide) Diblock Copolymers. *Macromolecules* **1996,** *29* (19), 6359-6361.
83. Israelachvili, J. N., *Intermolecular and surface forces*. Academic press: 2011.

84. Taubert, A.; Furrer, E.; Meier, W., Water-in-water mesophases for templating inorganics. *Chem. Commun.* **2004,** (19), 2170-2171.
85. Casse, O.; Shkilnyy, A.; Linders, J.; Mayer, C.; Häussinger, D.; Völkel, A.; Thünemann, A. F.; Dimova, R.; Cölfen, H.; Meier, W.; Schlaad, H.; Taubert, A., Solution Behavior of Double-Hydrophilic Block Copolymers in Dilute Aqueous Solution. *Macromolecules* **2012,** *45* (11), 4772-4777.
86. Stoenescu, R.; Meier, W., Vesicles with asymmetric membranes from amphiphilic ABC triblock copolymers. *Chemical communications (Cambridge, England)* **2002,** (24), 3016-7.
87. Liu, F.; Eisenberg, A., Preparation and pH Triggered Inversion of Vesicles from Poly(acrylic Acid)-block-Polystyrene-block-Poly(4-vinyl Pyridine). *J. Am. Chem. Soc.* **2003,** *125* (49), 15059-15064.
88. Wittemann, A.; Azzam, T.; Eisenberg, A., Biocompatible Polymer Vesicles from Biamphiphilic Triblock Copolymers and Their Interaction with Bovine Serum Albumin. *Langmuir* **2007,** *23* (4), 2224-2230.
89. Schlaad, H.; You, L.; Sigel, R.; Smarsly, B.; Heydenreich, M.; Mantion, A.; Mašić, A., Glycopolymer vesicles with an asymmetric membrane. *Chemical Communications* **2009,** (12), 1478-1480.
90. Liu, G.; Ma, S.; Li, S.; Cheng, R.; Meng, F.; Liu, H.; Zhong, Z., The highly efficient delivery of exogenous proteins into cells mediated by biodegradable chimaeric polymersomes. *Biomaterials* **2010,** *31* (29), 7575-7585.
91. Du, J.; Fan, L.; Liu, Q., pH-Sensitive Block Copolymer Vesicles with Variable Trigger Points for Drug Delivery. *Macromolecules* **2012,** *45* (20), 8275-8283.
92. Mason, A. F.; Thordarson, P., Polymersomes with Asymmetric Membranes Based on Readily Accessible Di- and Triblock Copolymers Synthesized via SET-LRP. *ACS Macro Letters* **2016,** *5* (10), 1172-1175.
93. Smith, P. K.; Krohn, R. I.; Hermanson, G. T.; Mallia, A. K.; Gartner, F. H.; Provenzano, M. D.; Fujimoto, E. K.; Goeke, N. M.; Olson, B. J.; Klenk, D. C., Measurement of protein using bicinchoninic acid. *Anal. Biochem.* **1985,** *150* (1), 76-85.
94. Schrage, S.; Sigel, R.; Schlaad, H., Formation of Amphiphilic Polyion Complex Vesicles from Mixtures of Oppositely Charged Block Ionomers. *Macromolecules* **2003,** *36* (5), 1417-1420.
95. Blanazs, A.; Massignani, M.; Battaglia, G.; Armes, S. P.; Ryan, A. J., Tailoring Macromolecular Expression at Polymersome Surfaces. *Advanced Functional Materials* **2009,** *19* (18), 2906-2914.
96. Liu, Q.; Chen, J.; Du, J., Asymmetrical Polymer Vesicles with a “Stealthy” Outer Corona and an Endosomal-Escape-Accelerating Inner Corona for Efficient Intracellular Anticancer Drug Delivery. *Biomacromolecules* **2014,** *15* (8), 3072-3082.
97. Discher, D. E.; Eisenberg, A., Polymer Vesicles. *Science* **2002,** *297* (5583), 967-973.
98. Palivan, C. G.; Goers, R.; Najer, A.; Zhang, X.; Car, A.; Meier, W., Bioinspired polymer vesicles and membranes for biological and medical applications. *Chemical Society Reviews* **2016,** *45* (2), 377-411.
99. Uehlein, N.; Otto, B.; Eilingsfeld, A.; Itel, F.; Meier, W.; Kaldenhoff, R., Gas-tight triblock-copolymer membranes are converted to CO2 permeable by insertion of plant aquaporins. *Scientific Reports* **2012,** *2*, 538.
100. Langowska, K.; Palivan, C. G.; Meier, W., Polymer nanoreactors shown to produce and release antibiotics locally. *Chemical Communications* **2013,** *49* (2), 128-130.

101. Lomora, M.; Garni, M.; Itel, F.; Tanner, P.; Spulber, M.; Palivan, C. G., Polymersomes with engineered ion selective permeability as stimuli-responsive nanocompartments with preserved architecture. *Biomaterials* **2015,** *53*, 406-14.
102. Gaitzsch, J.; Huang, X.; Voit, B., Engineering Functional Polymer Capsules toward Smart Nanoreactors. *Chemical Reviews* **2016,** *116* (3), 1053-1093.
103. Gaitzsch, J.; Hirschi, S.; Freimann, S.; Fotiadis, D.; Meier, W., Directed Insertion of Light-Activated Proteorhodopsin into Asymmetric Polymersomes from an ABC Block Copolymer. *Nano Letters* **2019,** *19* (4), 2503-2508.
104. Petersen, M. A.; Yin, L.; Kokkoli, E.; Hillmyer, M. A., Synthesis and characterization of reactive PEO-PMCL polymersomes. *Polymer Chemistry* **2010,** *1* (8), 1281-1290.
105. Gaitzsch, J.; Welsch, P. C.; Folini, J.; Schoenenberger, C.-A.; Anderson, J. C.; Meier, W. P., Revisiting monomer synthesis and radical ring opening polymerization of dimethylated MDO towards biodegradable nanoparticles for enzymes. *European Polymer Journal* **2018,** *101*, 113-119.
106. Moughton, A. O.; Hillmyer, M. A.; Lodge, T. P., Multicompartment Block Polymer Micelles. *Macromolecules* **2012,** *45* (1), 2-19.
107. Massignani, M.; LoPresti, C.; Blanazs, A.; Madsen, J.; Armes, S. P.; Lewis, A. L.; Battaglia, G., Controlling Cellular Uptake by Surface Chemistry, Size, and Surface Topology at the Nanoscale. *Small* **2009,** *5* (21), 2424-2432.
108. Wan, W.-M.; Pan, C.-Y., Formation of Polymeric Yolk/Shell Nanomaterial by Polymerization-Induced Self-Assembly and Reorganization. *Macromolecules* **2010,** *43* (6), 2672-2675.
109. Purbia, R.; Paria, S., Yolk/shell nanoparticles: classifications, synthesis, properties, and applications. *Nanoscale* **2015,** *7* (47), 19789-19873.
110. Du, J.; Armes, S. P., pH-Responsive Vesicles Based on a Hydrolytically Self-Cross-Linkable Copolymer. *Journal of the American Chemical Society* **2005,** *127* (37), 12800-12801.
111. Fetsch, C.; Gaitzsch, J.; Messager, L.; Battaglia, G.; Luxenhofer, R., Self-Assembly of Amphiphilic Block Copolypeptoids – Micelles, Worms and Polymersomes. *Scientific Reports* **2016,** *6* (1), 33491.
112. Sedlacek, O.; Monnery, B. D.; Filippov, S. K.; Hoogenboom, R.; Hruby, M., Poly(2-Oxazoline)s – Are They More Advantageous for Biomedical Applications Than Other Polymers? *Macromolecular Rapid Communications* **2012,** *33* (19), 1648-1662.
113. Zhang, N.; Huber, S.; Schulz, A.; Luxenhofer, R.; Jordan, R., Cylindrical Molecular Brushes of Poly(2-oxazoline)s from 2-Isopropenyl-2-oxazoline. *Macromolecules* **2009,** *42* (6), 2215-2221.
114. Luxenhofer, R.; Schulz, A.; Roques, C.; Li, S.; Bronich, T. K.; Batrakova, E. V.; Jordan, R.; Kabanov, A. V., Doubly amphiphilic poly(2-oxazoline)s as high-capacity delivery systems for hydrophobic drugs. *Biomaterials* **2010,** *31* (18), 4972-4979.
115. Kempe, K.; Rettler, E. F. J.; Paulus, R. M.; Kuse, A.; Hoogenboom, R.; Schubert, U. S., A systematic investigation of the effect of side chain branching on the glass transition temperature and mechanical properties of aliphatic (co-)poly(2-oxazoline)s. *Polymer* **2013,** *54* (8), 2036-2042.
116. Kempe, K.; Jacobs, S.; Lambermont-Thijs, H. M. L.; Fijten, M. M. W. M.; Hoogenboom, R.; Schubert, U. S., Rational Design of an Amorphous Poly(2-oxazoline) with a Low Glass-Transition Temperature: Monomer Synthesis, Copolymerization, and Properties. *Macromolecules* **2010,** *43* (9), 4098-4104.

117. Lübtow, M. M.; Keßler, L.; Appelt-Menzel, A.; Lorson, T.; Gangloff, N.; Kirsch, M.; Dahms, S.; Luxenhofer, R., More Is Sometimes Less: Curcumin and Paclitaxel Formulations Using Poly(2-oxazoline) and Poly(2-oxazine)-Based Amphiphiles Bearing Linear and Branched C9 Side Chains. *Macromolecular Bioscience* **2018,** *18* (11), 1800155.
118. Hoogenboom, R.; Thijs, H. M. L.; Fijten, M. W. M.; Lankvelt, B. M. v.; Schubert, U. S., One-pot synthesis of 2-phenyl-2-oxazoline-containing quasi-diblock copoly(2-oxazoline)s under microwave irradiation. *Journal of Polymer Science Part A: Polymer Chemistry* **2007,** *45* (3), 416-422.
119. Glassner, M.; D'hooge, D. R.; Young Park, J.; Van Steenberge, P. H. M.; Monnery, B. D.; Reyniers, M.-F.; Hoogenboom, R., Systematic investigation of alkyl sulfonate initiators for the cationic ring-opening polymerization of 2-oxazolines revealing optimal combinations of monomers and initiators. *European Polymer Journal* **2015,** *65* (Supplement C), 298-304.
120. Brissault, B.; Guis, C.; Cheradame, H., Kinetic study of poly(ethylene oxide-b-2-methyl-2-oxazoline) diblocs synthesis from poly(ethylene oxide) macroinitiators. *European Polymer Journal* **2002,** *38* (2), 219-228.
121. Tilstam, U., Sulfolane: A Versatile Dipolar Aprotic Solvent. *Organic Process Research & Development* **2012,** *16* (7), 1273-1278.
122. Vergaelen, M.; Verbraeken, B.; Monnery, B. D.; Hoogenboom, R., Sulfolane as Common Rate Accelerating Solvent for the Cationic Ring-Opening Polymerization of 2-Oxazolines. *ACS Macro Letters* **2015,** *4* (8), 825-828.
123. Robeson, L. M., *Polymer blends : a comprehensive review*. Hanser: Munich, 2007.
124. Privalko, V. P.; Lipatov, Y. S., Glass transition and chain flexibility of linear polymers. *Journal of Macromolecular Science, Part B* **1974,** *9* (3), 551-564.
125. Huang, H.; Chung, B.; Jung, J.; Park, H.-W.; Chang, T., Toroidal Micelles of Uniform Size from Diblock Copolymers. *Angewandte Chemie International Edition* **2009,** *48* (25), 4594-4597.
126. Egelhaaf, S. U.; Schurtenberger, P., Shape Transformations in the Lecithin-Bile Salt System: From Cylinders to Vesicles. *The Journal of Physical Chemistry* **1994,** *98* (34), 8560-8573.
127. Marsat, J.-N.; Stahlhut, F.; Laschewsky, A.; Berlepsch, H. v.; Böttcher, C., Multicompartment micelles from silicone-based triphilic block copolymers. *Colloid and Polymer Science* **2013,** *291* (11), 2561-2567.
128. Babinot, J.; Renard, E.; Le Droumaguet, B.; Guigner, J.-M.; Mura, S.; Nicolas, J.; Couvreur, P.; Langlois, V., Facile Synthesis of Multicompartment Micelles Based on Biocompatible Poly(3-hydroxyalkanoate). *Macromolecular Rapid Communications* **2013,** *34* (4), 362-368.
129. de Bruyn Ouboter, D.; Schuster, T. B.; Mantion, A.; Meier, W., Hierarchical Organization of Purely Peptidic Amphiphiles into Peptide Beads. *The Journal of Physical Chemistry C* **2011,** *115* (30), 14583-14590.
130. Sigg, S. J.; Postupalenko, V.; Duskey, J. T.; Palivan, C. G.; Meier, W., Stimuli-Responsive Codelivery of Oligonucleotides and Drugs by Self-Assembled Peptide Nanoparticles. *Biomacromolecules* **2016,** *17* (3), 935-45.
131. Allen, T. M.; Cullis, P. R., Drug Delivery Systems: Entering the Mainstream. *Science* **2004,** *303* (5665), 1818-1822.
132. Deraedt, C.; Astruc, D., Supramolecular nanoreactors for catalysis. *Coordination Chemistry Reviews* **2016,** *324*, 106-122.

133. Belluati, A.; Craciun, I.; Liu, J.; Palivan, C. G., Nanoscale Enzymatic Compartments in Tandem Support Cascade Reactions in Vitro. *Biomacromolecules* **2018,** *19* (10), 4023-4033.
134. Thamboo, S.; Najer, A.; Belluati, A.; von Planta, C.; Wu, D.; Craciun, I.; Meier, W.; Palivan, C. G., Mimicking Cellular Signaling Pathways within Synthetic Multicompartment Vesicles with Triggered Enzyme Activity and Induced Ion Channel Recruitment. *Advanced Functional Materials* **2019,** *29* (40), 1904267.
135. Folini, J.; Huang, C.-H.; Anderson, J. C.; Meier, W. P.; Gaitzsch, J., Novel monomers in radical ring-opening polymerisation for biodegradable and pH responsive nanoparticles. *Polymer Chemistry* **2019,** *10* (39), 5285-5288.
136. Zhao, L.; Li, N.; Wang, K.; Shi, C.; Zhang, L.; Luan, Y., A review of polypeptide-based polymersomes. *Biomaterials* **2014,** *35* (4), 1284-1301.
137. Pawar, P. V.; Gohil, S. V.; Jain, J. P.; Kumar, N., Functionalized polymersomes for biomedical applications. *Polymer Chemistry* **2013,** *4* (11), 3160-3176.
138. Belluati, A.; Mikhalevich, V.; Yorulmaz Avsar, S.; Daubian, D.; Craciun, I.; Chami, M.; Meier, W. P.; Palivan, C. G., How Do the Properties of Amphiphilic Polymer Membranes Influence the Functional Insertion of Peptide Pores? *Biomacromolecules* **2019**.
139. Rothman, J.; Lenard, J., Membrane asymmetry. *Science* **1977,** *195* (4280), 743-753.
140. Rigaud, J. L.; Paternostre, M. T.; Bluzat, A., Mechanisms of membrane protein insertion into liposomes during reconstitution procedures involving the use of detergents. 2. Incorporation of the light-driven proton pump bacteriorhodopsin. *Biochemistry* **1988,** *27* (8), 2677-2688.
141. Buch-Pedersen, M. J.; Pedersen, B. P.; Veierskov, B.; Nissen, P.; Palmgren, M. G., Protons and how they are transported by proton pumps. *Pflügers Archiv - European Journal of Physiology* **2008,** *457* (3), 573.
142. Pautot, S.; Frisken, B. J.; Weitz, D. A., Engineering asymmetric vesicles. *Proceedings of the National Academy of Sciences* **2003,** *100* (19), 10718-10721.
143. Goers, R.; Thoma, J.; Ritzmann, N.; Di Silvestro, A.; Alter, C.; Gunkel-Grabole, G.; Fotiadis, D.; Müller, D. J.; Meier, W., Optimized reconstitution of membrane proteins into synthetic membranes. *Communications Chemistry* **2018,** *1* (1), 35.
144. Lobling, T. I.; Borisov, O.; Haataja, J. S.; Ikkala, O.; Groschel, A. H.; Muller, A. H., Rational design of ABC triblock terpolymer solution nanostructures with controlled patch morphology. *Nat Commun* **2016,** *7*, 12097.
145. Konishcheva, E.; Daubian, D.; Gaitzsch, J.; Meier, W., Synthesis of Linear ABC Triblock Copolymers and Their Self-Assembly in Solution. *Helvetica Chimica Acta* **2018,** *101* (2), e1700287.
146. Hoogenboom, R.; Wiesbrock, F.; Leenen, M. A. M.; Thijs, H. M. L.; Huang, H.; Fustin, C.-A.; Guillet, P.; Gohy, J.-F.; Schubert, U. S., Synthesis and Aqueous Micellization of Amphiphilic Tetrablock Ter- and Quarterpoly(2-oxazoline)s. *Macromolecules* **2007,** *40* (8), 2837-2843.
147. Itel, F.; Najer, A.; Palivan, C. G.; Meier, W., Dynamics of Membrane Proteins within Synthetic Polymer Membranes with Large Hydrophobic Mismatch. *Nano Letters* **2015,** *15* (6), 3871-3878.
148. Lee, H.; Venable, R. M.; MacKerell, A. D.; Pastor, R. W., Molecular Dynamics Studies of Polyethylene Oxide and Polyethylene Glycol: Hydrodynamic Radius and Shape Anisotropy. *Biophys. J.* **2008,** *95* (4), 1590-1599.

# 7. Appendix

## 7.1 Chapter 2: PEO-*b*-PEHOx

### 7.1.1 Solubility issue of growing PEO-*b*-PEHOx in sulfolane

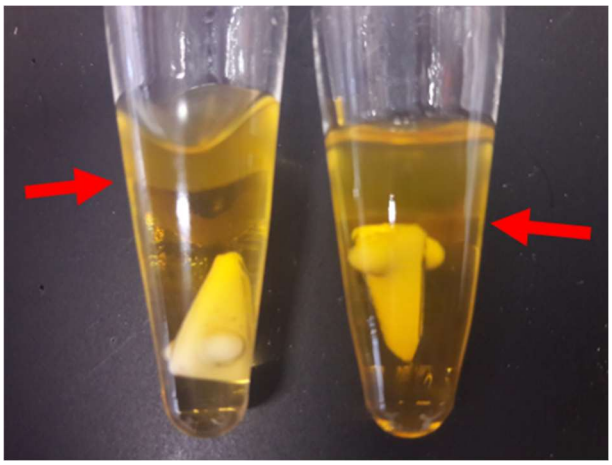

**Figure 45.** Picture of two microwave vials after polymerization of EHOx on PEO-Nos in sulfolane showing two different phases due two low solubility of the PEHOx block.

### 7.1.2 Calculation of EHOx block length by $^1$H NMR

The block ratio of AB PEO-*b*-PEHOx was determined by integrating the PEO backbone peak at 3.60 ppm as a reference (always 45 units for 2000 Da PEO used) to integrate peaks of PEHOx side chain at 0.86 and 1.24 ppm and calculate the EHOx block length as summarized in the following Table 6.

**Table 6**. Calculations of EHOx block length. [a] Integral "a" (m, 6H, $CH_3$)) 0.86 ppm. [b] Integral "b" (m, 9H, $CH(CH_2CH_3)$-$CH_2CH_2CH_2CH_3$)) 1.24 ppm. [c] Calculated via N(EHOx length)= (a/6+b/9)/2

| Diblock copolymers | Integral "a"[a] | Integral "b"[b] | EHOx length[c] |
|---|---|---|---|
| $PEO_{45}$-*b*-$PEHOx_8$ | 46 | 71 | 8 |
| $PEO_{45}$-*b*-$PEHOx_{26}$ | 153 | 230 | 26 |
| $PEO_{45}$-*b*-$PEHOx_{40}$ | 240 | 356 | 40 |
| $PEO_{45}$-*b*-$PEHOx_{57}$ | 344 | 516 | 57 |
| $PEO_{45}$-*b*-$PEHOx_{95}$ | 565 | 860 | 95 |
| $PEO_{45}$-*b*-$PEHOx_{128}$ | 764 | 1160 | 128 |
| $PEO_{45}$-*b*-$PEHOx_{151}$ | 901 | 1360 | 151 |
| $PEO_{45}$-*b*-$PEHOx_{171}$ | 1014 | 1563 | 171 |

### 7.1.3 Glass transition temperature ($T_g$) of the remaining AB polymers

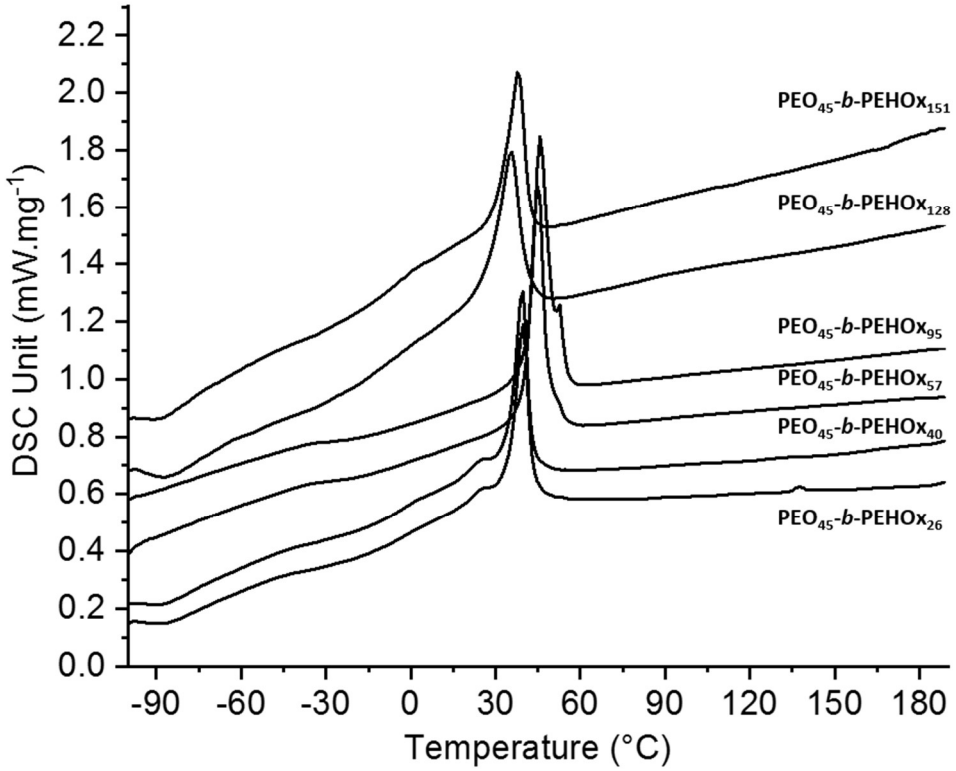


**Figure 46**. DSC measurements of diblocks copolymers: (starting from the bottom) $PEO_{45}$-*b*-$PEHOx_{26}$, $PEO_{45}$-*b*-$PEHOx_{40}$, $PEO_{45}$-*b*-$PEHOx_{57}$, $PEO_{45}$-*b*-$PEHOx_{95}$, $PEO_{45}$-*b*-$PEHOx_{128}$ and $PEO_{45}$-*b*-$PEHOx_{151}$

### 7.1.4 Supplementary Cryo-TEM images of SS of $PEO_{45}$-*b*-$PEHOx_{95}$

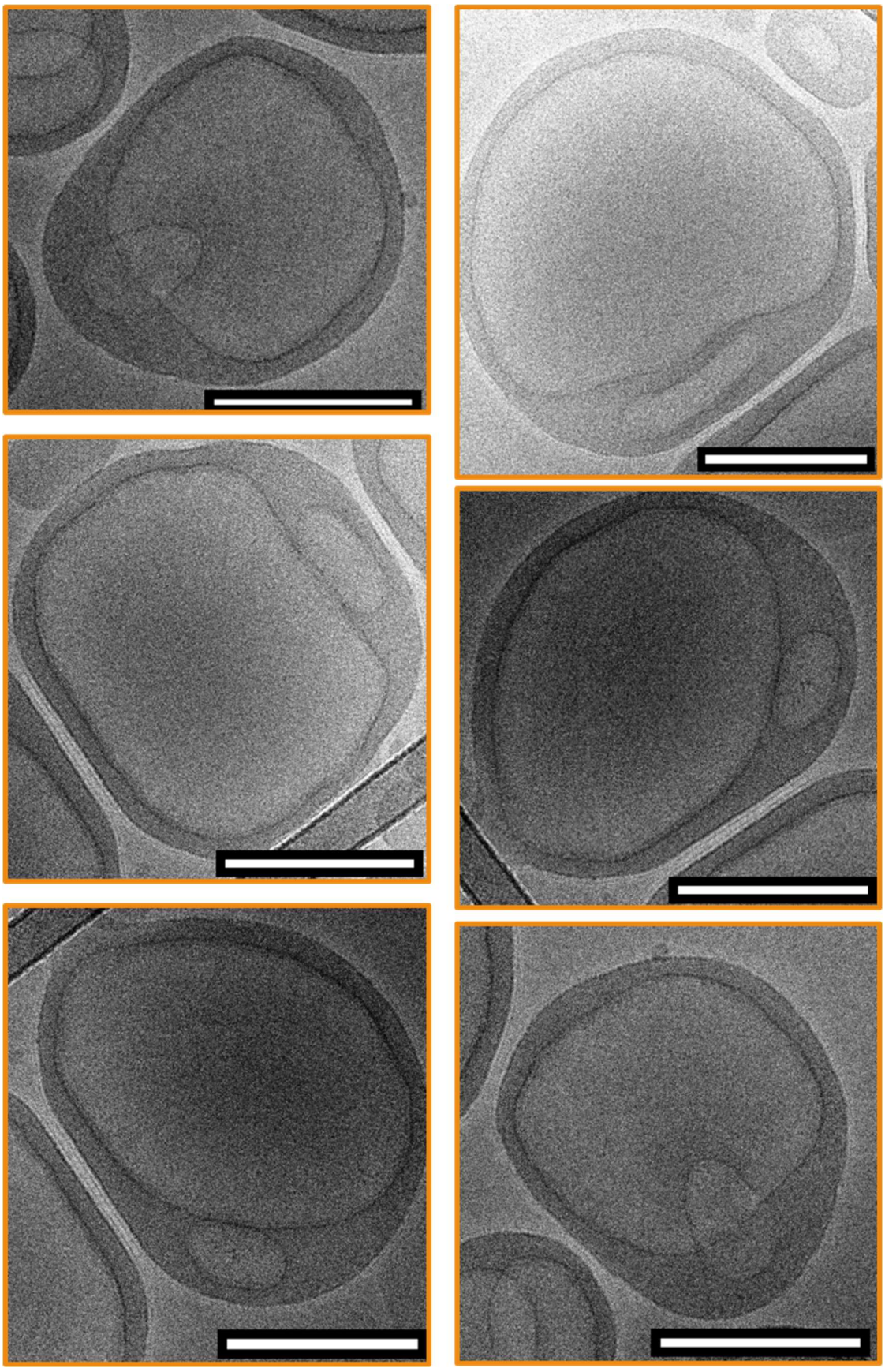

**Figure 47**. Supplementary Cryo-TEM images of SS of $PEO_{45}$-*b*-$PEHOx_{95}$. Scale bars 200 nm

### 7.1.5 Supplementary Cryo-TEM images of SS of $PEO_{45}$-b-$PEHOx_{128}$

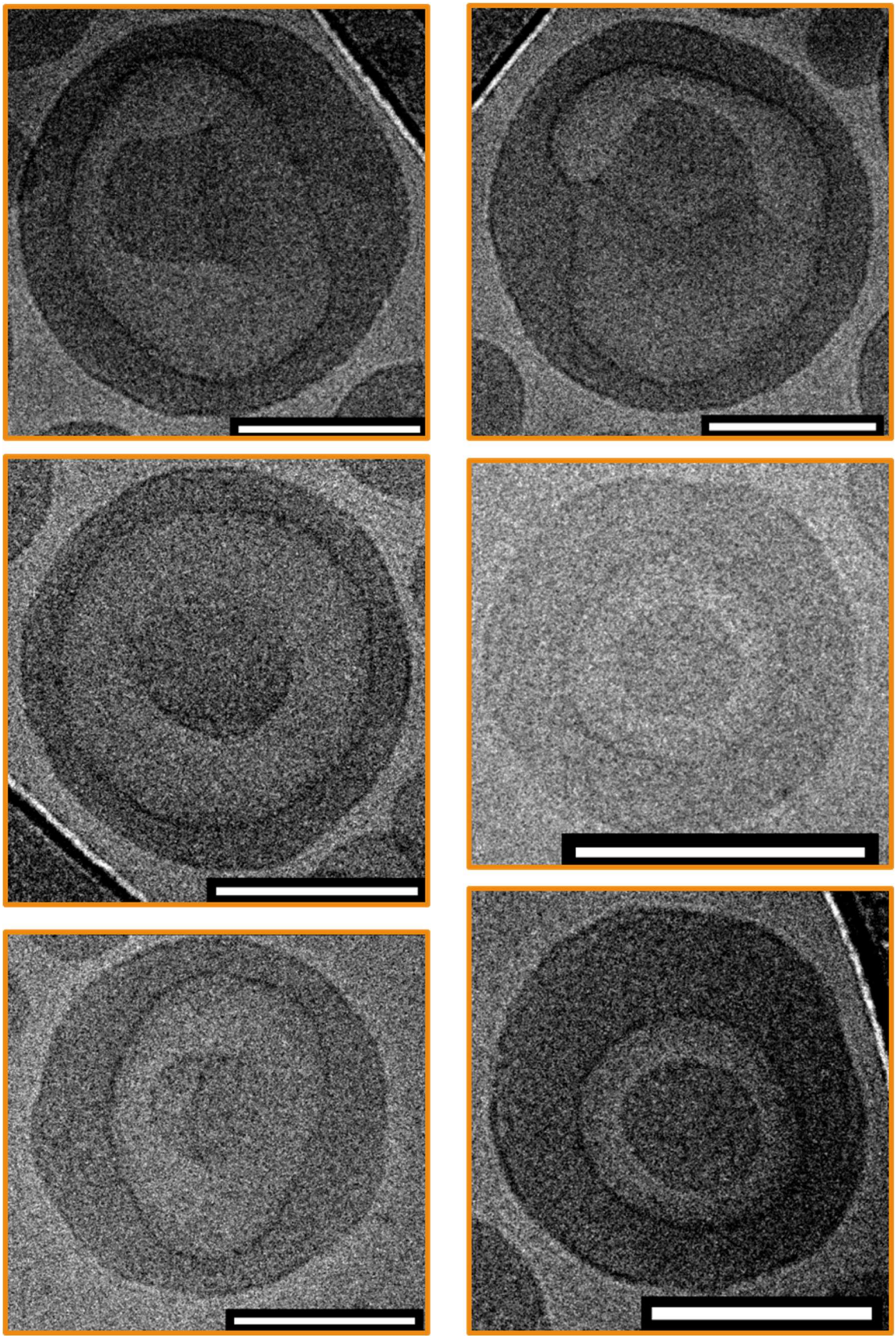

**Figure 48.** Supplementary Cryo-TEM images of $PEO_{45}$-*b*-$PEHOx_{128}$. Scale bars 100 nm

### 7.1.6 Determination of dn/dc value for SLS study

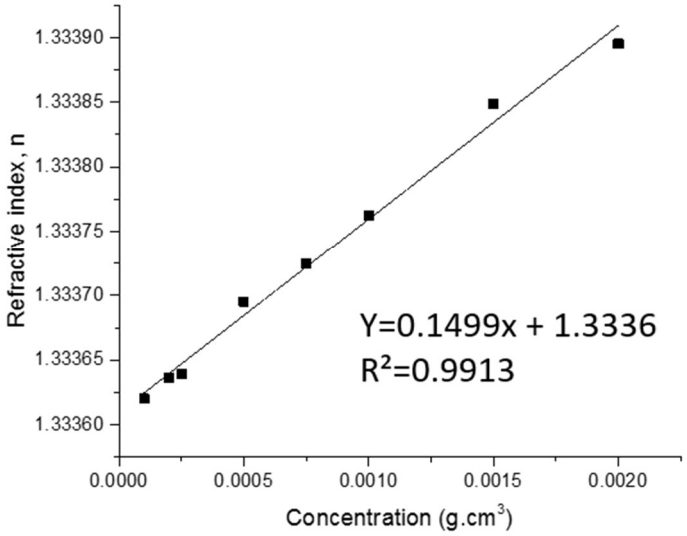


**Figure 49**. Determination of the refractive index increment value, dn/dc, of PEO-*b*-PEHOx

### 7.1.7 Length of the respective polymers and blocks

**A) Random conformation of PEO (coil):**

PEO has a an average bond length of 146 pm[148] (d = 146 pm = 1.46 Å) and has about 3 bonds per repeating unit (l=3). To end-to-end distance in the random coil, the tetraedric bond angle (109.5 degrees), the effective bond length and the number of repeating units must be taken in to account. PEO-45 has 45 repeating units (n=45).

$$R_{eff} = \frac{1+cos\theta}{1-cos\theta} * \sqrt{n * l} * d * sin\ \frac{109.5}{2}\Big)$$

$$R_{eff} = \frac{1.33}{0.67} * \sqrt{3 * 45} * 1.46A * 0{,}81 = 28\ A = 2.8nm$$

**B) Stretched conformation of PEHOx**

Although the average bond length of PEHOX is not reported, the chemical structure is similar to PEO (however, Nitrogen instead of Oxygen). Since any changes of the average bond length are not likely to be substantial, we rounded the above distance to 145 pm as bond length and 109.5 as angle for a perfect tetrahedron.

$$R_{contour} = n * l * \sin\left(\frac{\theta}{2}\right)$$

$$R_{contour} = 3 * 46 * 145nm * \sin\left(\frac{109.5}{2}\right) = 16.3nm \text{ for PEHOx-46}$$

$$R_{contour} = 3 * 57 * 145nm * \sin\left(\frac{109.5}{2}\right) = 20.2nm \text{ for PEHOx-57}$$

$$R_{contour} = 3 * 95 * 145nm * \sin\left(\frac{109.5}{2}\right) = 33.7nm \text{ for PEHOx-95}$$

For the block-copolymers, the contour length of PEO has to be taken into account as well:

$$R_{contour} = 3 * 45 * 146nm * \sin\left(\frac{109.5}{2}\right) = 16.1nm \text{ for PEHOx-46}$$

The overall length of $PEO_{45}$-*b*-$PEHOx_{46}$ is therefore 32.3 nm

The overall length of $PEO_{45}$-*b*-$PEHOx_{57}$ is therefore 36.1 nm

The overall length of $PEO_{45}$-*b*-$PEHOx_{95}$ is therefore 50.0 nm

### 7.1.8 MCMs formed are near-equilibrium self-assembled structures

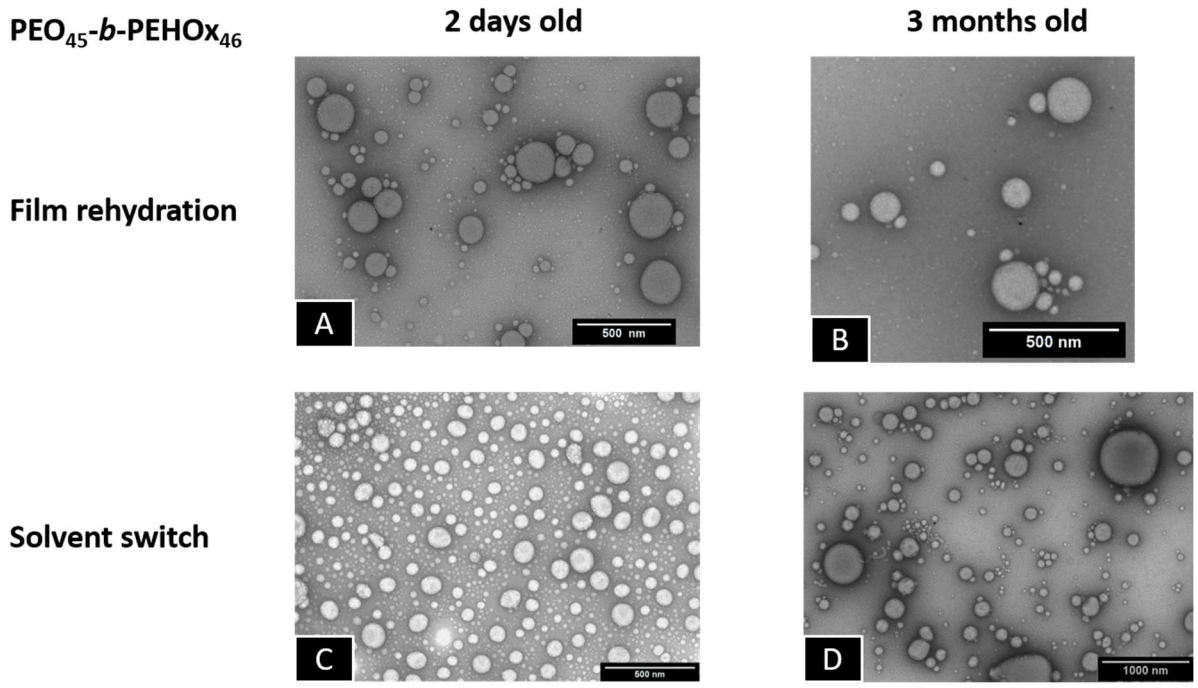


**Figure 50**. Representative TEM images of $PEO_{45}$-b-$PEHOx_{46}$ showing the stability of the spherical nanoparticles, MCMs, over months. Scale bars 500 nm – A, B, C. Scale bars 1000 nm – D.

### 7.1.9 Representative NMR spectrum of pseudo-vesicles and yolk/shell nanoparticles

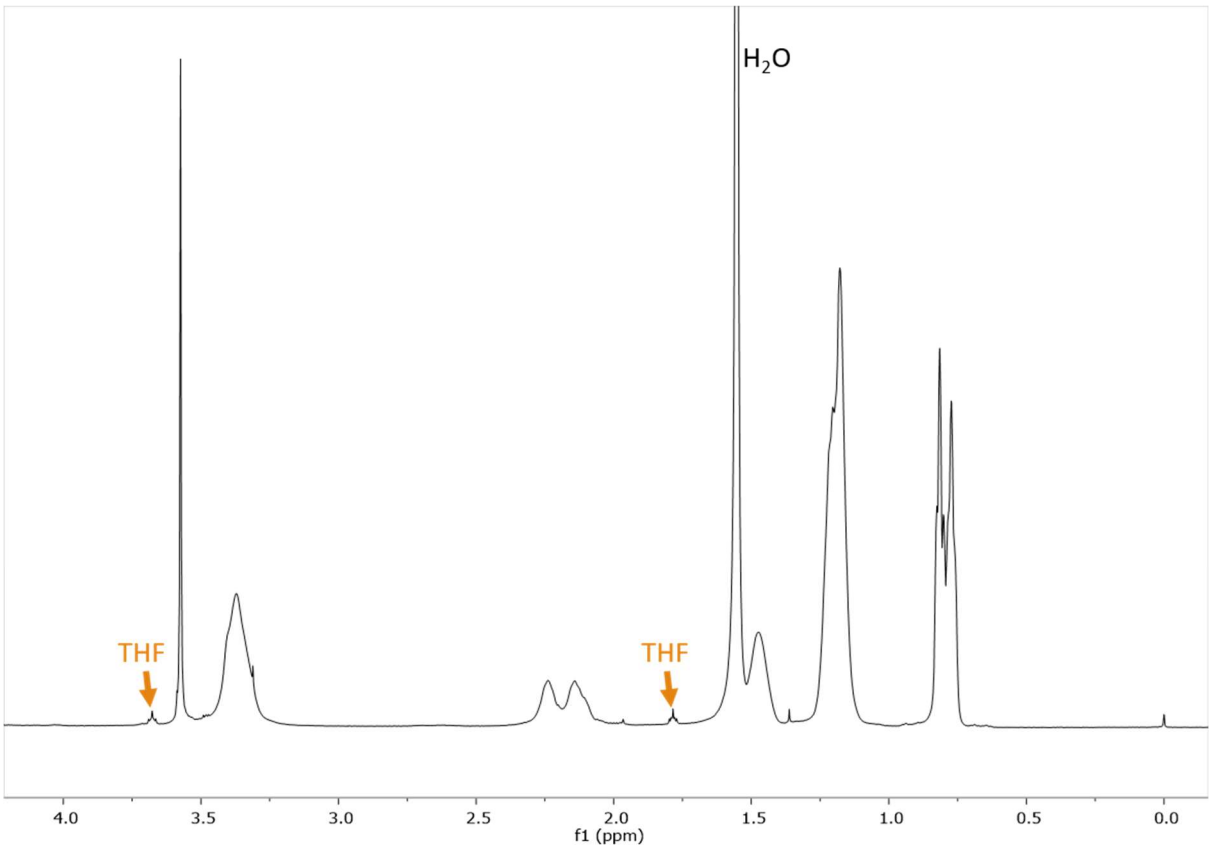


**Figure 51**. Representative $^{1}H$ NMR ($CDCl_3$) of pseudo-vesicles and yolk/shell nanoparticles showing the remaining traces of THF after self-assembly by solvent switch.

## 7.2 Chapter 3: PEO-*b*-PEHOx-*b*-PEtOz

### 7.2.1 Synthesis of PEO-*b*-PEHOx-*b*-PEtOz

**A) Calculation of EHOx and EtOz block length by by $^1$H NMR**

The block ratio of ABC PEO-b-PEHOx-b-PEtOz was determined by integrating the PEO backbone peak at 3.60 ppm as a reference (always 45 units for 2000 Da PEO used). Firstly, the peaks of PEHOx side chain at 0.86 ppm are integrated, integral "a" to calculate the PEHOx block length. The PEtOz block length is then calculated by integrating the peaks of the backbone of PEHOx and PEtOz at 3.43 ppm, integral "b", to which we subtract the number of H coming from PEHOx as summarized in the following Table 7.

**Table 7**. Calculations of EHOx block length for 5 different ABC triblock. [a] Integral "a" (m, 6H, $CH_3$) 0.86 ppm. [b]Integral "b" (m, 4H, N($COCH_2CH_2$)-$CH_2CH_2$) 3.43 ppm. [c] Calculated via N(PEHOx length)= a/6. [d]Calculated via N(PEtOz length)= (b-3-(N(PEHOx length)*4))/4. We subtract 3H from the integral b because of the methyl end-group of PEO which overlap with the peaks of backbone of PEHOx and PEtOz

| Triblock copolymers | Integral "a"[a] | Integral "b"[b] | PEHOx length[c] | PEtOz length[d] |
|---|---|---|---|---|
| $PEO_{45}$-*b*-$PEHOx_{30}$-*b*-$PEtOz_{14}$ | 182 | 179 | 30 | 14 |
| $PEO_{45}$-*b*-$PEHOx_{65}$-*b*-$PEtOz_{19}$ | 392 | 341 | 65 | 19 |
| $PEO_{45}$-*b*-$PEHOx_{53}$-*b*-$PEtOz_{56}$ | 319 | 440 | 53 | 56 |
| $PEO_{45}$-*b*-$PEHOx_{87}$-*b*-$PEtOz_{10}$ | 520 | 390 | 87 | 10 |
| $PEO_{45}$-b-$PEHOx_{138}$-b-$PEtOz_{14}$ | 827 | 610 | 138 | 14 |

### B) Remaining ABC triblock synthetized

**Table 8**. Remaining characterization of PEO-*b*-PEHOx-*b*-PEtOz triblock copolymers using $^1$H NMR, GPC ($CHCl_3$) and hydrophilic weight fraction, *f*. [a]Obtained from $^1$H NMR. [b]Obtained by GPC. [c]Calculated by the equation $f = (M_n(PEO)+M_n(PEtOz))/(M_n(PEO)+M_n(PEHOx)+M_n(PEtOz))$.[d]Ratio Monomer (EHOx) to Initiator (PEO-Nos*).*

| $PEO_t$-*b*-$PEHOx_i$-*b*-$PEtOz_g$ | $M_n$ [Da][a] | $Đ_M$[b] | *f* [%][c] | Ratio (Mono/Ini)[d] | $R_h$ [nm] | $R_g$ [nm] | $\rho = R_g / R_h$ |
|---|---|---|---|---|---|---|---|
| $A_{45}B_{49}C_9$ | 12600 | 1.35 | 23 | 50 | 103 ± 9 | 100 | 0.97 |
| $A_{45}B_{51}C_{11}$ | 13200 | 1.32 | 24 | 50 | 107 ± 12 | 103 | 0.96 |
| $A_{45}B_{45}C_{11}$ | 12000 | 1.36 | 26 | 50 | 102 ± 13 | 103 | 1.01 |
| $A_{45}B_{43}C_{11}$ | 11600 | 1.34 | 27 | 50 | 98 ± 9 | 98 | 1.00 |
| $A_{45}B_{57}C_{12}$ | 14400 | 1.35 | 22 | 60 | 105 ± 15 | 106 | 1.01 |
| $A_{45}B_{53}C_{16}$ | 14000 | 1.40 | 25 | 50 | 105 ± 16 | 105 | 0.98 |

## 7.2.2 Length of the polymer segments and their conformation

### A) Stretched conformation of PEO and PEHOx (contour length)

Although the average bond length of PEHOx is not reported, the chemical structure is similar to PEO (however, Nitrogen instead of Oxygen). Since any changes of the average bond length are not likely to be substantial, we rounded the above distance to 145 pm as bond length and 109.5 as angle for a perfect tetrahedron. The repeating unit has three atoms (l), which has to be multiplied with the number repeating units (n).

$$R_{contour} = l * n * \sin\left(\frac{\theta}{2}\right)$$

$R_{contour} = 3 * 10 * 145nm * sin\left(\frac{109.5}{2}\right) = 3.5nm$ for PEtOz-10

$R_{contour} = 3 * 45 * 145nm * sin\left(\frac{109.5}{2}\right) = 16.0nm$ for PEO-45

$R_{contour} = 3 * 48 * 145nm * sin\left(\frac{109.5}{2}\right) = 17.0nm$ for PEHOx-48

$R_{contour} = 3 * 65 * 145nm * sin\left(\frac{109.5}{2}\right) = 23.1\ nm$ for PEHOx-65

$R_{contour} = 3 * 87 * 145nm * \sin\left(\frac{109.5}{2}\right) = 30.9nm$ for PEHOx-87

$R_{contour} = 3 * 139 * 145nm * \sin\left(\frac{109.5}{2}\right) = 49.3nm$ for PEHOx-139

**B) Random conformation of PEO and PEHOx (ideal coil)**

The average bond length and effective bond length can be taken from the equation above (d = 145 pm and the tetraedric bond angle (109.5 degrees)). Similar to the equation above, the repeating unit has three atoms (l), which has to be multiplied with the number repeating units (n).

$R_{coil} = \frac{1+cos}{1-co} * \sqrt{l * n} * d * sin\left(\frac{109.5}{2}\right)$

$R_{coil} = \frac{1.33}{0.67} * \sqrt{3 * 45} * 145pm * sin\left(\frac{109.5}{2}\right) = 2.7nm$ for PEO-45

$R_{coil} = \frac{1.33}{0.67} * \sqrt{3 * 48} * 145pm * sin\left(\frac{109.5}{2}\right) = 2.8nm$ for PEHOX-48

$R_{coil} = \frac{1.33}{0.67} * \sqrt{3 * 65} * 145pm * sin\left(\frac{109.5}{2}\right) = 3.3nm$ for PEHOx-65

$R_{coil} = \frac{1.33}{0.67} * \sqrt{3 * 87} * 145pm * sin\left(\frac{109.5}{2}\right) = 3.8nm$ for PEHOx-87

$R_{coil} = \frac{1.33}{0.67} * \sqrt{3 * 139} * 145pm * sin\left(\frac{109.5}{2}\right) = 4.8nm$ for PEHOx-139

### C) Effective conformation of PEO and PEHOx, Mix of random coil and stretched

Since PEHOx is a polymer with a branched side chain, the ideal random coil cannot be formed. It also not completely stretched, but has a mixed conformation of both components. The amount of stretching (x) can be calculated, since the real length is known from Cryo-TEM. Since it is an ABC triblock this length can be taken as it has been measured as $R_{eff}$.

$R_{eff} = x * R_{contour} + (1 - x) * R_{coil}$ reforming the equation towards x yields

$x = \frac{R_{eff} - R_{coil}}{R_{contour} - R_{coil}}$ for the specific polymers, this yields x as dimensionless number:

$x_{PEO,45} = \frac{12.6-2,7}{16.0-2.8} = 75\%$ PEO-45 is 74% stretched within the cavities of the tubes

$x_{PEHOx,48} = \frac{6.3-2,8}{17.0-2.8} = 25\%$ PEHOx-48 is 25% stretched within the polymersome membrane

$x_{PEHOx,65} = \frac{7.8-3.3}{23.1-3.3} = 23\%$ PEHOx-65 is 23% stretched within the polymersome membrane

$x_{PEHOx,87} = \frac{9.9-3.8}{30.9-4.0} = 22\%$ PEHOx-87 is 22% stretched within the MCV membrane

$x_{PEHOx,138} = \frac{12.6-4.8}{49.3-4.8} = 18\%$ PEHOx-139 is 18% stretched within the membrane of the polymersomes with a thicker membrane

### 7.2.3 Supplementary Cryo-TEM images of polymersomes

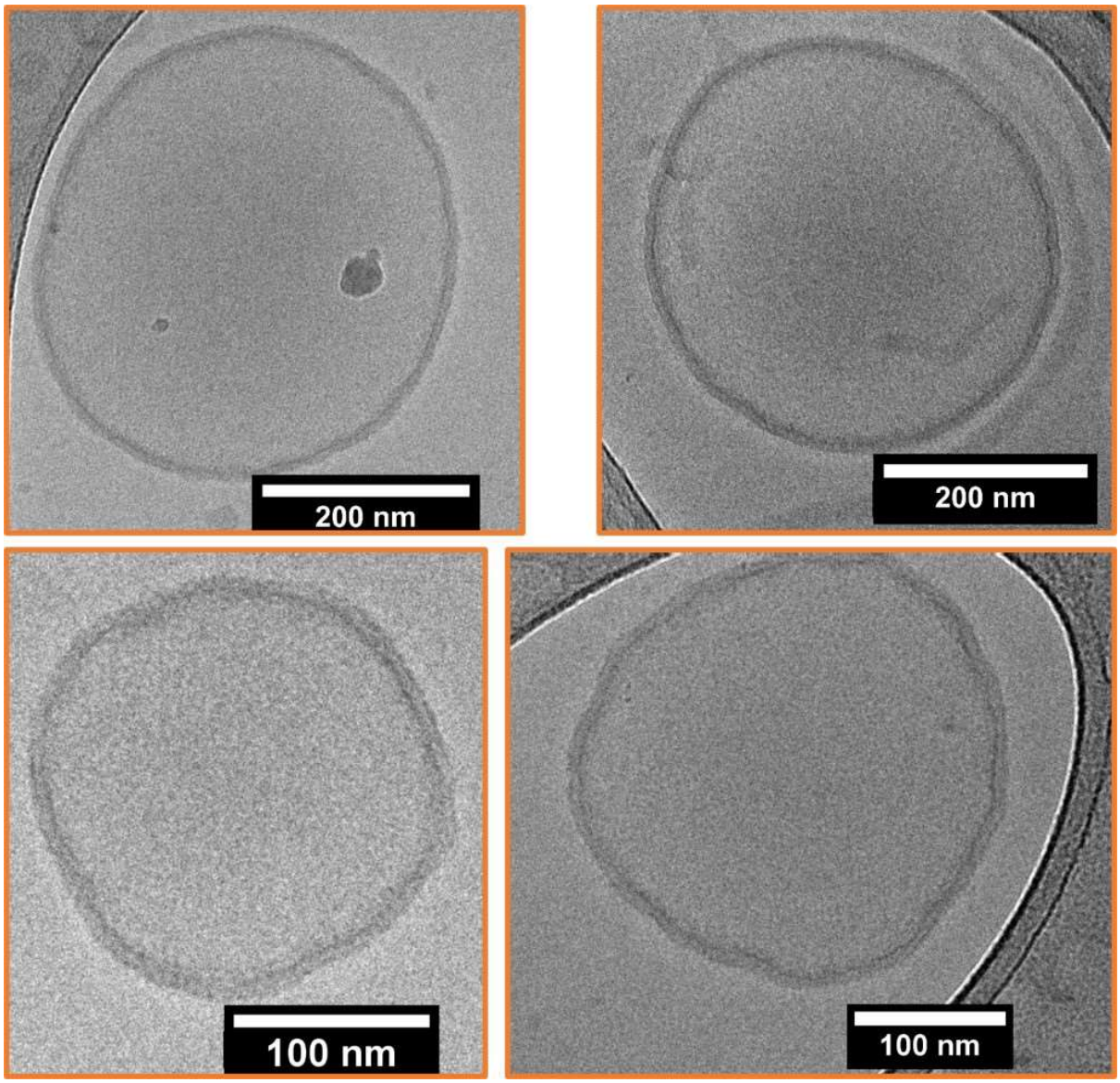


**Figure 52**. Supplementary Cryo-TEM images of polymersomes formed by film rehydration of $PEO_{45}$-*b*-$PEHOx_{48\text{-}65}$-*b*-$PEtOz_{8\text{-}35}$.

### 7.2.4 Supplementary Cryo-TEM images of multicompartment vesicles

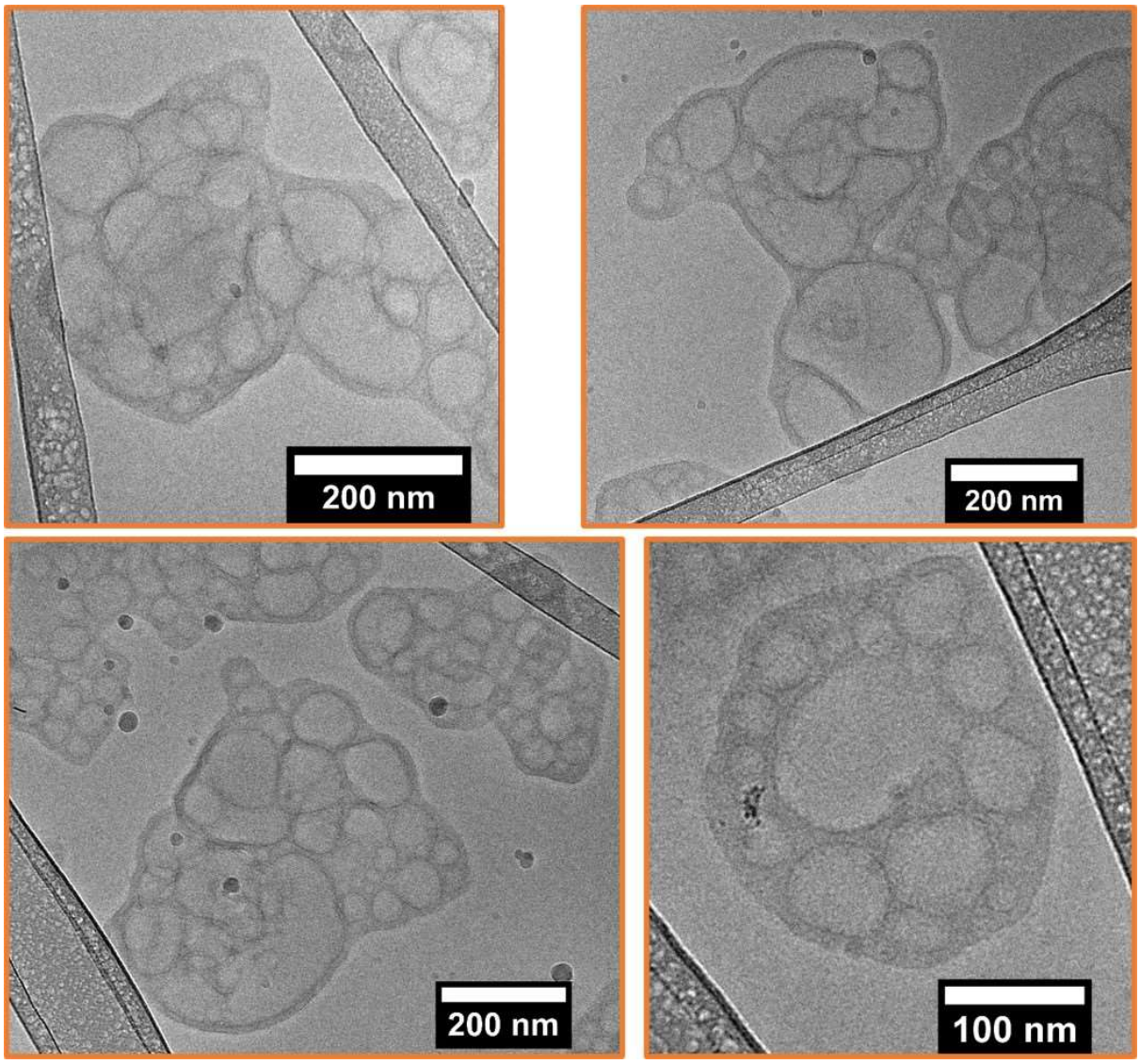


**Figure 53.** Supplementary Cryo-TEM images of multicompartment vesicles formed by film rehydration of $PEO_{45}$-*b*-$PEHOx_{87\text{-}96}$-*b*-$PEtOz_{10\text{-}11}$.

### 7.2.5 Supplementary Cryo-TEM images of tubes and polymersomes

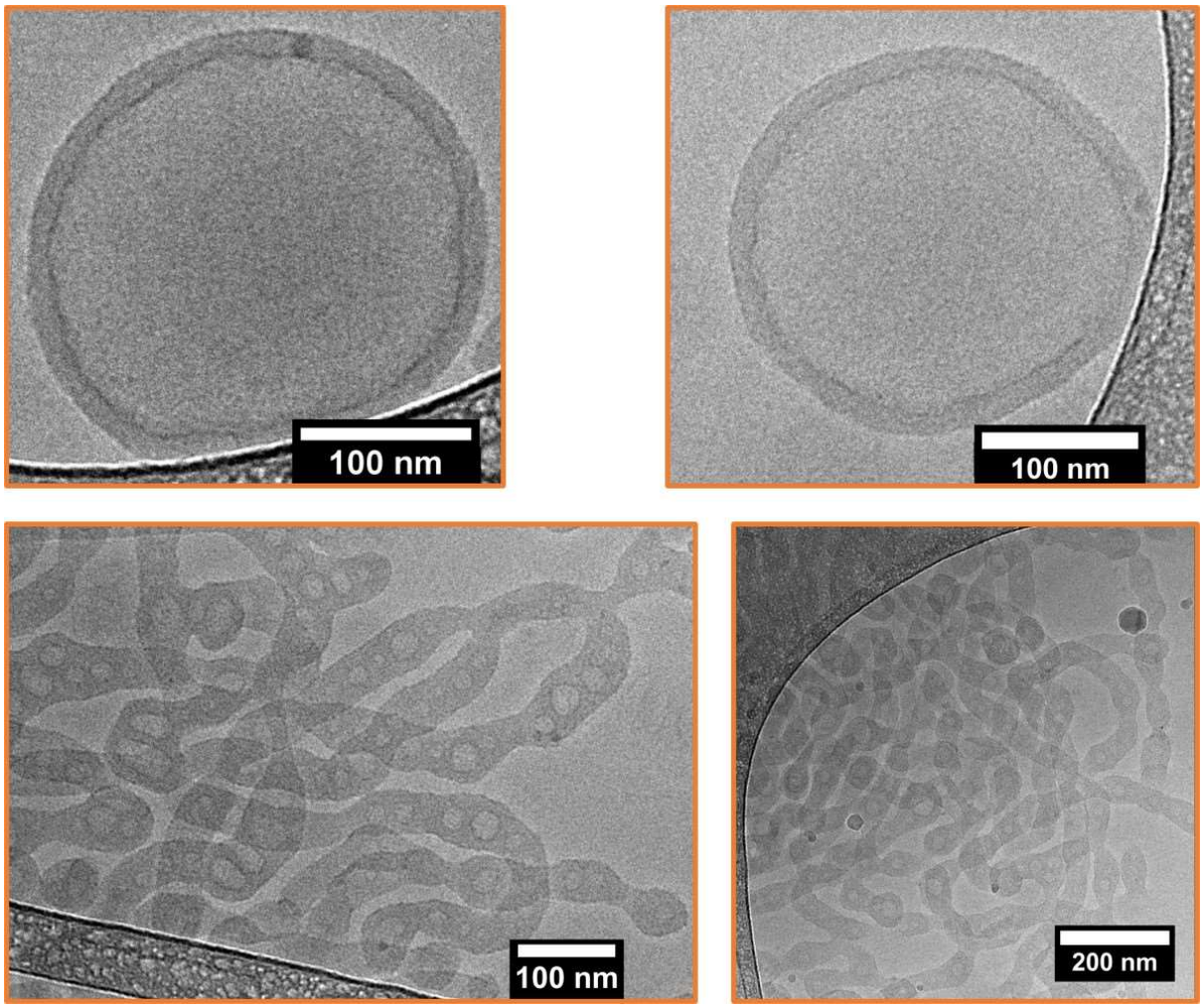


**Figure 54**. Supplementary Cryo-TEM images of tubes and polymersomes formed by film rehydration of $PEO_{45}$-*b*-$PEHOx_{138\text{-}139}$-*b*-$PEtOz_{10\text{-}11}$.